MEMOIRE DE DOCTORAT DE

L'ECOLE CENTRALE DE NANTES
ET L'ACADEMY OF SCIENTIFIC AND INNOVATIVE RESEARCH (AcSIR), INDE

ECOLE DOCTORALE N° 602
Sciences de l'Ingénierie et des Systèmes
Spécialité : *Robotique*

Par

Dhruva Rajesh KHANZODE

A Flexible robotic medical device based on under actuated tensegrity mechanism for minimally invasive surgery (MIS)

Projet de recherche doctoral présenté et soutenu à Chandigarh (INDE), le 18/12/2025
Unité de recherche : UMR6004 - Laboratoire des Sciences du Numérique de Nantes (LS2N)

Rapporteurs avant soutenance :

Renu John	Professor, IIT Hyderabad, Inde
Philippe Poignet	Professeur des universités, Université de Montpellier

Composition du Jury :

Président :	Suman Singh	Professor, AcSIR, Inde
Examinateurs :	Yannick Aoustin	Professeur des universités, Nantes Université
	Renu John	Professor, IIT Hyderabad, Inde
	Philippe Poignet	Professeur des universités, Université de Montpellier
	Sanjeev Verma	Chief Scientist, CSIR-Central Scientific Instruments Organisation, Inde

Directeur de recherches doctorales :	Damien Chablat	Directeur de Recherche CNRS, Ecole Centrale de Nantes
Co-dir. de recherches doctorales :	Emilie Duchalais	Professeur des universités, Praticien Hospitalier, CHU de Nantes
Co-enc. de recherches doctorales :	Ranjan Jha	Principal Scientist, CSIR-Central Scientific Instruments Organisation, Inde

Dedicated to

Lord Ganpati Bappa,

for blessing me with strength and wisdom.

My Family,

whose unconditional love and support

have been my foundation.

My Guides and Teachers,

for their constant encouragement and direction.

My Friends and Colleagues,

for their companionship, motivation, and kindness.

Together, you have been my strength throughout this journey.

ACKNOWLEDGMENT

I would like to express my deepest gratitude to my supervisor, Dr. Ranjan Jha, Principal Scientist, CSIR-CSIO Chandigarh, for his continuous guidance, encouragement, and support throughout this research journey. His invaluable mentorship has been instrumental in shaping the direction and quality of this work.

I am profoundly grateful to my co-supervisors, Prof. Damien Chablat, Directeur de recherche, CNRS LS2N Nantes, and Prof. Emilie Duchalais Dassonville, Chirurgie digestive et endocrinienne, Centre Hospitalier Universitaire (CHU) de Nantes, for their exceptional guidance, unwavering support, and invaluable mentorship throughout my PhD journey. Their insightful advice, constructive feedback, and constant encouragement have been instrumental in shaping both this thesis and my growth as a researcher. I am especially thankful for their generosity in sharing their interdisciplinary perspectives, which have greatly enriched my work and broadened my academic vision beyond what I could have imagined.

I would also like to extend my sincere thanks to the Director, CSIR-Central Scientific Instruments Organisation, for providing a supportive research environment, and to Dr. Sanjeev Soni and Dr. Suman Singh, Coordinators, AcSIR-CSIO, for their continuous support and guidance during my doctoral studies.

I would also like to express my gratitude to my Doctoral Advisory Committee (DAC) members at AcSIR: Dr. Sanjeev Verma, Chief Scientist, CSIR-CSIO, Dr. Neha Khatri, Principal Scientist, CSIR-CSIO, and Dr. Sudeshna Bagchi, Sr. Principal Scientist, CSIR-CSIO, for their valuable guidance and insightful suggestions during the course of this work.

I am equally grateful to my Comité de Suivi Individuel (CSI) members at École Centrale de Nantes: Prof. Yannick Austin, Department of Physics, Nantes University, and Dr. Aurélien Serandour, Department of Mathematics, Informatics and Biology, École Centrale de Nantes, for their constructive discussions and valuable feedback that helped refine my research.

I would like to extend my sincere thanks to my collaborators and team members, Dr.Alexandra Thomiries and Dr.Tinaig Menez from CHU Nantes, for their invaluable support, dedication, and contributions throughout this project. Their commitment and collaboration have been essential to the progress and success of this work.

I gratefully acknowledge the Indian Council of Medical Research (ICMR) for awarding me the ICMR-SRF Fellowship, which provided vital financial support and enabled me to carry out this work successfully.

I would also like to express my heartfelt gratitude to my friends and colleagues—Mr. Deepak Kumar, Mr. Pierre Mougenot, Mr. Dewan Mehnaz Mahmud, Mr. Sreejan Alapati, Mrs. Varsha B, Mr. Chudamani Sahu, Mr. Ishan Narayan, Mr. Kaushlesh Singh Shakya, Mr. Naman Gupta, Dr. Parul and Dr. Swarnima Agarwal —for their constant encouragement, companionship, and support throughout this journey. Their willingness to share ideas, offer guidance, and lend a listening ear during challenging times has been invaluable. Beyond professional support, their friendship, positivity, and sense of humour have made the long hours of research and writing far more enjoyable and meaningful. I am deeply thankful for the many ways they have contributed to making this PhD experience not just a rigorous academic endeavor, but also a truly fulfilling and memorable chapter of my life.

Finally, I extend my heartfelt gratitude to my family for their unconditional love, patience, and unwavering belief in me, without which this work would not have been possible.

Thank You

Dhruva Rajesh Khanzode

TABLE OF CONTENTS

ACKNOWLEDGMENT ii
LIST OF FIGURES vii
LIST OF TABLES ix
LIST OF TERMS AND ABBREVIATIONS x

1 Introduction **1**
1.1 Background 1
1.2 Clinical Problem Statement 2
1.3 Research Gaps 3
1.4 Research Objectives 4
1.5 Scope of the Thesis 4
1.6 Thesis Organization 4

2 Literature Review **8**
2.1 Minimally Invasive Surgery 8
2.1.1 History of Minimally Invasive Surgery 8
2.1.2 MIS v/s Conventional Open Surgery 9
2.1.3 Types of Minimally Invasive Procedures 11
2.1.4 Tools for Manual MIS Procedures 12
2.2 Surgical Robotics 14
2.2.1 History of Surgical Robotics 14
2.2.2 Current Surgical Platforms 16
2.2.3 Advantages of Robot-Assisted Surgery 19
2.2.4 Disadvantages of Robot-Assisted Surgery 21
2.3 Kinematic Modelling 23
2.3.1 Degrees of Freedom (DoF) 23
2.3.2 Forward and Inverse Kinematics 24
2.3.3 Transformation Matrices (DH Parameters) 26
2.3.4 Singularity in Robotic Systems 27
2.4 Piecewise Constant Curvature Approximation (PCCA) 28
2.5 Tensegrity 29
2.5.1 Tensegrity Structures and Their Relevance in Robotics 29
2.5.2 Structural Composition: Tension vs Compression 30
2.5.3 Kinematic modelling Challenges in Tensegrity Mechanisms 31
2.5.4 Actuation Strategies for Tensegrity Robots 31
2.6 Flexible Robotic Systems for Medical Applications 32
2.6.1 Introduction to Flexible Robotic Systems 32
2.6.2 Types of Actuation in Flexible/Continuum Robots 32
2.6.3 Why Tendon/Cable Actuation is Suited for Medical Surgery 33
2.6.4 Global Research and Developments in Tendon-Driven Continuum Robots 34

2.7 Surgical Staplers . . . 35
2.7.1 Early Developments (1900s–1930s) . . . 35
2.7.2 Advances in Materials and Stapling Systems (1930s–1950s) . . . 36
2.7.3 Vascular Staplers and Soviet Contributions (1940s–1960s) . . . 36
2.7.4 Commercialization and Global Adoption (1960s–1980s) . . . 37
2.7.5 Modern Innovations and Future Trends (1990s–Present) . . . 38
2.7.6 Classification of Surgical Staplers . . . 38
2.8 Summary of the Chapter . . . 39

3 Analysis of Surgical Workspace for Laparoscopic Rectal Procedures 42
3.1 Data Acquisition . . . 43
3.1.1 Imaging Protocol . . . 43
3.1.2 Image Capture . . . 44
3.2 Data Processing . . . 44
3.2.1 MRI Data Quality Check . . . 44
3.2.2 Segmentation . . . 45
3.2.3 Zone Identification . . . 45
3.2.4 3D Reconstruction . . . 47
3.2.5 Volume Analysis . . . 47
3.2.6 Positional Analysis . . . 48
3.3 Workspace Optimisation in MATLAB . . . 48
3.3.1 G-code Generation . . . 49
3.3.2 Coordinate Extraction . . . 50
3.3.3 Binary Masking . . . 50
3.3.4 Euclidean Distance Transform . . . 51
3.3.5 Optimization Algorithm . . . 51
3.3.6 2D Optimisation . . . 54
3.3.7 3D Optimisation . . . 54
3.4 Optimisation Results . . . 56
3.5 Summary of the Chapter . . . 58

4 Optimisation of Design Parameter for Surgical Tool 61
4.1 Simplified Workspace Representation . . . 61
4.2 Geometric Points and Parameters . . . 63
4.3 Bending Angle β and Tool Constraints . . . 63
4.4 Optimisation of Tool Parameters: . . . 64
4.4.1 Optimization for Straight Tool . . . 64
4.4.2 Optimization for Curved Tool . . . 65
4.5 Optimisation Results . . . 65
4.6 Summary of the Chapter . . . 69

5 Kinematic Modelling and Analysis 70
5.1 Kinematic Model . . . 70
5.2 Kinematics Equations of One Segment . . . 72
5.3 Force Transmissions between Segments . . . 74
5.4 Simulation-Based Evaluation of Bending Behaviour . . . 76
5.5 Summary of the Chapter . . . 78

6 Mechanical Design and Prototyping of the Flexible Surgical Stapler 80

6.1 Design Rationale and Requirements . . . 80
6.2 First-Generation Stapler Jaw Design . . . 80
6.2.1 Prototype Fabrication and Material Selection . . . 81
6.2.2 Experimental Evaluation . . . 82
6.3 Second-Generation Stapler Jaw Design . . . 82
6.3.1 Prototype Fabrication and Scaling . . . 84
6.3.2 Kinematic and Structural Considerations . . . 84
6.4 Stapler Wrist Design . . . 86
6.4.1 Mathematical Formulation . . . 86
6.4.2 Angular Deflection of a Single Segment . . . 88
6.4.3 Multisegment Deflection . . . 89
6.4.4 Force Optimization Using MATLAB . . . 90
6.4.5 Experimental Validation . . . 91
6.5 Stapler Actuation Mechanism . . . 91
6.5.1 Transmission Assembly . . . 93
6.5.2 Mathematical Representation of Stapler Firing, Jaw, and Wrist Transmission Assemblies . . . 94
6.5.3 Actuation Forces and Ergonomics . . . 96
6.5.4 Force Analysis and Safety Margins . . . 97
6.6 Ergonomic Evaluation of Design from Surgeons . . . 98
6.6.1 Design Integration . . . 102
6.7 Summary of the Chapter . . . 104

7 Conclusions **105**

8 Future Work **107**

References **109**

List of Publications **120**

Appendices

Appendix A Ethical Clearance certificate: CSIR-CSIO **123**

Appendix B Ethical Clearance certificate: CHU Nantes **124**

Résumé **125**

LIST OF FIGURES

2.1 (a) Open Surgery, (b) Minimally Invasive Surgery . . . 10
2.2 Instruments for Minimally Invasive Surgery . . . 12
2.3 Endoscopic Visualization System . . . 13
2.4 PUMA 200 robot for CT-guided neurosurgical brain biopsy . . . 15
2.5 da Vinci® Surgical System by Intuitive Surgical . . . 17
2.6 Zeus® system by Computer Motion . . . 17
2.7 The Versius® platform by CMR Surgical . . . 18
2.8 The Mantra® system from SSI Innovations, developed ingenuously in India . . . 19
2.9 Representation of Degrees of Freedom (DoF) for a free body . . . 24
2.10 Forward and Inverse Kinematics in Robotics . . . 25
2.11 General Representation of DH parameters in Robotics . . . 26
2.12 Tensegrity Structures . . . 30
2.13 First model of the Fischer-Hültl stapler . . . 35
2.14 The Petz Clamp . . . 36
2.15 Soviet UKL-60 stapler . . . 37
2.16 Commercial Surgical Stapler: (a) GIA Stapler, (b) TA Stapler, and (c) EEA Stapler. . . . 38
2.17 Endoscopic Surgical Staplers . . . 40
3.1 Segmentation of MRI slices . . . 46
3.2 Zone identification after segmentation of the pelvic region . . . 46
3.3 Three-dimensional representation of the pelvic workspace . . . 47
3.4 Flexible Surgical stapler inside the workspace . . . 48
3.5 Orientation of conventional tools inside the workspace . . . 49
3.6 Contour generation of the pelvic workspace at each slice using G-code . . . 49
3.7 Binary Masking of the workspace . . . 50
3.8 Anatomical Sections of workspace . . . 53
3.9 Optimisation Results for a layer . . . 53
3.10 Overall optimisation Results in 3D space . . . 54
3.11 Optimized section of 3-dimensional workspace . . . 55
3.12 3D representation of optimised workspace . . . 55
3.13 Flowchart of the workspace optimization process in MATLAB. . . . 57
3.14 Statistical distribution of basal and apical radii, with 5th percentile marked. . . . 58
4.1 Depiction of tool length analysis for straight tool and curved tool, respectively. . . 66
4.2 Maximum tool lengths for straight and curved tools along with corresponding wrist positions. . . . 67
4.3 Operation of the designed stapler in varying workspace sizes. . . . 67
4.4 Population coverage comparison between conventional staplers and the designed MK1 and MK2 staplers. . . . 68
4.5 Example showing the utilisation of MK1 and MK2 staplers for the same patient with $R_b = 25.10$ mm. . . . 68

5.1 The tensegrity mechanism understudy with a stacked multi−segmented model with a flexible beam. 72
5.2 Equilibrium of bending moment [81], where two forces f_1 and f_2 generate the torque $\mathcal{T}_1$. 73
5.3 Static equilibrium of three segments. 75
5.4 Simulation of the bending of one segment with $l_1 = l_2 = 1$ cm and $h_1 = 2$ cm. . 76
5.5 Simulation of bending for three segments with $\mu = 0$ (**left**) and $\mu = 0.2$ (**right**). 77
5.6 Bending singularity occurring due to reduced cross-section. 78
6.1 CAD model of the first-generation flexible stapler jaw. 81
6.2 SLA 3D-printed prototype of the first-generation flexible jaw. 82
6.3 Experimental setup for testing the bending behavior of the first-generation jaw. 83
6.4 Experimental results showing angular displacement (α) and tip coordinates (x, y) versus applied load. 83
6.5 Second-generation flexible stapler jaw with segmented solid sections joined by a flexible spine. 85
6.6 Comparison of actual-size and 250% scaled-up 3D-printed prototypes of the second-generation jaw. 85
6.7 Demonstration of the bending capability of the second-generation jaw using the 3D-printed prototype. 85
6.8 Single wrist segment with a flexural hinge. 86
6.9 Key dimensions of the wrist segment used in bending analysis. 87
6.10 Cross-sectional area considered for I_{yy} calculation. 88
6.11 Cross-sectional area considered for I_{xx} calculation. 89
6.12 Schematic of angular deflection in a single wrist segment under applied load F. 89
6.13 Bending moment distribution for a multi-segment wrist under load. 90
6.14 Experimental setup for measuring angular deflection of a single wrist segment. . 91
6.15 Comparison of experimental and calculated deflections for wrist segment under applied load. 92
6.16 Complete design of the surgical stapling instrument, showing all major components and actuation interfaces. 93
6.17 Actuation Sub-assemblies for the surgical stapler 94
6.18 Surgical Stapler with Ergonomic Handheld Design 97
6.19 First 3D printed prototype, **Prototype Noir** 98
6.20 Second 3D-printed prototype, **Prototype Christmas**, showing its key components: (a) long trigger, (b) short trigger, (c) thumb knob in position 1, (d) thumb knob in position 2, (e) rotation knob in position 1, (f) rotation knob in position 2, and (g) roller under the handle. 99
6.21 Detailed view of the cable-based actuation system for the surgical stapler, illustrating the transmission pathways for jaw, wrist, and firing mechanisms. 103
8.1 Envisioned CAD Design of Pin Arrangement in Flexible Cartridge 108
8.2 3D-Printed Prototype of Stapler Pin Arrangement in Flexible Cartridge 108
8.3 Envisioned Design of Motor Actuated Flexible Endoscopic Surgical Stapler . . 109

LIST OF TABLES

2.1 Comparison of current surgical robotic platforms 20
2.2 Advantages and disadvantages of conventional laparoscopic surgery versus robot-assisted surgery. 20
2.3 Comparison of human and robotic strengths and limitations in surgery. 22
2.4 Classification of surgical staplers according to geometry, function, and clinical application. 41
3.1 Observation of data from optimization results 59
3.2 Average coordinate axes of the workspace regions 59
6.1 Material properties of 3D-printed parts 81
6.2 Table for load v/s deflection of the tip of the 3D-printed lower jaw prototype. . . 84
6.3 Experimental vs Calculated Angular Deflection for Wrist Segment 92
6.4 Summary of ergonomic evaluations for the **Prototype Christmas** 100

LIST OF TERMS AND ABBREVIATIONS

3D	Three-Dimensional
CAD	Computer-Aided Design
CCA	Chef de Clinique Assistant
DH	Denavit–Hartenberg
DJ1	Junior Doctor, Year 1
DJ2	Junior Doctor, Year 2
FK	Forward Kinematics
IK	Inverse Kinematics
IPA	Interne – phase approfondissement (Advanced Internship)
IPS	Interne – phase socle (Basic Internship)
MIS	Minimally Invasive Surgery
MRI	Magnetic Resonance Imaging
PCCA	Piecewise Constant Curvature Approximation
PH	Praticien Hospitalier
PU-PH	Professeur des Universités–Praticien Hospitalier
SLA	Stereolithography
spec./non-spec.	Specialized / Non-specialized
STL	Stereolithography File Format

1

Introduction

1.1 BACKGROUND

Minimally invasive surgery (MIS) has developed progressively over the past two centuries, with each milestone driven by engineering advances that enabled surgical innovation. The central objective of MIS has been to minimize the degree of surgical trauma while maintaining clinical effectiveness. Patients have consistently benefited from this paradigm through reduced intraoperative blood loss, minimal scarring, lower incidence of wound infections and hernias, decreased postoperative pain, and faster recovery times. Historically, abdominal procedures often required large incisions ranging from 12–24 inches to provide the surgeon with adequate visualization and access to the operative field. Although effective, these open approaches were associated with significant patient discomfort and prolonged convalescence [1]. The introduction of laparoscopic techniques radically transformed this scenario by allowing procedures to be performed through small incisions of only 5–12 mm. Instead of direct visualization, surgeons rely on a laparoscope—a camera-based system introduced through one of the ports—to observe the operative site, while surgical instruments are passed through additional trocar-guided entry points. Unlike open surgery, which permits direct manipulation and tactile feedback, laparoscopy requires specially designed instruments capable of functioning within constrained spaces. These advances have significantly improved patient outcomes but simultaneously introduced new challenges for surgeons, including the steep learning curve associated with inverse hand-to-instrument motion mapping, reduced dexterity, and the absence of haptic feedback. As the range of laparoscopic and endoscopic procedures has expanded, so too has the demand for advanced instrumentation and systematic design strategies to develop or refine surgical tools.

In response to these challenges, robotic assistance was introduced to extend the possibilities of MIS. The convergence of robotics and minimally invasive approaches has marked a turning point in surgical practice. Robot-assisted multi-port surgery began to emerge in the mid-1990s

and gained widespread adoption following the introduction of the *da Vinci* Surgical System by Intuitive Surgical in the early 2000s. Robotic platforms addressed critical limitations of conventional laparoscopy by restoring dexterity through wristed instruments with additional degrees of freedom, offering tremor filtration, and providing high-definition, three-dimensional visualization [2]. These capabilities allowed surgeons to perform increasingly complex procedures in anatomically constrained environments that would otherwise challenge human precision and control. Nevertheless, limitations remain, particularly in surgeries involving deep or narrow operative fields such as the pelvis, where access and maneuverability continue to pose significant difficulties.

Colorectal surgery serves as a prime example of these challenges and opportunities. Minimally invasive approaches to colorectal procedures are especially advantageous, given the complex and confined anatomy of the pelvis. Achieving accurate positioning, orientation, and tissue handling in this region is technically demanding [3]. Although robotic platforms have enhanced surgical precision and facilitated difficult operations, procedures such as low anterior resection or rectal surgery still necessitate instruments with high degrees of maneuverability and reliability. The effectiveness of MIS and robotic-assisted colorectal surgery thus relies not only on the visualization and robotic systems but also on the continued development of specialized instruments that can operate effectively in constrained surgical environments.

Among the surgical instruments that have had a transformative impact, staplers are of particular significance. Since their introduction in 1908, surgical staplers have provided a reliable method of mechanical suturing, enabling efficient division of hollow organs and creation of anastomoses under sterile conditions. Early versions consisted of a stapler body, a cartridge or reload containing lines of staples, an anvil, and a firing mechanism, with some designs incorporating a blade to facilitate tissue transection following staple deployment [4]. Over the years, staplers have become indispensable for wound closure, tissue resection, transection, and anastomosis across multiple surgical domains. In colorectal surgery especially, staplers have played a pivotal role by enabling precise tissue joining, reducing operative times, and improving overall surgical efficiency and safety. Their progressive refinement reflects the broader trajectory of MIS, where advances in engineering directly translate into improved surgical capability and patient outcomes.

1.2 CLINICAL PROBLEM STATEMENT

Minimally invasive colorectal surgeries pose significant challenges due to the anatomical constraints of the pelvic region and the limitations of existing surgical instruments. Conventional endoscopic surgical staplers are rigid, which makes precise positioning and orientation within the confined pelvic space particularly difficult. This lack of maneuverability can compromise surgical efficiency and increase the complexity of procedures.

Furthermore, the restricted space in the pelvis limits the use of larger stapling tools, which are often required to achieve the desired cutting or stapling length. As a result, surgeons may need to use smaller tools multiple times to complete the procedure, increasing operative time and the risk of tissue trauma. These clinical challenges highlight the need for a flexible endoscopic stapler that can navigate the constrained pelvic anatomy while providing an extended stapling length, enabling precise and efficient tissue manipulation in minimally invasive surgery.

1.3 RESEARCH GAPS

Despite significant progress in surgical stapler technology, several critical challenges remain that hinder their full clinical effectiveness and adaptability. Identifying these gaps helps define the scope of this research and motivates the development of more advanced and flexible stapler systems.

1. **Limitations of conventional staplers:** Traditional laparoscopic staplers are inherently rigid, offering limited dexterity in anatomically constrained regions such as the deep pelvis or rectum. This lack of maneuverability can compromise precise positioning, reduce surgical efficiency, and increase the difficulty of performing complex procedures.

2. **Constraints in flexible robotic tools:** Continuum and tendon-driven surgical tools provide the potential for enhanced flexibility and access in confined spaces, but accurately modeling their behavior and ensuring reliable control under dynamic loads remain significant challenges. Maintaining robustness and clinical reliability under real surgical conditions is still an unresolved problem.

3. **Optimization of stapler size parameters:** The design of a flexible stapler must account for anatomical constraints, as it cannot be arbitrarily scaled for different patients. Therefore, careful analysis of key size parameters is necessary to determine an optimal stapler size that ensures safe and effective operation across a range of anatomical variations.

4. **Single-hand operability of the stapler:** In minimally invasive surgery, surgeons often manipulate multiple instruments simultaneously, and at any given moment, they may need to operate two tools, including the stapler. Current endoscopic staplers require two hands to position and orient the stapler jaws accurately, forcing the surgeon to temporarily release or forfeit control of another instrument. This creates a need for an endoscopic flexible stapler that can be articulated and maneuvered using a single hand, allowing the surgeon to maintain control over other tools and improving operational efficiency during complex procedures.

1.4 RESEARCH OBJECTIVES

Based on the research gaps, the objectives of this thesis are as follows:

- To design a novel tendon-based flexible surgical stapler with high dexterity.
- To derive the forward and inverse kinematics of the flexible surgical stapler.
- To analyze stiffness on the designed flexible surgical stapler.
- To derive optimal design parameters for flexible surgical staplers.
- To develop a prototype of the flexible surgical stapler.

1.5 SCOPE OF THE THESIS

This thesis focuses on the development of a flexible endoscopic surgical stapler designed to enhance the precision, safety, and efficiency of minimally invasive colorectal surgeries. The work addresses the limitations of conventional rigid staplers, which often struggle to navigate confined anatomical spaces and require complex handling, thereby constraining surgical effectiveness. By emphasizing flexibility, dexterity, and ergonomic operability, the research explores solutions that allow surgeons to manipulate the stapler efficiently while maintaining precise control over tissue handling, even in challenging surgical environments.

The scope of the thesis encompasses the conceptualization, design considerations, and overall framework for creating a tendon-driven, flexible stapler system. It emphasizes the integration of mechanical design principles with kinematic and ergonomic perspectives to define the boundaries and functional focus of the instrument. While specific technical implementations, detailed modeling, and experimental validations are addressed in the subsequent chapters, the primary aim here is to establish a foundation for a next-generation surgical tool capable of improving workflow, reducing procedural limitations, and paving the way for broader applications of flexible instruments in minimally invasive surgery. In doing so, the thesis also highlights areas for future exploration, including clinical validation, material selection, and long-term performance, thereby providing a roadmap for the continued evolution of surgical stapler technology.

1.6 THESIS ORGANIZATION

The remainder of this thesis is organized into the following chapters, each focusing on a specific aspect of the research :

CHAPTER 2: LITERATURE REVIEW

The literature review traces the progression of minimally invasive surgery (MIS), from its history and advantages over open surgery to its main types and enabling tools. It then turns to

surgical robotics, outlining their evolution, current platforms, and the balance between benefits—such as precision, dexterity, and ergonomics—and limitations including cost, bulk, and rigidity.

To establish a theoretical basis, the review introduces key concepts of kinematic modeling, such as degrees of freedom, forward and inverse kinematics, Denavit–Hartenberg parameters, and singularities. Since rigid-body methods fall short for continuum and tendon-driven mechanisms, the Piecewise Constant Curvature Approximation (PCCA) is presented as a more suitable modeling framework. Tensegrity-inspired mechanisms are also discussed for their potential to enhance stability and lightweight actuation. Finally, flexible robotic systems are reviewed for their medical applications, alongside the development of surgical staplers from early designs to modern devices.

CHAPTER 3: ANALYSIS OF SURGICAL WORKSPACE FOR LAPAROSCOPIC RECTAL PRECEDURES

This chapter presents a comprehensive workspace analysis for laparoscopic rectal surgery, focusing on the spatial constraints of the pelvic region and their implications for surgical planning and instrument design. The process begins with high-resolution MRI data acquisition, particularly T2-weighted scans, which provide detailed visualization of pelvic anatomy. Imaging protocols, slice capture, and artifact minimization ensure accurate datasets. The data are processed through quality checks, segmentation of six anatomical zones, and three-dimensional reconstruction using tools such as 3D Slicer. These reconstructions are exported in `.stl` format for computational modeling, volumetric assessment, and positional analysis in SOLIDWORKS.

Subsequently, MATLAB-based optimization techniques are applied to evaluate instrument reachability and collision avoidance. Key steps include contour extraction, binary masking, Euclidean Distance Transform for identifying maximal free space, and Lamé curve fitting to approximate workspace boundaries. A two-stage optimization process addresses anatomical non-uniformities, producing smooth 3D workspace models with apical, intermediate, and basal regions.

Analysis of MRI datasets from 77 patients highlights sex-based anatomical variations, with female workspaces generally larger. Importantly, percentile-based statistics, particularly 5th percentile values, inform surgical stapler design for constrained cases. Results reveal misalignments and curved access pathways, confirming the necessity of flexible wrist mechanisms to ensure safe, effective stapling in rectal surgery.

CHAPTER 4: OPTIMISATION OF DESIGN PARAMETER FOR SURGICAL TOOL

This chapter focuses on the optimization of design parameters for a flexible endoscopic surgical stapler, informed by the previously defined anatomical workspace. Based on surgeon consultations and MRI-based reconstructions, tool navigation was found to occur primarily within the intermediate and basal pelvic regions, allowing design efforts to concentrate on these zones. A simplified cylindrical workspace was derived, characterized by working radius, working height, wrist joint height, dead lengths, curvature angle, and maximum tool length. The analytical modeling of tool trajectory and positioning was possible thanks to these parameters.

Two design cases were investigated: straight and curved tools. The straight tool optimization aimed to maximize effective length while ensuring safe bending angles, solved using MATLAB's *fmincon*. The curved tool analysis incorporated constant rigid segments and bending arcs, evaluated parametrically. Results demonstrated significant limitations of conventional staplers, which failed to operate effectively in up to 18% of the patient population. In contrast, the optimized designs achieved broader anatomical coverage. Two stapler prototypes were proposed: MK1 (55.7 mm) for smaller workspaces and MK2 (67.1 mm) for larger anatomies, with overlapping usability. These designs, incorporating adjustable bending and orientation, enhance surgical accessibility, minimize tissue trauma, and outperform conventional rigid staplers in both adaptability and patient coverage.

CHAPTER 5: MECHANICAL DESIGN AND PROTOTYPING OF THE FLEXIBLE SURGICAL STAPLER

This chapter presents the design and development of the flexible stapler jaw, a key component of the endoscopic stapler system. The clinical requirements demanded a balance between flexibility for navigating confined pelvic anatomy and rigidity for consistent tissue compression and stapling. This presentation describes how to compute the position of intermediate and end points of each segment using PCCA and detailed mathematical formulations, which creates a comprehensive framework for multi-segment analysis, including bending simulations and singularity analysis.

The first-generation design utilized a slotted tube structure with cable-driven actuation, providing controlled bending while maintaining structural continuity. A scaled SLA 3D-printed prototype, fabricated with a flexible–rigid resin mix, enabled mechanical testing. Experimental evaluation confirmed predictable angular displacement under variable loads, validating the feasibility of the design. However, limitations included reduced rigidity under high loads, restricted tip orientation, and difficulties in integrating a removable anvil.

To address these issues, the second-generation jaw was developed with a segmented structure

connected by a flexible spine. This configuration enhanced both rigidity and articulation, while a mechanical hinge restricted opening to 15°, ensuring safe and repeatable deployment. A modular, removable anvil further improved adaptability and simplified maintenance. Scaled and full-size prototypes confirmed smooth bending, stable kinematics, and compatibility with cable actuation, resulting in a robust and versatile stapler jaw.

The chapter also presents the design and validation of the tool's flexible wrist, which employs a flexural hinge design. In addition, the tendon-driven actuation mechanism is described and analysed, with its performance compared against the limitations of human ergonomics validated by surgeon inputs. The chapter concludes that iterative refinement through design, fabrication, and testing enabled a clinically viable solution, forming the foundation for integration with the wrist and actuation mechanisms.

CHAPTER 6 AND 7: CONCLUSIONS AND FUTURE WORK

This research establishes a systematic framework for the conceptualization, design, and prototyping of flexible endoscopic surgical staplers, addressing key limitations of conventional rigid instruments in anatomically constrained regions. By combining advanced kinematic modeling, patient-specific anatomical analysis, iterative prototyping, and ergonomic actuation design, the work demonstrates that flexibility, precision, and reliability can be simultaneously achieved in minimally invasive surgical tools. The development of a modular jaw with a flexible spine, a flexural hinge-based wrist, and a cable-driven single-handed actuation system provides a proof-of-concept for controlled articulation, mechanical stability, and intuitive operation. Experimental validation confirms that the theoretical models accurately predict bending behavior and actuation requirements, highlighting the practical feasibility of the proposed designs.

Despite these advances, several critical challenges remain to achieve clinical readiness. Future investigations must focus on developing a flexible stapler cartridge capable of reliable staple deployment under dynamic bending, selecting and validating materials that balance compliance, strength, and biocompatibility, and conducting rigorous fatigue and sterilization testing. Clinical evaluation will be essential to benchmark device performance, assess ergonomics in surgical workflows, and guide iterative refinements.

By integrating mechanical design principles with patient-specific considerations and ergonomic actuation strategies, this work lays a foundation for next-generation flexible surgical instruments. The methodologies and insights presented here provide a roadmap for extending flexible tool architectures to other constrained surgical environments, supporting broader adoption of minimally invasive technologies and advancing the safety, efficiency, and precision of complex surgical procedures.

2

Literature Review

2.1 MINIMALLY INVASIVE SURGERY

2.1.1 HISTORY OF MINIMALLY INVASIVE SURGERY

The origins of minimally invasive surgery (MIS) can be traced back to the early attempts at reducing surgical trauma by limiting the size of incisions. While traditional surgery relied on large openings to provide direct access and visibility, pioneers in the 20th century began exploring techniques that could achieve the same outcomes with smaller portals. The introduction of endoscopes in the early 1900s laid the groundwork, but it was not until the second half of the century that major technological breakthroughs transformed these ideas into clinical practice.

One of the most influential innovations was the *Hopkins rod-lens system*, which provided improved illumination and sharper images compared with earlier fibre optic technologies. When coupled with the miniaturisation of video cameras, this allowed surgeons to obtain a magnified and detailed view of the operative field without directly opening large sections of the body. The ability to visualise internal structures on a monitor also meant that the entire surgical team could share the same operative field, fostering collaboration and reducing surgeon fatigue, as operators no longer needed to remain in uncomfortable positions at the eyepiece [5].

Equally critical was the advent of *insufflation systems*, which made it possible to expand body cavities safely using carbon dioxide gas. This expansion created sufficient working space for the introduction and manipulation of instruments. The establishment of a gas-filled cavity was a turning point, enabling complex operations to be carried out laparoscopically in a manner comparable to open techniques.

By the late 1980s and early 1990s, laparoscopic cholecystectomy had become the first widely accepted MIS procedure. Its success triggered a rapid adoption of minimally invasive techniques across other domains, including appendectomy, hysterectomy, hernia repair, gastric by-

pass, prostatectomy, and myomectomy [6]. Advances in endoscopes and flexible instruments further expanded the scope of MIS, permitting interventions in regions that were once inaccessible without extensive open incisions.

The global growth of MIS has been remarkable. A 2015 industry report estimated that more than 7.5 million laparoscopic procedures were performed worldwide, with projections indicating annual increases of 10–15%. Today, in many high-volume surgical centres, over 90% of specific operations such as appendectomy, tubal ligation, and cholecystectomy are carried out using minimally invasive approaches.

In parallel, educational methods evolved to accommodate the unique challenges of MIS. Early complications during the learning curve highlighted the necessity of structured training, leading to the development of *surgical simulators, animal models, virtual reality platforms, and mentoring programs*. These tools helped shorten the transition period for new surgeons and ensured safer adoption of the techniques [3].

The history of MIS therefore reflects a gradual yet profound transformation of surgery. What began as an experimental attempt to reduce trauma has evolved into a central paradigm of modern surgical practice. The synergy between optics, video technology, and access devices redefined the boundaries of what surgeons could achieve. Importantly, MIS also catalysed subsequent innovations in robotics, computer-assisted surgery, and image-guided navigation, setting the stage for the present era of technologically advanced surgical systems [7].

2.1.2 MIS V/S CONVENTIONAL OPEN SURGERY

Open surgery has long been regarded as the standard approach for treating a wide range of conditions. Its defining characteristic is the creation of large incisions to provide direct access and exposure of the operative site [8]. While this offers certain advantages, such as tactile feedback, wide visibility, and unrestricted instrument manoeuvrability, it also carries considerable drawbacks, particularly in terms of postoperative morbidity and patient recovery. MIS emerged as a response to these limitations, and its comparison with open surgery highlights both its benefits and its challenges.

The most notable advantage of MIS is the reduction in incision size. Smaller incisions are associated with less postoperative pain, which decreases reliance on analgesics and minimises complications linked to immobility, such as atelectasis and venous thromboembolism. By reducing surgical trauma, MIS also allows for shorter hospital stays and quicker return to daily activities, lowering overall healthcare costs in the long term. Cosmetic results are markedly improved, with patients often valuing the minimal scarring as an important benefit [9].

Clinical studies have also demonstrated other advantages. Minimally invasive approaches can

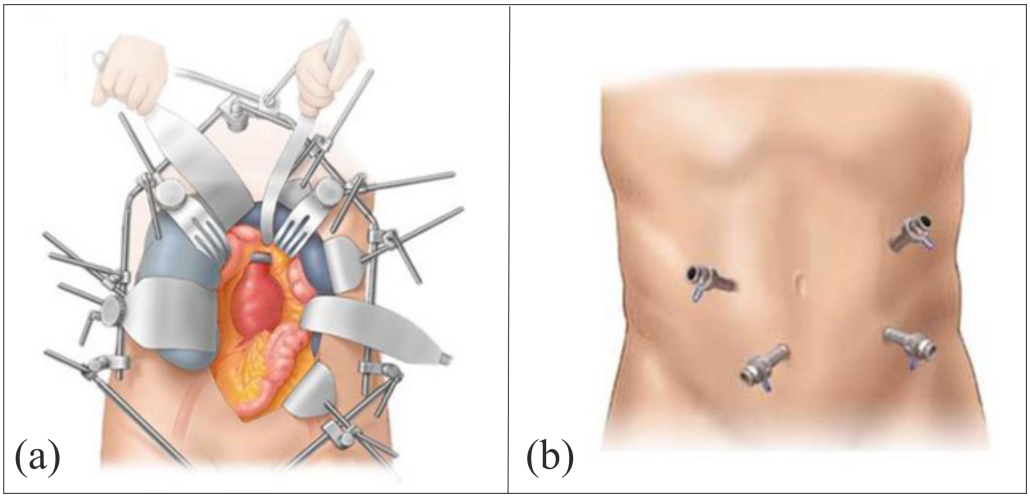

Fig. 2.1 *(a) Open Surgery, (b) Minimally Invasive Surgery*

sometimes provide superior visualisation of certain anatomical regions due to magnification and the ability to angle the camera into narrow spaces. Moreover, the smaller degree of tissue manipulation reduces the systemic inflammatory response and may lessen the risk of adhesive intestinal obstruction, a common complication after open abdominal surgery. Nevertheless, the adoption of MIS also introduced new challenges [10]. The steep learning curve is a critical limitation; complications are most frequently observed in the early stages of a surgeon's experience. For example, in laparoscopic fundoplication, evidence suggests that the first 20 procedures carry the highest risk of errors. Recognising this, structured training, simulation, and mentorship programs have become integral to surgical education.

There are also technical disadvantages unique to MIS. Creating a pneumoperitoneum carries risks such as inadvertent organ injury during trocar insertion, haemodynamic changes due to increased intra-abdominal pressure, and, though rare, gas embolism. Specific complications include port-site hernias and, in oncological surgeries, the possibility of port-site metastases. MIS procedures also tend to have longer operative times compared with open surgeries, particularly during the initial learning phase, which can strain operating room efficiency. From the healthcare system's perspective, MIS involves higher upfront costs due to specialised instruments, energy devices, and imaging systems. However, these expenses are frequently offset by the economic benefits of reduced hospitalisation and faster patient recovery [11].

In essence, while open surgery remains indispensable in certain contexts—especially in emergencies requiring rapid access—MIS has demonstrated clear patient-centred benefits. The balance between the advantages and disadvantages depends on the specific clinical situation, surgeon expertise, and available infrastructure. Ultimately, the ongoing refinement of tools, imaging systems, and training strategies continues to narrow the gap between the two approaches, consolidating MIS as the preferred option in many surgical specialties.

2.1.3 TYPES OF MINIMALLY INVASIVE PROCEDURES

Minimally invasive surgery is a broad field encompassing diverse techniques, each designed for specific anatomical regions or conditions. The most widely practiced type is *laparoscopy*, which involves inserting a laparoscope and instruments into the abdominal cavity through small ports. This approach is used in procedures ranging from appendectomy and cholecystectomy to bariatric surgery and colectomy. Its versatility and reproducibility have made it the cornerstone of abdominal MIS.

Thoracoscopy [12] represents another major category, providing access to the chest cavity. It is commonly employed for lung resections, pleural biopsies, and thymectomies, offering the benefits of reduced postoperative pain and shorter recovery compared with traditional thoracotomy. Similarly, *arthroscopy* [13] is widely used in orthopaedics, enabling minimally invasive treatment of joint disorders such as ligament tears, cartilage injuries, and meniscal repairs.

Other important techniques include *hysteroscopy* [14] for intrauterine interventions, *ureteroscopy* [15] for treating kidney stones and urological conditions, and *endoscopic sinus surgery* for addressing chronic sinus disease. Each of these procedures leverages the principles of MIS to provide targeted interventions with reduced morbidity.

A major innovation in the field is *Natural Orifice Translumenal Endoscopic Surgery (NOTES)* [16], which allows surgeons to access internal organs through natural body orifices such as the mouth, vagina, or rectum. NOTES can reduce postoperative pain and scarring to an absolute minimum by eliminating external incisions. Although technically demanding, NOTES has been applied in procedures such as cholecystectomy and experimental neurosurgery, generating significant interest in the surgical community.

Another evolving area is *image-guided keyhole neurosurgery* [17], which combines advanced navigation systems with endoscopic access to treat brain tumours and vascular malformations. This approach enables surgeons to reach deep intracranial targets with minimal disruption of surrounding tissue, a feat that would be highly invasive with conventional craniotomy.

Endoscopic submucosal dissection and other advanced *gastrointestinal endoscopic procedures* further illustrate the expansion of MIS into areas once managed exclusively through open surgery. These techniques enable precise removal of lesions with minimal disruption of normal anatomy.

Overall, the diversity of MIS reflects its adaptability and continuous evolution. While each type presents unique challenges in terms of access, instrumentation, and learning curve, the unifying principle remains the same: to achieve effective surgical outcomes with the least possible trauma to the patient. As technology advances, the scope of MIS is expected to expand further, incorporating hybrid approaches that combine laparoscopy, robotics, and natural orifice



Fig. 2.2 *Instruments for Minimally Invasive Surgery*

techniques for optimal results.

2.1.4 TOOLS FOR MANUAL MIS PROCEDURES

The success of minimally invasive surgery depends heavily on the availability and refinement of specialised instruments that can perform complex tasks in restricted spaces. Traditional tools had to be miniaturised, redesigned, and optimised for use through narrow trocars or flexible endoscopes. Over time, a wide array of *manual MIS instruments* has been developed, each serving specific purposes.

Basic tools include grasper forceps, needle drivers, scissors, and retrieval pouches, which enable tissue manipulation, suturing, and specimen removal. Innovations such as the *Endo Stitch* system [18] have simplified suturing within confined operative fields, while stapling devices like the *MicroCutter XCHANGE* [19] provide reliable haemostasis and anastomosis in gastrointestinal surgery. These tools replicate the functions of open surgical instruments while overcoming the limitations of restricted access.



Fig. 2.3 *Endoscopic Visualization System*

Energy-based devices are another essential category. Monopolar and bipolar cautery systems are widely used for tissue dissection and haemostasis. More advanced instruments, such as *harmonic scalpels*, convert electrical energy into high-frequency mechanical vibrations, enabling precise cutting with simultaneous coagulation. Radiofrequency ablation systems, argon-enhanced electrosurgery, and lasers extend these capabilities, allowing surgeons to ablate tumours, seal vessels, and minimise intraoperative bleeding. Despite their effectiveness, these devices require careful handling, as limited visualisation increases the risk of inadvertent burns or collateral tissue damage.

Equally vital are imaging and visualisation systems. Early fibre-optic endoscopes have largely been replaced by high-resolution *charge-coupled device (CCD) cameras* and digital imaging systems, which provide colour, magnified views projected on monitors. Modern rod-lens laparoscopes enhance clarity and ergonomics, while tip-mounted cameras reduce lens-related distortions. More recently, *three-dimensional (3D) laparoscopic systems* have restored depth perception, improving hand–eye coordination and reducing surgical errors. Platforms such as *Olympus VISERA* deliver 3D 4K video with wide angulation, significantly enhancing procedural accuracy [20]. Computational stereo algorithms further expand these possibilities by reconstructing depth information from two-dimensional images.

Despite these advancements, manual MIS tools still face limitations. The lack of wrist-like articulation at the instrument tip complicates triangulation and tissue handling. Frequent instrument exchanges prolong procedures, while cluttered working spaces challenge efficiency. Nevertheless, the continuous refinement of instrument design, including articulating end-effectors and ergonomic handles, has steadily improved functionality.

The role of training cannot be overstated. Surgeons must adapt to the altered hand–eye coordination and the absence of tactile feedback in MIS. Virtual reality simulators and bench-top trainers have become essential for skill acquisition before clinical application.

In summary, the toolbox of manual MIS procedures has expanded significantly, transforming what can be achieved through small incisions or natural orifices. While current limitations persist, ongoing innovation—supported by advances in robotics, imaging, and ergonomics—continues to push the boundaries of what manual MIS can accomplish. These tools not only enable safer and more efficient procedures but also lay the foundation for hybrid and robot-assisted techniques that represent the future of surgical practice.

2.2 SURGICAL ROBOTICS

2.2.1 HISTORY OF SURGICAL ROBOTICS

The concept of robotics has long fascinated both scientists and the general public. The term "robot" was first introduced in 1921 by the Czech playwright Karel Čapek in his play *Rossum's Universal Robots*, derived from the Czech word *robota*, meaning forced labor. Initially, robots were imagined as simple machines capable of repetitive manual tasks, designed to substitute for human labor. Over time, their meaning expanded to encompass advanced, programmable machines with varying degrees of autonomy. By the mid-20th century, robots had become vital in industrial sectors, capable of performing tasks with precision, reliability, and endurance far beyond human capacity [21]. Robotics was routinely employed in hazardous settings such as deep-sea exploration, chemical manufacturing, and microelectronics production.

The application of robotics in medicine, however, lagged behind industrial developments. In the 1970s, the National Aeronautics and Space Administration (NASA) and the Defense Advanced Research Projects Agency (DARPA) began investigating the feasibility of robotic and teleoperated systems for surgery. Their motivation was clear: astronauts in space and soldiers on the battlefield often lacked access to specialized surgeons. Robotic platforms, controlled remotely, were envisioned as a means of delivering surgical expertise to locations where human presence was impractical or dangerous. This early research laid the foundation for telepresence and telesurgery concepts, which remain relevant today.

The first true milestone in robotic surgery came in 1985, when a modified PUMA 200 industrial robot was employed for a computed tomography (CT)-guided neurosurgical brain biopsy

[22]. This demonstrated the potential of robots for image-guided, high-precision interventions. Shortly thereafter, the PROBOT system was developed in the United Kingdom for prostate resection, while the ROBODOC system in the United States was designed for orthopedic applications, specifically precise femoral milling during hip replacement surgery. ROBODOC became the first medical robot approved by the U.S. Food and Drug Administration (FDA), highlighting its clinical viability [23]. These early systems, however, were limited by primitive computer interfaces, cumbersome set-ups, and the requirement for extensive preoperative planning.



Fig. 2.4 *PUMA 200 robot for CT-guided neurosurgical brain biopsy*

During the 1990s, advances in virtual reality, computing power, and robotics converged to create the foundation of modern telemanipulation systems. At NASA Ames Research Center and the Stanford Research Institute (SRI), engineers developed dexterous telemanipulators intended to give surgeons a sense of direct interaction with the surgical field, despite physical distance. The concept of telepresence—whereby a surgeon operates as if present at the site—was a crucial leap forward. These efforts aligned with military objectives of reducing wartime mortality by enabling remote operations on injured soldiers [24]. Parallel to these efforts, commercial ventures began to flourish. Computer Motion introduced the Automated Endoscopic System for Optimal Positioning (AESOP) [25], a voice-controlled robotic arm that positioned laparoscopic cameras. This was followed by the Zeus system, a master–slave telemanipulator that included a voice-controlled camera and modular, table-mounted robotic arms.

Meanwhile, Intuitive Surgical developed the da Vinci Surgical System, derived from SRI's telepresence research. The da Vinci platform provided stereoscopic three-dimensional imaging and articulated instruments mimicking the movements of the human wrist. In 2003, Computer Motion and Intuitive Surgical merged, leading to the discontinuation of the Zeus platform and

consolidating the surgical robotics market. This merger marked a turning point in the evolution of surgical robotics, giving da Vinci a near-monopoly position that persists today [26].

Thus, the history of surgical robotics reflects the interplay of industrial innovation, military applications, and medical necessity. From its origins in neurosurgery and orthopedics to its present role in minimally invasive procedures, surgical robotics has steadily expanded the boundaries of what is technically feasible in the operating room [27].

2.2.2 CURRENT SURGICAL PLATFORMS

Modern surgical robotics has evolved into sophisticated master–slave telemanipulation systems, where the surgeon operates from a console (the master), and the robotic arms (the slave) translate the surgeon's motions into precise actions within the patient's body. This design eliminates many limitations of conventional laparoscopy, such as restricted range of motion and poor ergonomics, while introducing new possibilities in precision, stability, and remote operation.

The most widely adopted system is the da Vinci® Surgical System by Intuitive Surgical [28]. Introduced in the late 1990s, it rapidly became the global standard for robotic-assisted surgery. The da Vinci platform provides stereoscopic high-definition three-dimensional visualization, tenfold magnification, and wrist-like instrument articulation (EndoWrist® technology). The surgeon operates in a seated, ergonomic position, controlling instruments via intuitive hand controllers and foot pedals. Successive generations of da Vinci, culminating in the da Vinci Xi and da Vinci SP (single-port), have refined ergonomics, reduced instrument collisions, and integrated advanced imaging modalities such as near-infrared fluorescence for real-time anatomical guidance. These systems are now widely used in urology, gynecology, cardiothoracic surgery, and general surgery.

Earlier competitors such as the Zeus® system by Computer Motion [29] played a key role in shaping the field. Zeus introduced modular robotic arms, a voice-controlled camera system (AESOP), and precise motion scaling. However, after the merger with Intuitive Surgical in 2003, the Zeus line was discontinued in favor of da Vinci. Despite its discontinuation, Zeus demonstrated the value of modularity and voice-controlled interfaces, concepts that continue to influence newer platforms.

Beyond da Vinci, other robotic systems have sought to address its limitations or offer niche advantages. The TELELAP Alf-X® system, developed in Italy [30], incorporates force-feedback technology, enabling surgeons to feel resistance during tissue manipulation—a feature absent in most current robotic systems. Its innovative eye-tracking technology allows surgeons to control camera movements simply by gaze direction, improving workflow efficiency. Titan Medical introduced the Amadeus prototypes, which featured haptic feedback and compact designs tailored for confined anatomical spaces, although development has since shifted toward



Fig. 2.5 *da Vinci® Surgical System by Intuitive Surgical*

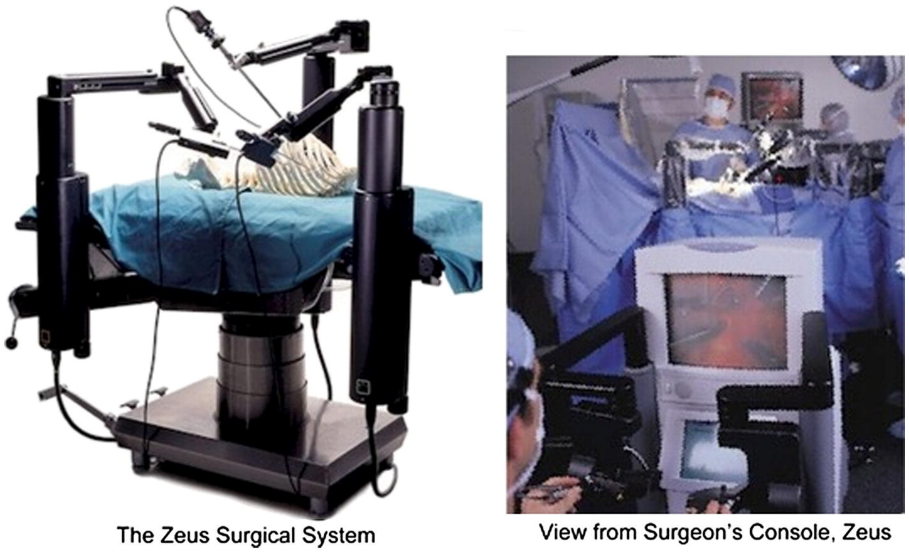

Fig. 2.6 *Zeus® system by Computer Motion*

single-access robotic systems. Similarly, AVRA Surgical Robotics has developed modular systems with wireless control, increasing flexibility and adaptability for varied procedures [31].

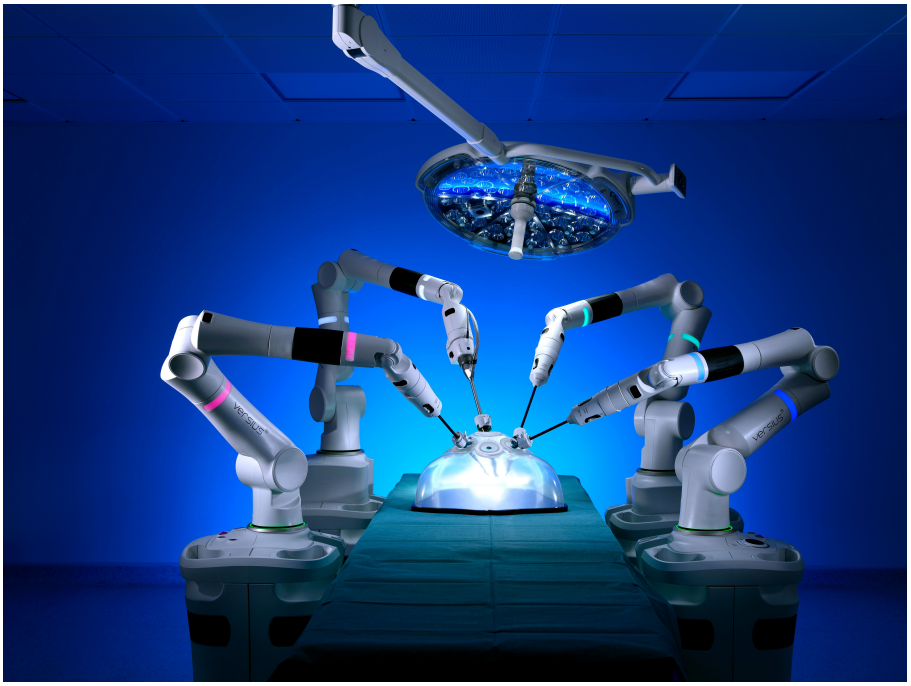

Fig. 2.7 *The Versius® platform by CMR Surgical*

Several newer systems are now being used in clinical practice to diversify the market and address da Vinci's limitations. The Versius® platform by CMR Surgical [32] adopts a modular architecture, with independent robotic arms positioned around the patient, providing greater flexibility in operating room setup and improved ergonomics through an open-console design (Figure 2.7). Hugo RAS®, developed by Medtronic [33], similarly emphasizes modularity and portability, with compact robotic arms and an open-console system intended to lower costs and improve accessibility in diverse healthcare settings. The Mantra® system from SSI Innovations in India has emerged as a cost-effective alternative, offering articulated instruments, 3D vision, and a design philosophy aimed at expanding access to robotic surgery in developing regions (Figure 2.8) [34]. In contrast, Stryker's Mako SmartRobotics® [35] platform focuses on orthopedic applications, particularly hip and knee replacements, where it combines CT-based surgical planning with robotic-arm guidance and haptic feedback to improve accuracy in bone preparation and implant placement.

Recent developments also focus on miniaturization and single-port approaches. The da Vinci SP system, for example, enables the introduction of multiple articulated instruments through a single incision, reducing trauma and improving cosmetic outcomes. Parallel efforts are integrating robotic systems with advanced imaging technologies such as MRI and CT, further expanding their potential for real-time image-guided interventions.

The global market for surgical robotics is also diversifying. Emerging companies from Europe



Fig. 2.8 *The Mantra® system from SSI Innovations, developed ingenuously in India*

and Asia are developing cost-effective platforms to challenge da Vinci's dominance. While these newer systems are not yet as widely adopted, they represent the next wave of innovation aimed at improving accessibility and affordability.

In summary, current surgical platforms represent a combination of ergonomic design, enhanced visualization, and precise motion control. While da Vinci remains the dominant system, continuous innovation from competitors such as CMR's Versius, Medtronic's Hugo RAS, SSI's Mantra, and Stryker's Mako is reshaping the landscape, ensuring that the field of surgical robotics remains dynamic and forward-looking.

2.2.3 ADVANTAGES OF ROBOT-ASSISTED SURGERY

The advent of robot-assisted surgery has been driven largely by the desire to overcome the limitations of conventional laparoscopic techniques. Traditional minimally invasive surgery, though highly beneficial compared to open surgery, is hindered by restricted instrument movement, counterintuitive hand–eye coordination, and a lack of tactile feedback. Robot-assisted systems have introduced solutions to many of these challenges, significantly enhancing surgical precision, ergonomics, and clinical outcomes.

One of the foremost advantages is improved visualization. Robotic systems such as da Vinci provide three-dimensional, high-definition views of the surgical field with up to tenfold magnification. This enhanced visualization allows surgeons to identify critical anatomical structures with greater accuracy, reducing the risk of inadvertent injury. Additionally, the immersive stereoscopic display restores depth perception, which is absent in conventional two-dimensional laparoscopy [36].

Table 2.1 *Comparison of current surgical robotic platforms*

Platform	**Manufacturer / Origin**	**Key Features**	**Primary Applications**
da Vinci®	Intuitive Surgical (USA)	3D HD vision, EndoWrist®, multiple generations (Xi, SP)	Urology, gynecology, thoracic, general surgery
Versius®	CMR Surgical (UK)	Modular independent arms, open console, ergonomic design	General, colorectal, gynecology, urology
Hugo RAS®	Medtronic (USA)	Modular arms, portable carts, open console, cost-oriented	Hernia repair, prostate, soft tissue procedures
Mantra®	SSI Innovations (India)	Cost-effective, articulated instruments, 3D vision, access-focused design	General, gynecology, urology (emerging markets)
Mako SmartRobotics®	Stryker (USA)	CT-based planning, robotic-arm guidance, haptic boundary control	Orthopedics (hip and knee replacement)

Table 2.2 *Advantages and disadvantages of conventional laparoscopic surgery versus robot-assisted surgery.*

	Conventional Laparoscopic Surgery	Robot-Assisted Surgery
Advantages	Well-developed technology Affordable and widely available Proven clinical efficacy	3D visualization Improved dexterity Seven degrees of freedom Elimination of fulcrum effect Reduction of physiologic tremors Motion scaling Microsurgical capability Tele-surgery potential Ergonomic working position
Disadvantages	Loss of tactile sensation Loss of three-dimensional visualization Limited degrees of freedom Fulcrum effect present Amplification of tremors Compromised ergonomics	Absence of tactile sensation Very high cost High set-up and maintenance costs Steep learning curve Requires additional staff support New technology with limited validation

Dexterity is another major benefit. Robotic instruments are equipped with articulated joints, often mimicking the movements of the human wrist with seven degrees of freedom. This eliminates the fulcrum effect inherent in laparoscopic surgery, where instrument tips move in the opposite direction to the surgeon's hands. Motion scaling enables fine manipulations, such as microsuturing and anastomosis, which would be exceedingly difficult with conventional tools. Tremor filtration further refines precision, ensuring stable instrument movements even during lengthy procedures [37].

Ergonomics also plays a crucial role. Surgeons performing lengthy laparoscopic procedures often experience physical strain due to awkward instrument positioning and prolonged standing [38]. Robotic systems allow surgeons to operate from a seated console with natural hand positioning, reducing fatigue and musculoskeletal stress. This ergonomic advantage not only improves surgeon comfort but may also enhance performance and prolong surgical careers.

From a clinical perspective, robot-assisted surgery has been associated with reduced intraoperative blood loss, shorter hospital stays, and faster recovery times compared to traditional approaches. Studies in urology, gynecology, and colorectal surgery have demonstrated lower conversion rates to open surgery, improved postoperative pain control, and superior cosmetic outcomes. For patients, these translate into reduced morbidity and earlier return to normal activities.

Robot-assisted systems present new possibilities, such as remote tele-surgery, where procedures can be carried out remotely. This has implications for improving access to expert surgical care in underserved regions [39]. Furthermore, robotic platforms provide unique training opportunities. Virtual reality simulators and built-in performance metrics enable trainees to practice skills in a safe, controlled environment, accelerating learning curves.

The advantages can be summarized in structured form (see Tables 2.2 and 2.3). Robot-assisted systems combine the strengths of human cognitive abilities with machine precision, bridging gaps left by traditional minimally invasive surgery.

2.2.4 DISADVANTAGES OF ROBOT-ASSISTED SURGERY

Despite the many advantages, robot-assisted surgery is accompanied by several disadvantages that temper its universal adoption. The most significant limitation is cost. Robotic systems typically exceed one million U.S. dollars in acquisition expenses, with recurring costs for disposable instruments, maintenance contracts, and software upgrades. Hospitals must weigh these costs against potential benefits in patient outcomes, which are not always consistently superior to conventional minimally invasive approaches [40]. For smaller healthcare institutions, the financial burden may be prohibitive, restricting access to advanced surgical technology. Another drawback is the size and complexity of robotic systems. Operating rooms are often

Table 2.3 *Comparison of human and robotic strengths and limitations in surgery.*

Human Strengths	Human Limitations	Robot Strengths	Robot Limitations
• Strong hand–eye coordination	• Limited dexterity beyond natural scale	• High geometric accuracy	• No clinical judgment
• Dexterity and adaptability	• Prone to fatigue and tremors	• Stable and tireless	• Lack of qualitative assessment
• Integration of diverse information	• Restricted geometric accuracy	• Motion scaling	• No tactile feedback
• Rudimentary haptics	• Limited use of quantitative data	• Sensor-based data acquisition	• Expensive technology
• Ability to apply qualitative judgment	• Limited sterility and infection risk	• Sterilizable components	• Rapid technological changes
• Good judgment and decision-making	• Susceptible to radiation/infection	• Resistant to radiation and infection	• Requires further validation

limited in space, and the addition of large robotic platforms can lead to crowding and workflow inefficiencies. The robotic arms, though precise, may obstruct surgical staff, complicate instrument exchange, or increase operative time during the learning curve. These logistical issues are compounded in high-volume hospitals where rapid room turnover is essential.

The absence of tactile feedback remains a critical limitation. Conventional open surgery allows surgeons to rely on their sense of touch to assess tissue characteristics such as firmness, texture, or vascular pulsation. In robotic systems, this tactile dimension is largely absent, making surgeons heavily reliant on visual cues. While research into haptic feedback technologies is ongoing, no mainstream system has yet incorporated reliable, real-time force feedback as a standard feature. Training and proficiency development also pose challenges [41]. Mastering robotic platforms requires extensive training, often through simulation modules, animal labs, and proctored cases. The learning curve is steep, particularly for complex procedures, and inadequate training can negate the advantages of the system. Furthermore, surgical teams must adapt to new workflows, necessitating ongoing education for nurses, anesthesiologists, and operating room staff.

Another disadvantage lies in the relative novelty of the technology. Although short-term studies demonstrate safety and feasibility, robust long-term data are limited. Randomized controlled trials comparing robotic-assisted surgery with laparoscopy often reveal equivalent outcomes, raising questions about cost-effectiveness. As such, insurers and healthcare policymakers remain cautious in supporting widespread robotic adoption without stronger evidence of clinical superiority. Upgradability is a concern as well. Technology evolves rapidly, and existing robotic systems may become obsolete within a decade, necessitating costly upgrades or replacements. This raises concerns for institutions that must justify the initial investment while anticipating future expenditures [42]. Ethical issues, such as equitable access to robotic surgery, also emerge. Wealthier hospitals in developed regions may adopt these systems, while under-

funded facilities remain reliant on traditional methods, exacerbating disparities in healthcare delivery.

Lastly, robotic systems may increase dependence on technology. Technical malfunctions, although rare, can interrupt procedures and pose safety risks. Surgeons must be prepared to convert to open or laparoscopic surgery in such instances, necessitating dual proficiency. This dependence underscores the importance of maintaining traditional surgical skills alongside robotic training. Therefore, while robot-assisted surgery represents a groundbreaking advance in surgical technology, its disadvantages—high cost, logistical complexity, absence of haptic feedback, steep learning curve, and uncertain long-term outcomes—must be addressed for the field to mature. The future of surgical robotics will likely involve balancing these challenges against its transformative potential, ensuring that benefits are equitably distributed and cost-effectiveness is demonstrated [43].

2.3 KINEMATIC MODELLING

Kinematics is a foundational discipline in robotics and mechanical engineering that focuses on the study of motion without considering the forces or torques that cause it. It is involved in describing the position, orientation, velocity, and acceleration of bodies or mechanisms in space. In the context of robotic systems, especially those used in surgical applications, kinematics is essential for determining the control of robotic arms, manipulators, or flexible tools [44].

Rigid body kinematics typically deals with the transformation of coordinates in space, utilizing mathematical tools such as vectors, matrices, and coordinate frames. The fundamental aim is to model how different parts of a mechanical system move relative to one another. This modelling includes both forward kinematics and inverse kinematics.

The scope of kinematics extends to various types of robotic systems, including serial manipulators, parallel manipulators, and continuum robots. For each type, specific mathematical frameworks and assumptions are used. For example, in serial manipulators, the transformation of each link is calculated relative to a base frame using homogeneous transformation matrices. In contrast, continuum robots may require piecewise models or curve approximations like constant curvature [45].

Understanding kinematics is also vital for defining control systems, workspace analysis, and collision avoidance in robotics. In surgical contexts, precision in motion and repeatability are of utmost importance, which makes kinematic accuracy crucial [46].

2.3.1 DEGREES OF FREEDOM (DOF)

Degrees of Freedom (DoF) is a concept in the study of kinematics, serving as a quantitative measure of the number of independent parameters required to define the configuration of a

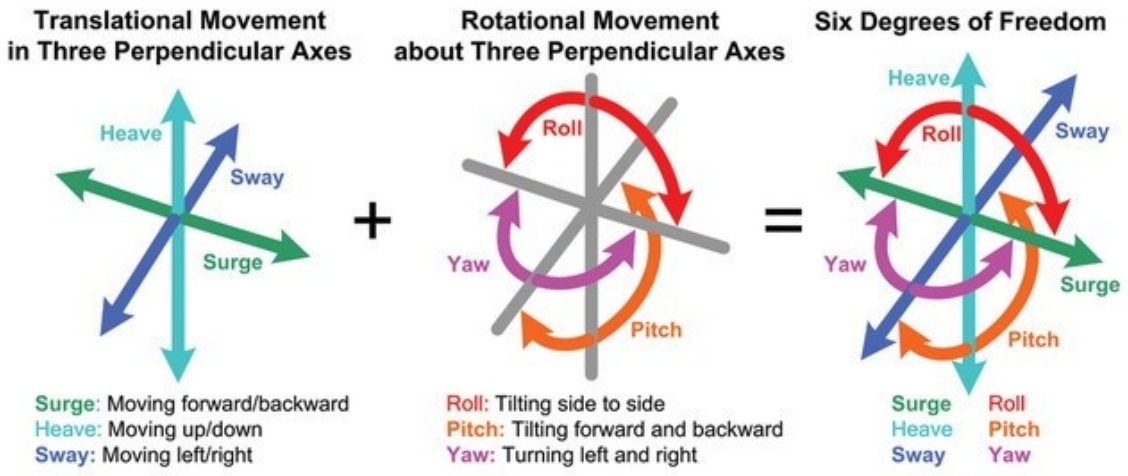

Fig. 2.9 *Representation of Degrees of Freedom (DoF) for a free body*

mechanical system. In the context of robotics, it refers to the number of independent motions, such as translations and rotations, that a robotic mechanism or manipulator can perform. For example, a rigid body in three-dimensional space has six degrees of freedom: three translational (movement along x, y, z axes) and three rotational (about these axes) [47].

Understanding DoF is essential in designing robotic mechanisms that are capable of achieving the desired mobility for specific tasks. A serial manipulator, like a traditional robotic arm, typically comprises a sequence of joints and links, where each joint contributes one or more degrees of freedom. Revolute joints offer rotational DoF, while prismatic joints provide translational movement. The total DoF of such a mechanism is the sum of the individual joint contributions, constrained by the mechanical structure [48].

The concept of DoF is not only theoretical, but it has real-world implications in the design and control of surgical robots, where high dexterity and precision are required in constrained environments. For instance, a laparoscopic instrument may be limited to fewer degrees of freedom due to the entry-point constraint, necessitating innovative mechanical designs to maintain functionality internally. Similarly, continuum robots often exhibit theoretically infinite DoF, which are practically approximated using models like Piecewise Constant Curvature to make analysis and control tractable [49].

2.3.2 FORWARD AND INVERSE KINEMATICS

Forward and inverse kinematics form the base of robotic motion analysis and are essential parts in determining the relationship between a robot's joint configurations and the position

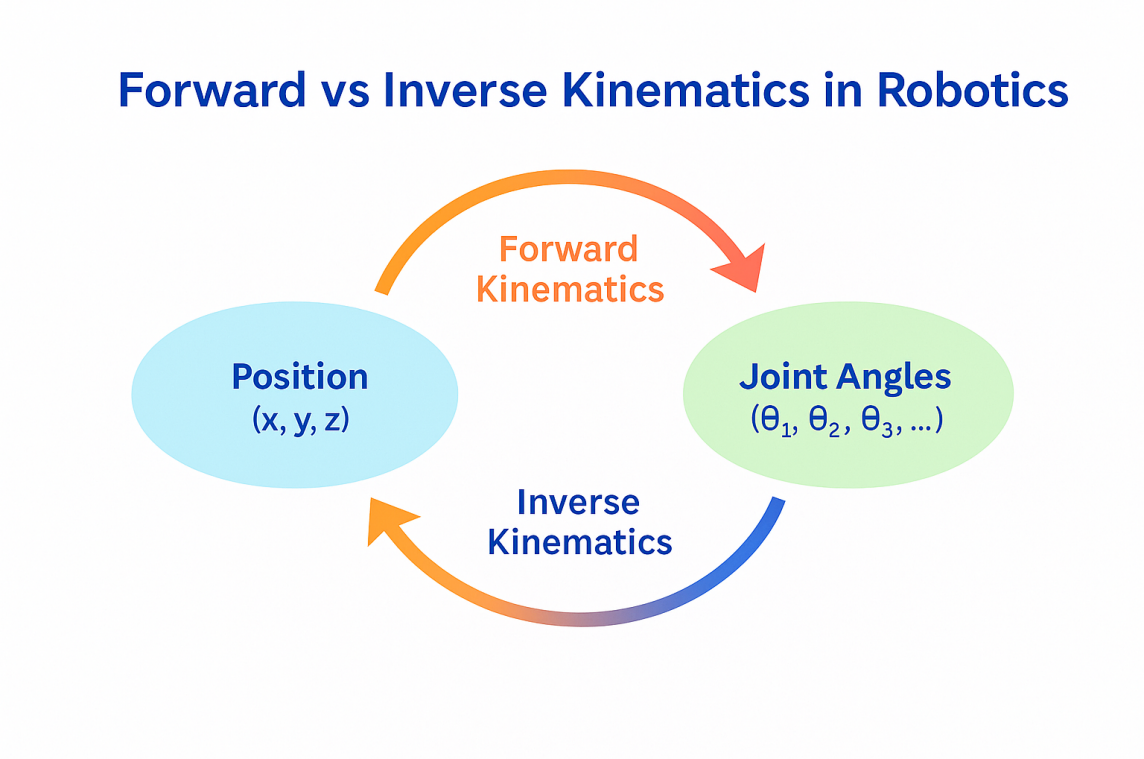

Fig. 2.10 *Forward and Inverse Kinematics in Robotics*

and orientation of its end-effector. In forward kinematics, given the joint parameters, such as angles in revolute joints or displacements in prismatic joints, the main objective is to compute the end-effector's pose (position and orientation) in 3D space. Alternatively, inverse kinematics addresses the reverse problem: determining the required joint parameters to achieve a desired end-effector pose [50].

Forward kinematics is typically straightforward, relying on the successive application of transformation matrices along the robot's kinematic chain. These transformations account for rotations and translations, often represented using homogeneous transformation matrices derived from the Denavit–Hartenberg (DH) Parameters. This method allows the representation of complex multi-joint systems by breaking them into smaller, manageable segments [51].

Inverse kinematics, on the other hand, is more computationally complex and may involve multiple or no solutions, depending on the configuration and constraints of the robotic system. Analytical solutions exist for simpler manipulators with a known structure and limited degrees of freedom, but most practical robotic systems—especially those used in minimally invasive surgery—require numerical methods or optimization-based approaches to solve the inverse kinematics problem [52].

In surgical robotics, precise inverse kinematics is vital for tasks such as tool path tracking, trajectory planning, and motion compensation. The confined and sensitive anatomical environment necessitates sub-millimetre accuracy, making robust and real-time kinematic solvers

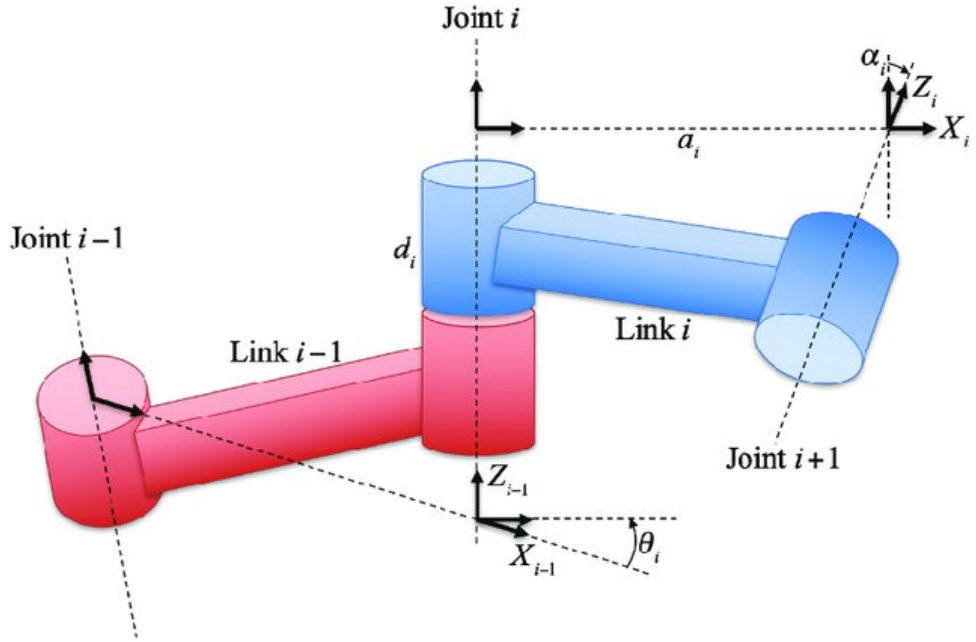

Fig. 2.11 *General Representation of DH parameters in Robotics*

a key component of system performance. Additionally, the flexibility of continuum manipulators often demands alternative formulations that approximate their geometry using constant curvature or spline-based models.

2.3.3 TRANSFORMATION MATRICES (DH PARAMETERS)

Transformation matrices are an essential mathematical tool used in robotic kinematics to describe the position and orientation of one coordinate frame relative to another. A widely adopted method for systematically representing these transformations is the Denavit–Hartenberg (DH) convention. This method introduces a standardized way of assigning coordinate frames to links and joints in a serial robotic manipulator, which simplifies the derivation of kinematic equations [53].

The DH convention involves four parameters per link: link length (a), link twist (α), link offset (d), and joint angle (θ). These parameters represent geometric relations between successive coordinate frames attached to each joint or link. By applying these parameters in sequence, one can construct homogeneous transformation matrices that encapsulate both rotation and translation. These 4×4 matrices allow efficient concatenation of multiple transformations across a kinematic chain [54].

In a serial manipulator with n joints, the overall transformation from the base frame to the end-effector is obtained by multiplying the individual transformation matrices of all the joints. This composite transformation is critical in forward kinematics, enabling the computation of the end-effector pose given a set of joint parameters.

The use of DH parameters not only aids in computational modelling but also provides clarity in the design and simulation of robotic systems. Many commercial robotics software packages, including MATLAB and ROS-based platforms, implement DH conventions for defining robot models and performing kinematic analyses [55].

However, it's important to note the limitations of the classic DH convention, particularly for more complex structures such as parallel robots or continuum robots, where alternative parameterizations like the modified DH method or product of exponentials (PoE) formulation might be more suitable.

2.3.4 SINGULARITY IN ROBOTIC SYSTEMS

In robotic kinematics, singularities are critical configurations where a manipulator loses one or more degrees of freedom, leading to instability or inability to perform certain motions. Mathematically, singularities occur when the Jacobian matrix $\mathbf{J}$, which maps joint velocities $\dot{q}$ to end-effector velocities $\dot{\mathbf{x}}$ through $\dot{\mathbf{x}} = \mathbf{J}\dot{\mathbf{q}}$, loses rank and becomes non-invertible [56]. At such points, small end-effector displacements may require disproportionately large joint motions, or joint inputs may fail to produce motion in specific Cartesian directions [57].

Singularities are generally classified into three types: boundary singularities at the edges of the workspace, structural singularities determined by manipulator geometry, and kinematic singularities that depend on the specific configuration and affect the differential relationship between joint and end-effector velocities. A classic example is a planar 3R arm, which becomes singular when its links align collinearly. In this configuration, certain Cartesian motions become unachievable regardless of joint velocities, and manipulability, often quantified using Yoshikawa's manipulability index $w = \sqrt{\det(\mathbf{J}\mathbf{J}^T)}$, drops to zero [56]. Practically, singularities can lead to excessive joint velocities, poor force transmission, and reduced precision, which is critical in applications like surgical robotics [58].

Serial Robot Singularities

For serial manipulators, singularities occur when the Jacobian matrix loses rank, expressed as

$$\det(\mathbf{J}(\mathbf{q})) = 0$$

for non-redundant manipulators, or

$$\det(\mathbf{J}(\mathbf{q})\mathbf{J}^T(\mathbf{q})) = 0$$

for redundant manipulators [57]. These configurations correspond to alignments of joint axes or workspace boundaries where the manipulator loses the ability to move in certain Cartesian directions. Consequences include reduced dexterity, the need for arbitrarily high joint velocities to achieve finite end-effector motions, and compromised force transmission. Understanding and predicting these singularities is crucial for planning safe trajectories and for the design of controllers that can handle near-singular configurations [56, 58].

Parallel Robot Singularities

Parallel manipulators exhibit more complex singularities due to their closed-loop architectures. Two Jacobians are defined: matrix $\mathbf{A}$, representing constraints, and matrix $\mathbf{B}$, representing actuation mapping. Singularities are classified as [59]:

1. **Serial singularities:** $\det(\mathbf{B}) = 0$, preventing the manipulator from generating certain end-effector velocities.
2. **Parallel singularities:** $\det(\mathbf{A}) = 0$, where the end-effector acquires uncontrollable motions even without actuator input [60, 61].

These internal singularities can occur within the workspace, not just at boundaries, and may cause abrupt or uncontrolled motions. Constraint singularities, a subset where unexpected degrees of freedom appear, further complicate control [62]. Such singularities are particularly relevant in precision-dependent domains like robotic surgery, where safety and accuracy are paramount [58].

2.4 PIECEWISE CONSTANT CURVATURE APPROXIMATION (PCCA)

The *piecewise constant curvature approximation* (PCCA) is a foundational concept in the modelling of continuum robots, which include highly flexible systems such as snake-like manipulators, soft robotic arms, and steerable catheters. Unlike rigid-link manipulators composed of discrete joints and links, continuum robots bend smoothly and continuously. This continuous deformation introduces challenges for conventional kinematic and dynamic modelling approaches. PCCA addresses these challenges by approximating the backbone of the robot as a sequence of circular arcs, each maintaining constant curvature within its segment [63].

In practice, each arc segment is parameterized by its length, radius of curvature, and bending plane angle, allowing the robot's shape to be described with relatively simple geometry. This representation makes it possible to employ standard rigid-body tools, such as homogeneous transformation matrices, to derive forward and inverse kinematics. As a result, the highly nonlinear behaviour of continuum structures can be captured efficiently through manageable analytical expressions. The effectiveness of this approach for cable-driven continuum robots

has been demonstrated through workspace analysis [64], highlighting its balance between computational efficiency and physical fidelity.

PCCA is simple enough for real-time applications such as surgical navigation and motion planning, yet sufficiently accurate to support design and control strategies in tendon-driven, concentric tube, and pneumatically actuated systems. Experimental validation in tendon-driven surgical robots confirmed that the model predicts global motion well, though deviations appear under non-ideal actuation or large deformations [65]. More recently, the approach has been extended to millimeter-scale continuum robots, where partitioning the structure into multiple arc segments allows accurate modelling of large-angle deformation [66].

Beyond its kinematic simplicity, PCCA also integrates naturally with sensor-based feedback control, particularly when paired with curvature-sensing technologies such as fiber Bragg grating sensors or magnetic trackers [67]. Its modular nature facilitates calibration, optimization, and learning-based approaches. However, PCCA is not without limitations: it neglects torsional effects, shear deformation, and spatially varying stiffness, and accuracy decreases under significant external loads or highly nonuniform bending. Despite these challenges, PCCA remains the most widely used and versatile modelling framework in continuum robotics, forming the basis for ongoing advances in design, control, and surgical deployment.

2.5 TENSEGRITY

2.5.1 TENSEGRITY STRUCTURES AND THEIR RELEVANCE IN ROBOTICS

Tensegrity structures derive from the combination of tension and integrity, forming stable, spatial networks of isolated rigid elements (struts) that do not touch but are held in place by a continuous network of tensile components (cables or tendons). This equilibrium-based structure results in a lightweight, flexible, and robust form, capable of absorbing shocks and withstanding large deformations [68].

Their application in robotics stems from unique mechanical properties such as structural compliance, passive reconfiguration, and fault tolerance. These features are invaluable in soft robotics, planetary exploration, and biomedical devices where rigid systems pose limitations. For example, NASA's Super Ball Bot project utilizes a tensegrity robot for planetary landings due to its high impact absorption and reconfigurability [69].

Tensegrity mechanisms, by nature, distribute stresses evenly and recover their shape after deformation, reducing the need for active stabilization. These properties make them ideal for navigating unpredictable environments. In medical robotics, particularly for minimally invasive procedures, their compliant nature will ensure patient safety while maneuvering through soft tissue.

Despite their advantages, control and modelling of tensegrity systems present challenges due

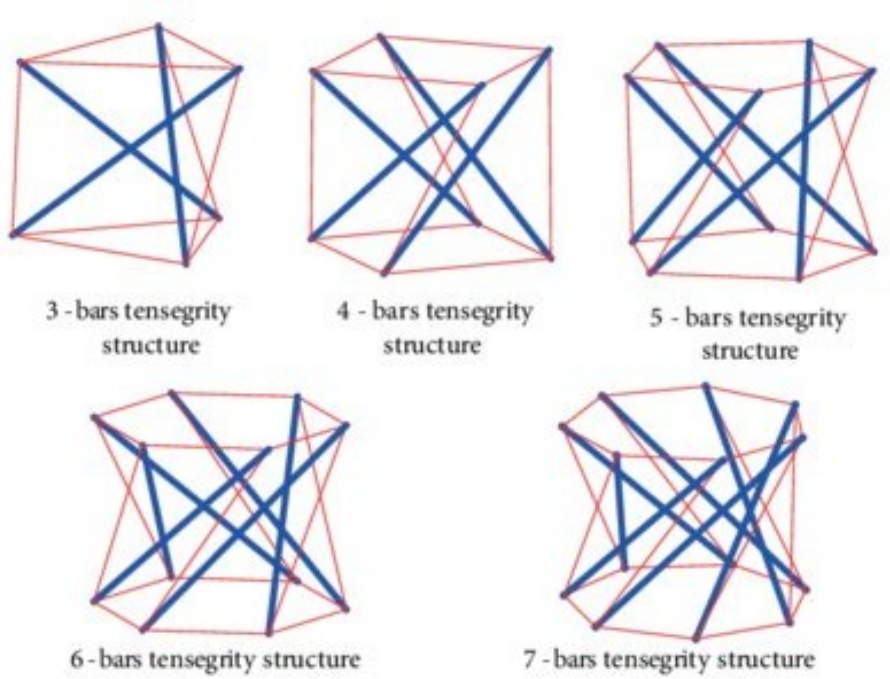

Fig. 2.12 *Tensegrity Structures*

to nonlinearities, underactuation, and dynamic coupling between geometry and internal forces. Recent advances in machine learning, inverse statics, and tensegrity-specific optimization algorithms are helping overcome these limitations, paving the way for their broader adoption in robotic applications.

2.5.2 STRUCTURAL COMPOSITION: TENSION VS COMPRESSION

At the heart of tensegrity architecture lies the distinct separation of tensile and compressive elements. Rigid struts handle compression while flexible cables maintain tension, keeping the struts suspended without direct contact. This configuration allows tensegrity structures to maintain global shape through local force equilibrium [70].

This division results in a compliant structure with significantly fewer compressive pathways, enhancing lightness and flexibility. The pre-tensioning of cables stabilizes the form and can be adjusted for fine-tuned behaviour. In robotic applications, this is advantageous as it provides mechanical robustness without the weight penalty typical of rigid structures.

The balance between tension and compression is not just structural; it is functional. It affects how the robot moves, deforms, or interacts with its environment. For example, in surgical tools designed with tensegrity-inspired architecture, controlled cable tensioning can lead to smooth and compliant tip articulation for navigating tight anatomical spaces [71].

2.5.3 KINEMATIC MODELLING CHALLENGES IN TENSEGRITY MECHANISMS

Tensegrity systems pose significant challenges in kinematic modelling due to their nonlinear, highly coupled behaviour. Unlike traditional serial or parallel manipulators, where the position of joints can be mapped directly through link transformations, tensegrity robots lack fixed joint centers and instead rely on continuously changing geometries governed by tension and compression equilibrium [72].

This means that solving for position, orientation, and deformation requires balancing internal cable forces against external loads while satisfying geometric constraints. Closed-form solutions are rare. Instead, methods such as static equilibrium modelling, force density analysis, and numerical optimization are used.

Moreover, because tensegrity robots often operate with fewer actuators than degrees of freedom (underactuated systems), their motion is dictated not just by direct input but also by passive deformation and internal force distribution. This complicates inverse kinematics, as multiple configurations can produce the same end-effector position [73].

Recent approaches employ optimization-based techniques and dynamic relaxation methods to predict shape and motion. The field is also exploring learning-based models where neural networks approximate system behaviour under varying conditions.

2.5.4 ACTUATION STRATEGIES FOR TENSEGRITY ROBOTS

Actuating a tensegrity robot involves manipulating internal cable tensions to alter its shape or move its end-effectors. This presents both mechanical and algorithmic challenges due to the nonlinear interactions between tensile forces and overall geometry [74].

Cable-driven actuation is the most common method, using motors or shape memory alloys (SMAs) to retract or release cables. Actuation can be either centralized (motors off the structure pulling via tendons) or embedded (motors located on the robot body). Centralized systems reduce weight on the moving structure but increase routing complexity [75].

SMAs and other smart materials offer compact solutions but are limited by speed and control precision. Pneumatic or hydraulic actuation, while effective in generating large forces, introduces bulk and response lag. The trade-off between compactness, controllability, and responsiveness must be considered based on the application [76].

Control strategies involve either open-loop actuation with predefined patterns or closed-loop feedback using sensors like encoders, tension gauges, or IMUs. Optimization-based control, reinforcement learning, and model predictive control are increasingly being used to manage the dynamic behaviour of tensegrity structures during locomotion or manipulation tasks [73].

2.6 FLEXIBLE ROBOTIC SYSTEMS FOR MEDICAL APPLICATIONS

2.6.1 INTRODUCTION TO FLEXIBLE ROBOTIC SYSTEMS

Flexible robotic systems, often referred to as continuum robots, represent a class of robotic mechanisms characterized by their ability to bend continuously along their length rather than relying on discrete joints. Unlike traditional rigid-link manipulators, continuum robots are capable of executing smooth, snake-like motions that allow them to reach confined and tortuous anatomical regions. Their structural compliance makes them inherently safer for interactions with delicate biological tissues, as external forces are distributed along their flexible backbone rather than being concentrated at rigid interfaces. This capability has positioned them as highly promising tools in the field of minimally invasive surgery, where constrained access and maneuverability are major limitations [77].

The fundamental principle of flexible robotic systems lies in approximating continuous curvature through either backbone bending or controlled tendon tensioning. By exploiting compliance and elasticity, these systems provide dexterity and workspace coverage in environments inaccessible to conventional endoscopes or laparoscopic tools. Applications range from endoluminal procedures and neurosurgery to transoral and cardiac catheterization interventions. Additionally, their modularity allows them to be miniaturized to sub-centimeter diameters, a requirement for navigation within small anatomical lumens.

The introduction of flexible robotic systems into the clinical domain has been motivated by the demand for greater surgical precision, reduced invasiveness, and improved patient outcomes. By mimicking the natural motions of biological structures such as the human finger or octopus arm, continuum robots provide surgeons with intuitive and versatile instruments that extend the possibilities of operative interventions in anatomically challenging regions [78].

2.6.2 TYPES OF ACTUATION IN FLEXIBLE/CONTINUUM ROBOTS

Actuation plays a central role in determining the performance, dexterity, and clinical viability of continuum robots. Several actuation modalities have been explored: tendon-driven actuation, concentric tube mechanisms, fluidic or pneumatic actuation, and shape-memory alloys.

Tendon-driven actuation is the most widely adopted approach. In this configuration, cables or tendons are routed along the flexible backbone and anchored at the distal end. By adjusting tendon tension, bending moments are induced, resulting in controlled tip deflection. Tendon-driven systems offer high force transmission, compact actuator placement outside the patient, and scalable designs. Challenges include tendon friction, hysteresis, and slack compensation, but advances in modelling and calibration have mitigated many of these issues [79].

Concentric tube robots consist of multiple pre-curved superelastic tubes nested together. By rotating and translating individual tubes, complex three-dimensional shapes can be achieved. These robots provide high precision and stiffness at small diameters, making them suitable for delicate procedures such as intracranial interventions. However, they are limited by reduced curvature range, low payload capacity, and challenges in miniaturization [80].

Fluidic or pneumatic actuation relies on the inflation of chambers or bellows to achieve deformation. Such designs, often categorized as soft robots, provide excellent compliance and safety but typically suffer from low output force, bulky external pumps, and reduced accuracy, restricting their widespread surgical use. Shape-memory alloys and electroactive polymers offer compact actuation without external tendons or transmission components. Despite this advantage, slow response times, hysteresis, and heat generation have limited their practicality in clinical scenarios. Overall, while several actuation strategies exist, tendon-driven continuum robots currently provide the best balance between dexterity, force output, miniaturization, and integration into surgical workflows [79].

2.6.3 WHY TENDON/CABLE ACTUATION IS SUITED FOR MEDICAL SURGERY

Tendon-driven actuation has emerged as the most clinically feasible strategy for continuum robots in surgery due to its inherent scalability and remote actuation capability [65]. By placing motors and actuators outside the patient's body, tendons transmit motion along highly flexible shafts of sub-centimeter diameters, a critical feature for minimally invasive access. This architecture reduces the size and rigidity of the in-body portion of the robot, enabling navigation through narrow lumens and confined anatomical spaces.

From a control perspective, tendon-driven systems provide surgeons with direct, high-bandwidth manipulation of distal tips, essential for precise dissection, suturing, and stapling tasks [77]. The mechanical advantage of tendons allows for high force transmission relative to the robot's diameter, which is vital for tissue manipulation. Moreover, the adaptability of tendon routing enables multi-segment designs with independent bending directions, replicating natural biological flexibility.

Although tendon friction, hysteresis, and slack pose challenges, advancements in tension-propagation modelling, calibration algorithms, and closed-loop force sensing have addressed these limitations. Consequently, tendon-driven continuum robots represent the optimal compromise between dexterity, miniaturization, and clinical usability, making them the preferred actuation paradigm in surgical applications [81].

2.6.4 GLOBAL RESEARCH AND DEVELOPMENTS IN TENDON-DRIVEN CONTINUUM ROBOTS

Recent years have seen significant progress in the design, modelling, and clinical translation of tendon-driven continuum robots. Foundational work provided mechanics-based models that describe the relationship between tendon displacement and backbone curvature, accounting for compression and routing effects. These models remain essential for precise control and kinematic inversion in surgical contexts.

Building upon this foundation, advanced designs have been created for applications such as neurosurgery and endoluminal procedures. Multi-segment tendon-driven neuroendoscopes have been developed with dual-segment flexibility, incorporating models that account for tendon friction and hysteresis to improve steering accuracy and repeatability. Other designs focus on transoral and endoluminal access, using extensible tendon-driven segments capable of "follow-the-leader" insertion along tortuous anatomical paths [82]. Such features are essential for safe and effective navigation in confined regions. Innovations in mechanical design have extended the degrees of freedom available in tendon-driven segments. Compact, fully actuated modules with helical tendon routing and backbone rotation have been shown to provide enhanced control in multiple directions, improving deployment in constrained surgical workspaces. These designs enable precise follow-the-leader performance and orientation control, which are critical for surgical procedures requiring complex navigation and targeted intervention [79].

Calibration and compensation have also become central research directions. Data-driven methods that combine machine learning with linear regression have been employed to correct tendon slack, elasticity, and nonlinearities, achieving sub-degree accuracy in surgical platforms [83]. Such approaches significantly improve the reliability of cable-driven systems during long operations, where mechanical properties can vary over time. Dynamic modelling has advanced beyond quasi-static approximations, enabling control strategies that account for cable tension propagation and external loading. Optimization-based controllers minimize tendon forces while maintaining accuracy, ensuring safe and stable operation during complex tasks such as tissue manipulation or suturing [84].

Applications are steadily moving from laboratory prototypes toward clinical integration. Platforms designed for minimally invasive surgery have demonstrated the ability to cover complex workspaces and perform dexterous maneuvers within anatomical constraints [85]. Quasi-static models tailored for transoral surgical units further extend the theoretical basis required for safe deployment in delicate regions such as the pharynx or larynx. Together, these developments are steadily transforming tendon-driven continuum robots from experimental concepts into practical surgical instruments. Their ability to combine dexterity, safety, and miniaturization positions them as a cornerstone technology for the future of minimally invasive and image-guided

surgery.

2.7 SURGICAL STAPLERS

2.7.1 EARLY DEVELOPMENTS (1900S–1930S)

The concept of mechanical tissue approximation emerged in the early twentieth century as an alternative to hand-sewn sutures, which were often associated with leakage and infection in gastrointestinal procedures. In 1907, the French surgeon Jeannel argued that the presence of metallic foreign bodies in tissues posed minimal risk, opening the way for staple-based closure techniques.

In 1908, Hungarian surgeon Hümer Hültl [86], in collaboration with engineer Victor Fischer, introduced the first surgical stapler. The device applied two staggered rows of U-shaped steel staples, which were intentionally left in a "B" configuration to maintain tissue perfusion. Although innovative, the instrument was bulky, weighing more than 3 kilograms, required significant manual effort, and needed nearly two hours for reloading. Nevertheless, it was successfully used in gastric cancer surgery and gradually gained clinical interest.

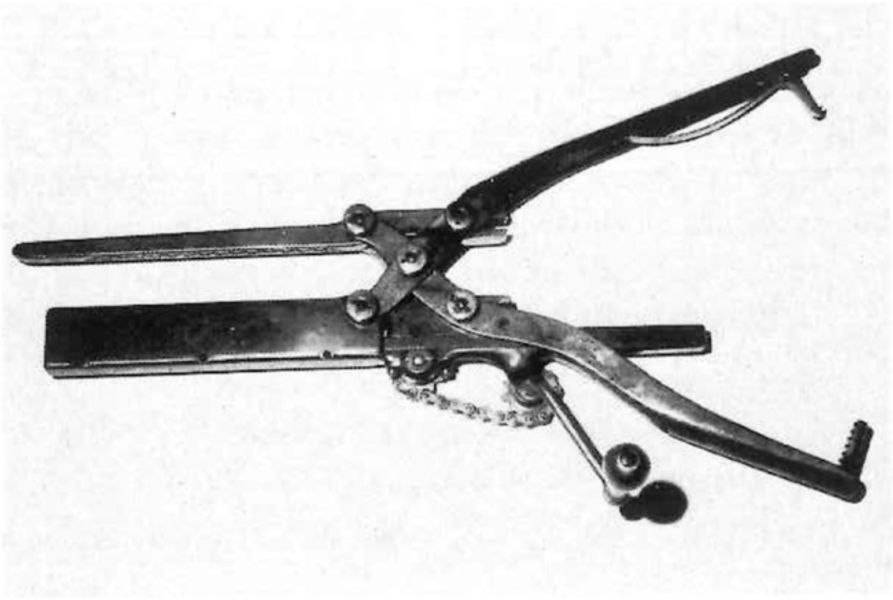

Fig. 2.13 *First model of the Fischer-Hültl stapler*

In 1920, Aladár Petz designed a lighter and more practical stapler weighing just over 1 kilogram and consisting of fewer components. Produced under the trade name *Aesculap* in Germany, Petz's device became popular in Hungary and Germany, maintaining dominance for several decades. Further refinements followed in the 1930s, including angled staple placement for better vascularity, graded compression for tissue-specific applications, and preloaded, interchangeable cartridges introduced by Friedrich in Germany. These modifications marked the transition of staplers into more practical surgical tools.

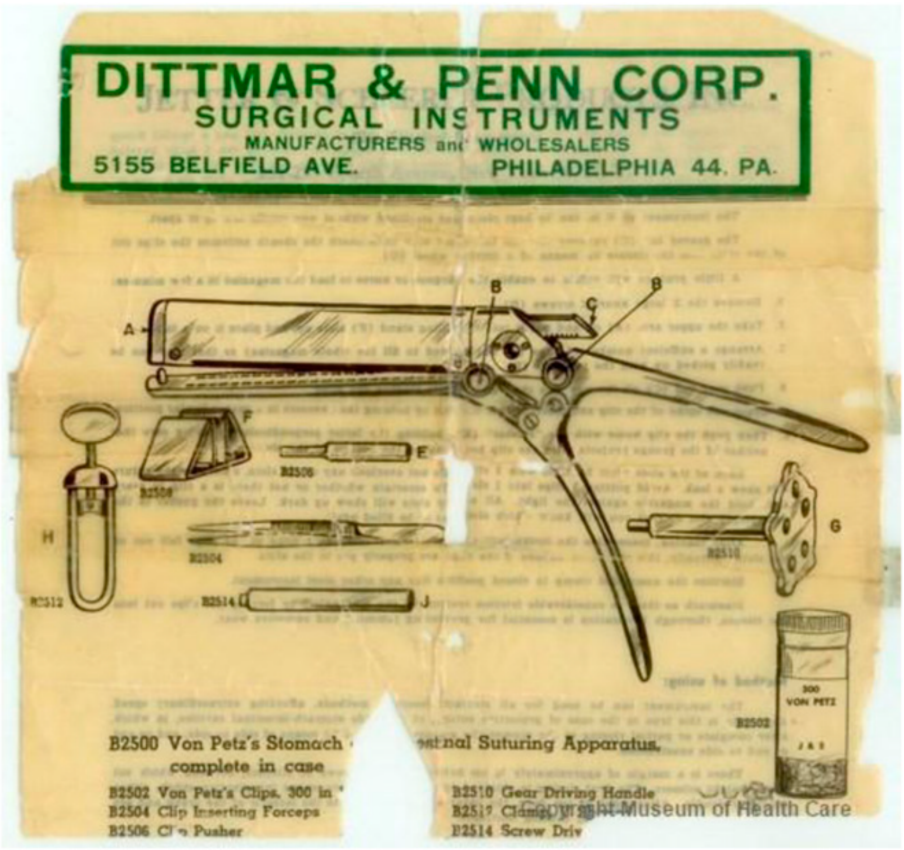

Fig. 2.14 *The Petz Clamp*

2.7.2 ADVANCES IN MATERIALS AND STAPLING SYSTEMS (1930S–1950S)

Material science significantly influenced the evolution of stapling devices. Early staples, commonly made of silver, were soft and provided inconsistent closure. Subsequent experimentation with copper, nickel, and zinc alloys improved strength, while tantalum was introduced in the 1940s for its bioinertness and corrosion resistance [4]. Later, cobalt alloys and titanium became standard for internal use, while stainless steel was widely adopted for skin closure.

The limitations of conventional suturing, particularly evident during World War II with high rates of hemorrhage and vascular trauma, underscored the need for efficient and reliable alternatives. This drove research toward specialized staplers for vascular and thoracic applications [87].

2.7.3 VASCULAR STAPLERS AND SOVIET CONTRIBUTIONS (1940S–1960S)

The Soviet Union was a pioneer in vascular stapling. In 1945, engineer Vasiliy Gudov developed the first vascular stapler designed for rapid vessel anastomosis. By the early 1950s, models such as SSA-1, SL-6, and SL-10 were introduced, though their complexity limited widespread adoption. Surgeons like Vladimir Demikhov and Pavel Androsov applied these instruments in

transplantation and vascular trauma surgeries, respectively [88].

Soviet engineers also developed staplers for bronchial, gastrointestinal, and pulmonary applications, creating more than 600 prototypes by the 1960s. Only a small proportion entered clinical practice, yet these innovations laid the groundwork for specialized stapling systems. Despite these advances, Soviet devices were eventually surpassed by Western designs that emphasized disposability, ergonomics, and commercial scalability.

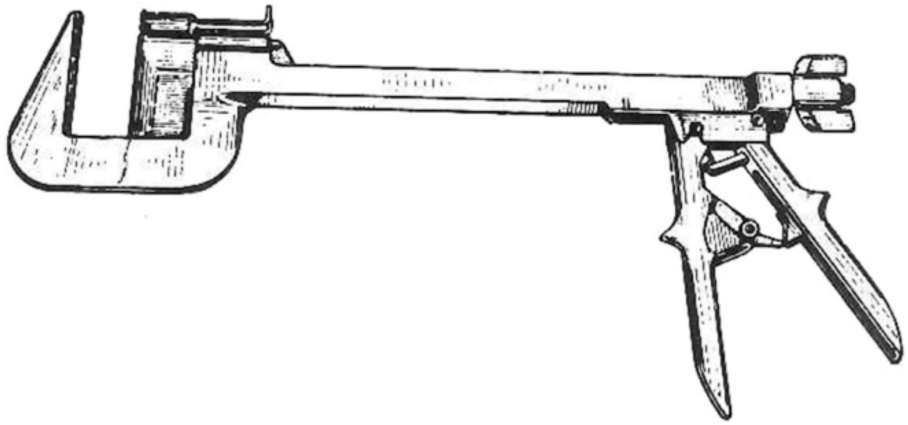

Fig. 2.15 *Soviet UKL-60 stapler*

2.7.4 COMMERCIALIZATION AND GLOBAL ADOPTION (1960S–1980S)

The modern era of stapling began in the United States. In 1964, surgeon Mark Ravitch collaborated with entrepreneur Leon Hirsch to establish the United States Surgical Corporation (USSC). Along with Felicien Steichen, they reverse-engineered Soviet staplers and introduced key improvements, including stainless steel construction, disposable cartridges, and standardized staple sizes coded by color [89].

Under the *Auto Suture* brand, USSC introduced widely adopted instruments such as:

- **TA (Thoracoabdominal) stapler:** for tissue approximation.
- **GIA (Gastrointestinal Anastomosis) stapler:** enabling simultaneous cutting and stapling.
- **EEA (End-to-End Anastomosis) stapler:** designed for circular anastomosis in colorectal and esophageal surgery.

An aggressive training strategy, where company representatives assisted surgeons directly in operating rooms, accelerated adoption. By the 1970s, staplers became standard surgical tools worldwide. Competitors such as Ethicon (Johnson and Johnson) entered the market in 1977, and USSC later merged into Tyco Healthcare, eventually becoming part of Covidien in 2007.



Fig. 2.16 *Commercial Surgical Stapler: (a) GIA Stapler, (b) TA Stapler, and (c) EEA Stapler.*

2.7.5 MODERN INNOVATIONS AND FUTURE TRENDS (1990S–PRESENT)

With the growth of minimally invasive surgery, stapler designs evolved toward endoscopic and robotic applications. Devices such as the *Endo GIA* [90, 91] allowed intracorporeal stapling through trocars, expanding stapler use in laparoscopic surgery. Modern staplers include ergonomic handles, powered firing mechanisms, integrated cutting blades, and three-dimensional staple formation, all aimed at reducing ischemia and improving closure reliability [92].

The integration of robotic staplers into robotic surgical systems represents the latest advancement, offering greater precision and surgeon control [93]. At the same time, disposable cartridges and plastic components have raised environmental and economic concerns. Reusable metal staplers may regain relevance unless future tissue fusion technologies replace mechanical stapling altogether.

2.7.6 CLASSIFICATION OF SURGICAL STAPLERS

Modern surgical staplers are available in a wide range of designs that differ according to their application, mechanism, and anatomical target. Their classification is generally based on geometry, mode of operation, and surgical specialty. The most commonly recognized categories include:

- **Thoracoabdominal (TA) staplers:** Primarily used in thoracic and abdominal surgery, these instruments are designed for linear tissue approximation without cutting. They apply parallel rows of staples, making them suitable for closing visceral stumps (such

as bronchi or stomach) and for reinforcing sutures in large, thick tissue structures. TA staplers are often employed in open procedures where secure closure is required across substantial tissue planes.

- **Gastrointestinal Anastomosis (GIA) staplers:** These staplers combine cutting and stapling in a single action, enabling surgeons to transect and join hollow organs efficiently. A GIA stapler places two or more staggered rows of staples on either side of a central cutting blade, producing a hemostatic closure while simultaneously dividing the tissue. They are commonly applied in bowel resections, gastric bypass procedures, and other gastrointestinal surgeries where both resection and anastomosis are required.

- **Endo GIA staplers:** Specifically developed for minimally invasive surgery, Endo GIA staplers are designed to pass through trocars during laparoscopic or thoracoscopic procedures. They offer rotatable and articulating tips to access confined spaces and fire multiple rows of staples with integrated cutting capability. These instruments are indispensable in advanced laparoscopic interventions such as colectomies, lung resections, and bariatric surgery, where precise control in restricted anatomy is critical.

- **End-to-End Anastomosis (EEA) staplers:** Also known as circular staplers, EEA devices are used to create end-to-end or end-to-side connections between hollow organs. The instrument delivers one or more concentric rings of staples while simultaneously excising a central tissue disc, thereby establishing a patent lumen. EEA staplers are particularly important in colorectal surgery for low pelvic anastomoses and in esophageal reconstruction, where hand-sewn sutures are technically challenging.

- **Dermal staplers:** Designed for external use, dermal staplers are lightweight, disposable devices used to approximate skin edges rapidly and with minimal tissue trauma. They are especially valuable in emergency care and trauma surgery, where speed is essential. Compared with sutures, skin staples reduce operative time, lower the risk of needlestick injury, and often yield favorable cosmetic outcomes with reduced scarring.

In addition to these categories, staplers may also be distinguished by their actuation method (manual, powered, or robotic), their staple line configuration (linear, circular, or curved), and their intended reusability (disposable versus reusable). This wide variety of designs highlights the adaptability of stapling technology across multiple surgical domains.

2.8 SUMMARY OF THE CHAPTER

The literature review outlines the development of minimally invasive surgery (MIS), beginning with its history and the shift from open surgery to less invasive methods. It compares MIS with traditional approaches in terms of patient outcomes and recovery, presents the main types of MIS, and highlights the tools that have supported its growth.



Fig. 2.17 *Endoscopic Surgical Staplers*

The discussion then moves to surgical robotics, tracing its history, surveying current robotic platforms, and weighing their advantages and drawbacks. While robotics has brought improvements in precision, dexterity, and ergonomics, challenges such as cost, bulk, and rigidity continue to limit their application.

To build the theoretical foundation, the review introduces key principles of kinematic modelling, including degrees of freedom, forward and inverse kinematics, Denavit–Hartenberg parameters, and singularities. Since rigid-link approaches are not sufficient for continuum and tendon-driven robots, the Piecewise Constant Curvature Approximation (PCCA) is presented as a suitable modelling method. Tensegrity-inspired mechanisms are also highlighted for their ability to improve structural stability, distribute forces efficiently, and enable lightweight actuation.

Flexible robotic systems designed for medical applications are then examined, with emphasis on their ability to navigate confined anatomical regions. Within this context, surgical staplers are reviewed, from early designs to modern devices. Current staplers remain restricted by their size and rigidity, underscoring the need for flexible, tendon-driven alternatives.

Taken together, the literature highlights the growing demand for robotic staplers that combine flexibility, adaptability, and precise control. These ideas carry forward into the following chapters, where the focus turns to understanding the stapler's workspace in the pelvic region,

Table 2.4 *Classification of surgical staplers according to geometry, function, and clinical application.*

Stapler Type	Configuration/Function	Typical Clinical Applications
Thoracoabdominal (TA)	Linear stapler without cutting blade	Closure of visceral stumps (bronchus, stomach, bowel); reinforcement of thick tissue in thoracic and abdominal surgery
Gastrointestinal Anastomosis (GIA)	Linear stapler with integrated cutting blade	Bowel resections, gastric bypass, intestinal anastomoses; enables simultaneous division and closure
Endo GIA	Linear stapler, rotatable and articulating, passes through laparoscopic trocar	Minimally invasive procedures such as colectomy, lung resection, bariatric surgery; stapling in confined spaces
End-to-End Anastomosis (EEA)	Circular stapler with central cutting punch	Low anterior resection in colorectal surgery, esophageal reconstruction, end-to-side or end-to-end anastomoses of hollow organs
Dermal Stapler	Small, lightweight device for external use	Rapid skin closure in trauma, emergency surgery, and general wound management; reduced operative time and favorable cosmetic outcomes

analysis of design parameters for reliable use, and developing the mechanical design of a flexible endoscopic stapler. Through kinematic analysis, CAD modelling, and prototyping, these chapters extend the insights from the literature into concrete steps toward building a functional flexible endoscopic surgical stapler.

3

Analysis of Surgical Workspace for Laparoscopic Rectal Procedures

The workspace analysis for laparoscopic rectal surgery constitutes a pivotal component of surgical planning, as it provides a detailed understanding of the spatial constraints and maneuverability within the pelvic region. Effective workspace evaluation facilitates the optimization of instrument trajectories, minimizes potential conflicts with anatomical structures, and enhances the overall safety and efficiency of the procedure.

This section presents a systematic approach to workspace analysis, encompassing the acquisition of anatomical and procedural data, subsequent processing, and optimization of the surgical workspace. Data acquisition involves capturing high-fidelity imaging of the pelvic anatomy using modalities such as computed tomography (CT) or magnetic resonance imaging (MRI), which allows for the accurate reconstruction of three-dimensional models of relevant organs and tissues. Following acquisition, the data are processed to delineate boundaries, identify critical anatomical landmarks, and quantify the available operational volume for laparoscopic instruments.

Subsequently, optimization techniques are applied to evaluate different surgical approaches, including the assessment of instrument reachability, collision avoidance, and angular constraints within the confined pelvic cavity. The combination of precise modeling and computational analysis provides surgeons and robotic systems with valuable insights into feasible instrument paths, thereby supporting preoperative planning and intraoperative decision-making. Overall, a thorough workspace analysis not only enhances procedural efficiency but also contributes to improved patient safety and surgical outcomes.

3.1 DATA ACQUISITION

The data acquisition phase constitutes the foundational step in workspace analysis, involving the collection of high-resolution medical imaging data of the pelvic region. Accurate and detailed imaging is essential to capture the complex anatomical structures, which directly influence the reliability of subsequent modeling, simulation, and optimization processes.

In laparoscopic rectal surgery, T2-weighted magnetic resonance imaging (MRI) scans are the preferred modality due to their superior soft-tissue contrast, enabling clear delineation of pelvic organs, mesorectal fascia, and surrounding vascular and neural structures. Imaging protocols are designed to minimize motion artifacts while maximizing spatial resolution, often incorporating multiple planes (axial, sagittal, and coronal) to facilitate comprehensive three-dimensional reconstruction.

Additionally, patient-specific anatomical variations are accounted for by acquiring images under standardized positioning and preparation conditions. The resulting imaging data serve as the basis for constructing accurate three-dimensional pelvic models, which are subsequently used for instrument trajectory planning, collision analysis, and workspace optimization. Incorporating high-quality data at this stage ensures that the downstream computational analyses reflect realistic surgical constraints, thereby enhancing the precision and safety of laparoscopic procedures.

3.1.1 IMAGING PROTOCOL

MRI scanners are configured to acquire T2-weighted sequences, which provide enhanced soft-tissue contrast and enable the clear differentiation of critical anatomical structures within the pelvic region. This imaging modality is particularly effective for visualizing the rectum, mesorectal fascia, surrounding musculature, and adjacent organs, which are essential for accurate workspace modeling in laparoscopic rectal surgery.

Key imaging parameters, including echo time (TE) and repetition time (TR), are carefully optimized to achieve a balance between high spatial resolution and reasonable acquisition time. Slice thickness, field of view (FOV), and in-plane resolution are adjusted to minimize partial volume effects and motion artifacts, thereby ensuring the anatomical fidelity of the reconstructed data.

Furthermore, multi-planar acquisitions, typically in the axial, sagittal, and coronal planes, are employed to capture the three-dimensional morphology of the pelvis comprehensively. Patient positioning and immobilization techniques are standardized to reduce variability and improve reproducibility across different scans. Collectively, these protocol considerations ensure that the acquired images provide a robust and precise foundation for subsequent data processing,

three-dimensional reconstruction, and surgical workspace analysis.

3.1.2 IMAGE CAPTURE

Sequential slices of the pelvic region are acquired using the MRI scanner, typically with a slice thickness of 3–5 mm to ensure complete coverage of the anatomical structures relevant to laparoscopic rectal surgery. The imaging protocol is designed to capture the entire pelvis, including the rectum, mesorectal fascia, pelvic floor musculature, and adjacent organs, while maintaining high spatial resolution.

Each slice is stored in a standardized digital format, such as DICOM, which preserves critical metadata including acquisition parameters, orientation, and spatial calibration. These high-resolution images provide a detailed representation of the patient-specific pelvic anatomy, forming the foundation for subsequent preprocessing, segmentation, and three-dimensional reconstruction.

To enhance image quality, measures such as respiratory gating, patient immobilization, and motion artifact reduction techniques are employed. Collectively, the careful capture of sequential slices ensures that the resulting dataset is both comprehensive and precise, enabling accurate modeling of the surgical workspace and supporting reliable planning of instrument trajectories and access strategies.

3.2 DATA PROCESSING

The data processing phase involves several steps to transform raw MRI data into a format suitable for detailed analysis and modeling. This stage is critical to ensure that the imaging data accurately represents the patient-specific anatomy and provides a reliable basis for workspace analysis.

3.2.1 MRI DATA QUALITY CHECK

The acquired MRI data undergoes a comprehensive quality check to identify and correct any deformities, errors, or artifacts that may have been introduced during the imaging process. Common issues include motion artifacts, signal loss, intensity inhomogeneities, and geometric distortions.

Motion artifacts, caused by patient movement or physiological activity such as respiration, are corrected using image registration and alignment techniques. Signal loss and intensity inconsistencies are addressed through normalization and filtering procedures, while geometric distortions are minimized by calibrating the imaging data according to known anatomical references.

Performing a rigorous quality check ensures that subsequent preprocessing, segmentation, and three-dimensional reconstruction steps are based on accurate and artifact-free data. This is essential for generating reliable models of the pelvic workspace, which directly impact the precision of instrument trajectory planning and surgical decision-making.

3.2.2 SEGMENTATION

Segmentation is a critical step in workspace analysis, involving the identification and delineation of different tissue types within each MRI slice (Fig. 3.1). Accurate segmentation is essential for defining anatomical boundaries, distinguishing between critical structures, and establishing the limits of the available surgical workspace.

In laparoscopic rectal surgery, the pelvic region is typically segmented into six zones: pelvic bone, ligaments, vascular tissues, genitals and urinary tract, rectum, and probable/available workspace [94]. Each zone is segmented based on tissue characteristics, intensity contrasts, and anatomical landmarks identifiable in T2-weighted MRI images.

Segmentation can be performed using a combination of semi-automated and manual approaches. Semi-automated techniques, such as thresholding, region growing, and edge detection algorithms, accelerate the process while preserving anatomical accuracy. Manual refinement by experienced clinicians ensures that subtle structures and critical boundaries are accurately captured, especially in regions with complex overlapping tissues or low contrast.

The resulting segmented data serves as the foundation for subsequent three-dimensional reconstruction and workspace modeling. Accurate segmentation directly influences the precision of instrument path planning, collision avoidance, and evaluation of reachable workspace volumes, which are essential for both preoperative planning and the optimization of minimally invasive surgical strategies.

3.2.3 ZONE IDENTIFICATION

Each MRI slice is segmented into the previously described zones based on both anatomical and functional significance, as illustrated in Fig. 3.2. This classification provides a comprehensive and structured representation of the pelvic anatomy, which is essential for subsequent computational modeling, workspace analysis, and surgical planning. Accurate identification of zones enables the differentiation of critical structures such as the rectum, vascular tissues, and pelvic bones, thereby facilitating precise evaluation of instrument reachability and avoidance of sensitive areas during laparoscopic procedures.

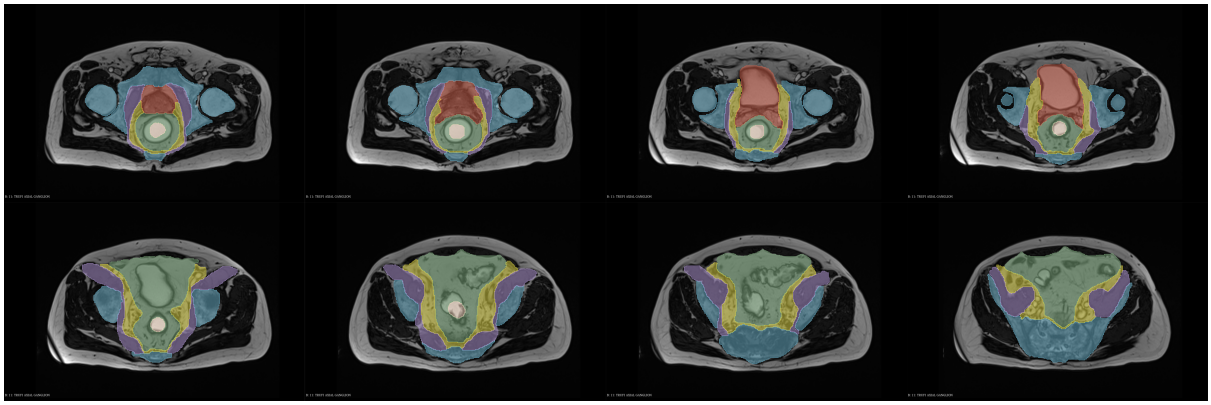

Fig. 3.1 *Segmentation of MRI slices*

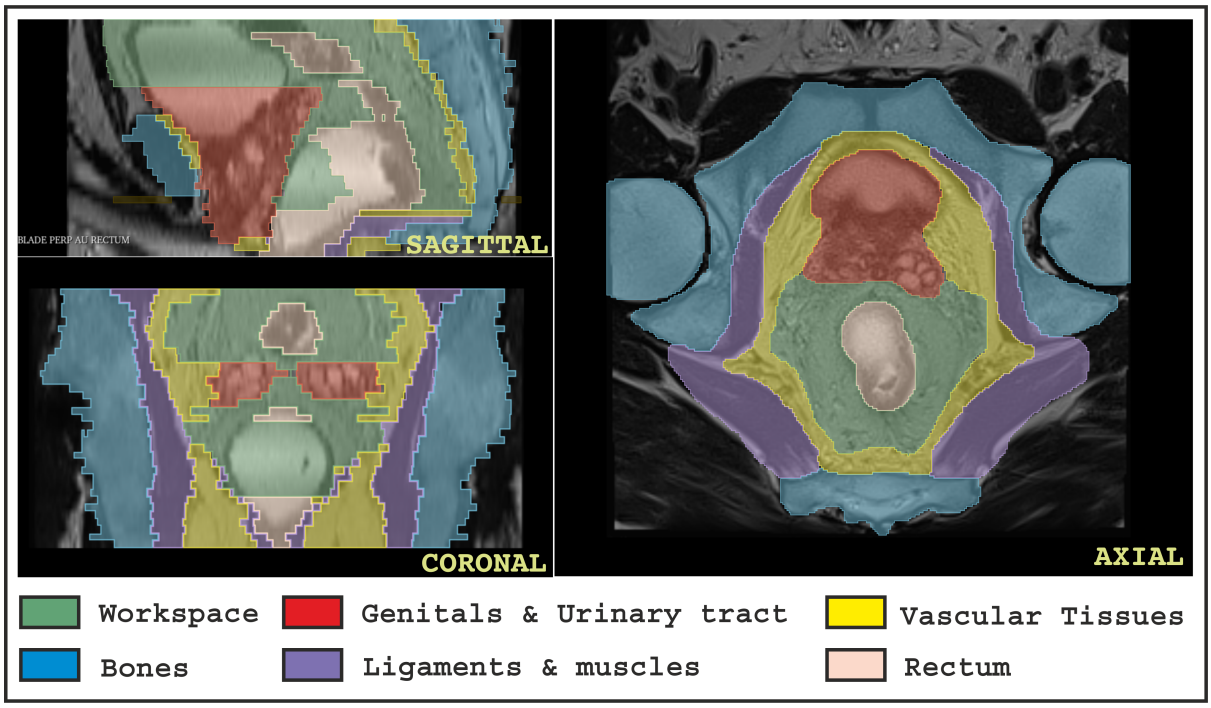

Fig. 3.2 *Zone identification after segmentation of the pelvic region*

3D Slicer Software Advanced segmentation tools, such as the open-source 3D Slicer software, are employed to achieve precise delineation of segmented zones within each MRI slice. The software provides a user-friendly interface combined with powerful algorithms for thresholding, region growing, and manual refinement, enabling accurate segmentation even in anatomically complex regions. Additionally, 3D Slicer facilitates volumetric rendering and export of segmented structures into formats suitable for three-dimensional reconstruction, computational analysis, and surgical simulation. The integration of such software ensures reproducibility, efficiency, and high fidelity of the segmented data, which forms the basis for subsequent workspace modeling and preoperative planning.

3.2.4 3D RECONSTRUCTION

Following segmentation, a three-dimensional (3D) reconstruction of the pelvic region is generated by integrating the segmented data from each MRI slice (Fig. 3.3). This comprehensive 3D model provides a spatially accurate and detailed representation of the pelvic anatomy, enabling quantitative analysis, visualization, and surgical planning.

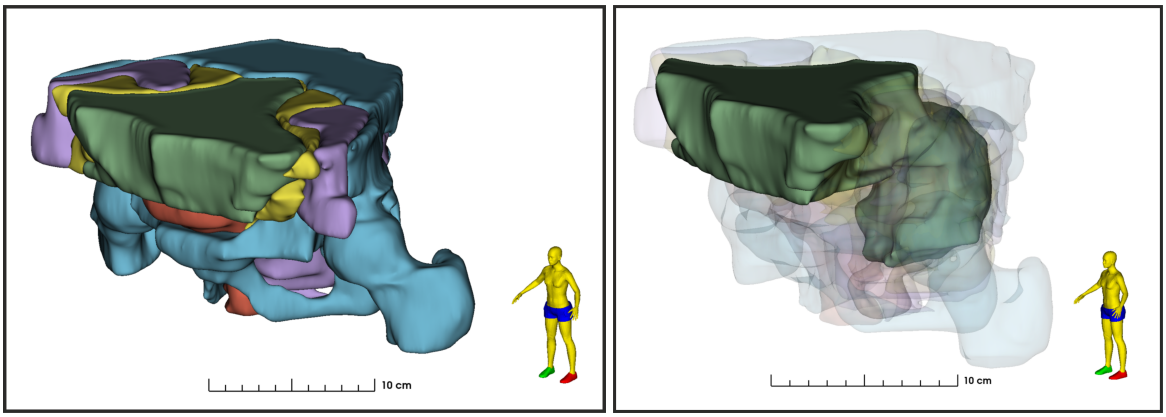

Fig. 3.3 *Three-dimensional representation of the pelvic workspace*

Integration of Segmented Data The segmented data from individual MRI slices are carefully aligned and integrated to create a coherent 3D reconstruction of the pelvic region. This process involves spatial registration, correction of slice misalignments, and interpolation between adjacent slices to ensure anatomical continuity. The resulting 3D model accurately captures the geometric relationships among pelvic bones, ligaments, vascular structures, and soft tissues, providing a robust framework for subsequent workspace analysis.

Exporting 3D Data The reconstructed 3D models are exported in standard formats such as `.stl`, which is widely used for representing surface geometry of anatomical structures. Exporting in `.stl` format ensures compatibility with computational modeling software, surgical simulation platforms, and robotic planning tools. This enables further processing, including virtual instrument trajectory planning, collision analysis, and workspace optimization, ultimately supporting enhanced preoperative planning and safer laparoscopic interventions.

3.2.5 VOLUME ANALYSIS

The exported `.stl` files from the 3D reconstruction are imported into SOLIDWORKS CAD software for volumetric analysis. SolidWorks enables precise computation of the volume of each segmented anatomical zone, providing critical quantitative insights into the spatial distribution of tissues within the pelvic cavity.

Volumetric analysis is essential for understanding the relative sizes and proportions of various structures, such as the rectum, vascular tissues, ligaments, and pelvic bones. These measurements facilitate informed decisions regarding instrument design, surgical approach, and workspace optimization. Moreover, knowledge of volumetric constraints is crucial for planning minimally invasive procedures, where spatial limitations can significantly influence instrument maneuverability and access strategies.

3.2.6 POSITIONAL ANALYSIS

In addition to volume, the positional relationships of each segmented zone are analyzed both individually and relative to one another. This analysis provides a detailed understanding of the anatomical layout, including the proximity, orientation, and potential interactions of critical structures. Positional data are essential for assessing feasible instrument trajectories, identifying areas at risk of collision, and optimizing surgical access pathways.

Figures 3.4 and 3.5 illustrate the visualization of the proposed flexible surgical stapler, featuring bendable jaws and movable wrists, alongside conventional rigid endoscopic staplers operating within the identified workspace. According to feedback from experienced surgeons, the stapler orientation depicted in Fig. 3.5(c) is most commonly employed during procedures, as it minimizes interference from the rectum while allowing precise positioning and orientation of the surgical instrument. This insight informs both the ergonomic design of novel surgical tools and the planning of laparoscopic interventions.

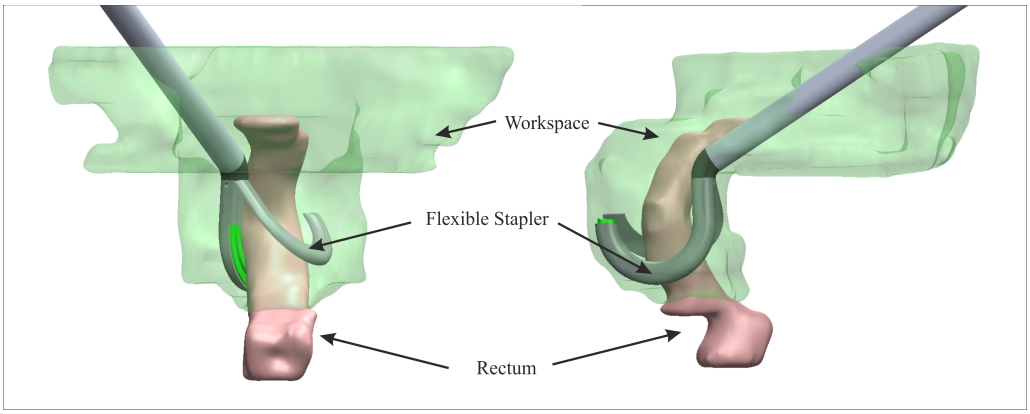

Fig. 3.4 *Flexible Surgical stapler inside the workspace*

3.3 WORKSPACE OPTIMISATION IN MATLAB

Further quantitative analysis of the pelvic workspace is performed using MATLAB to facilitate numerical modeling, optimization, and visualization.

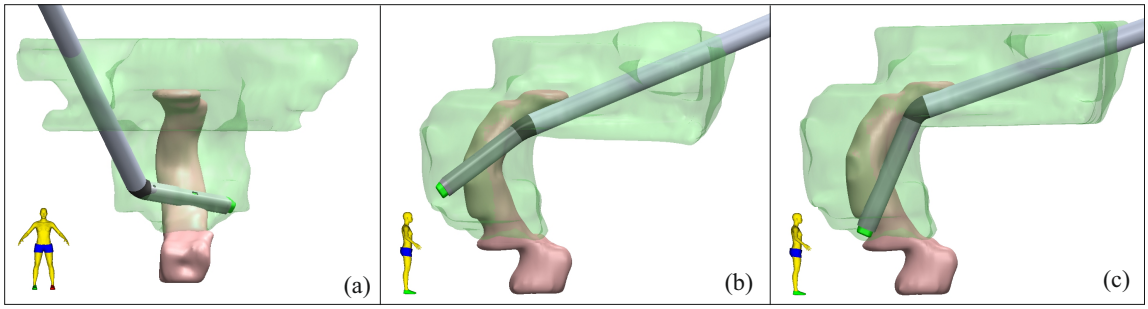

Fig. 3.5 *Orientation of conventional tools inside the workspace*

3.3.1 G-CODE GENERATION

The `.stl` files of the reconstructed workspace model are imported into MATLAB to generate G-code representing the entire 3D structure. The G-code specifies the slice thickness and provides a detailed representation of the contour for each slice (Fig. 3.6). By converting the 3D model into this format, the workspace is transformed into a discretized representation suitable for computational analysis, enabling precise evaluation of instrument reachability, collision detection, and optimization of trajectories.

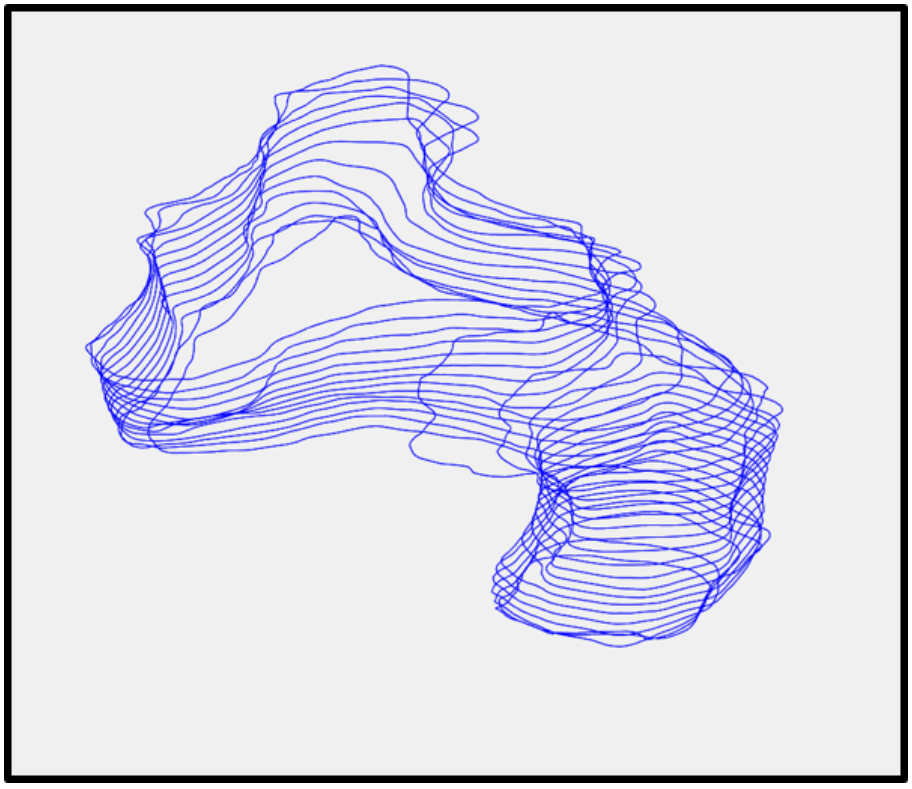

Fig. 3.6 *Contour generation of the pelvic workspace at each slice using G-code*

3.3.2 COORDINATE EXTRACTION

Once the contours are generated, the coordinates of each slice are extracted and organized in a clockwise pattern to maintain continuity of the curve. This structured dataset represents the 3D boundary of the anatomical structures at each slice. Accurate coordinate extraction is essential for defining the geometry of the workspace, as it enables precise reconstruction of surfaces, computation of reachable areas, and modeling of potential instrument paths.

3.3.3 BINARY MASKING

Binary masking is performed on each slice to differentiate the interior and exterior of the workspace contour. Pixels located inside the contour are assigned a value of 1, while those outside are assigned a value of 0, as shown in Fig. 3.7. This process provides an unambiguous definition of the available workspace within the pelvic cavity and serves as the foundation for numerical analysis and optimization algorithms. Mathematically, the binary mask can be represented as:

$$M(x,y) = \begin{cases} 1 & \text{if pixel } (x,y) \text{ is inside the contour,} \\ 0 & \text{if pixel } (x,y) \text{ is outside the contour.} \end{cases} \tag{3.1}$$

Binary masking is particularly useful for evaluating the reachable workspace of laparoscopic instruments, collision-free zones, and planning optimal trajectories for flexible surgical tools within the confined anatomical region.

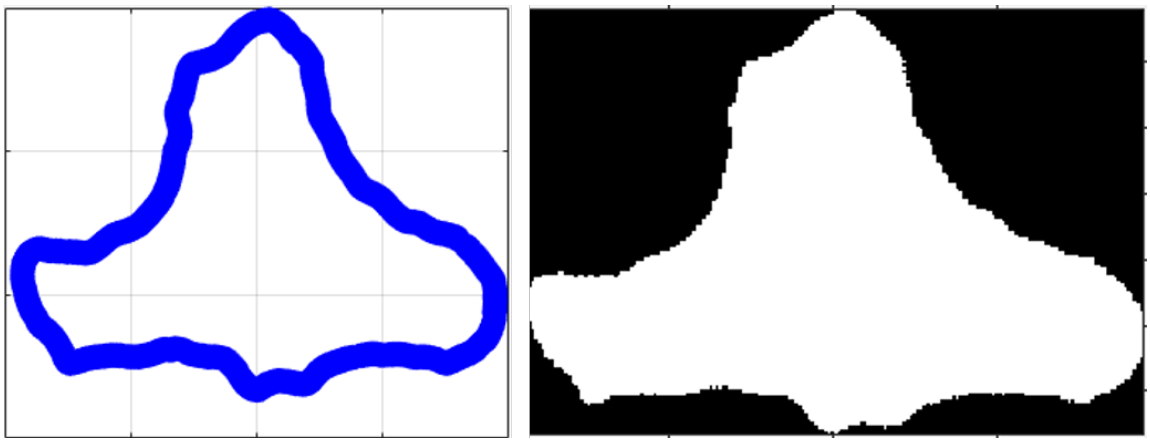

Fig. 3.7 *Binary Masking of the workspace*

3.3.4 EUCLIDEAN DISTANCE TRANSFORM

The Euclidean Distance Transform (EDT) is a widely used technique in image processing that computes the distance from each pixel in a binary image to the nearest foreground pixel. The result is a distance map in which each background pixel is assigned a value representing the shortest Euclidean distance to a foreground pixel, thereby providing a quantitative measure of spatial relationships within the image.

In a binary image, pixels are classified as either foreground (typically represented by 1) or background (typically represented by 0). The EDT assigns to each background pixel the Euclidean distance to the closest foreground pixel. This produces a continuous distance field, which can be leveraged to analyze geometric properties, optimize paths, or detect spatial constraints within the region of interest.

One of the primary applications of the EDT is the identification of the maximal inscribed circle within a given shape. By locating the pixel with the maximum distance value in the distance map, it is possible to determine the center and radius of the largest circle that can fit entirely within the shape. In the context of laparoscopic pelvic workspace analysis, this allows the determination of the largest instrument tip or surgical tool that can maneuver within confined anatomical regions without collision.

Overall, the EDT provides a robust computational framework for evaluating distances, identifying free space, and supporting optimization tasks in surgical workspace modeling, instrument design, and trajectory planning. Its application ensures precise quantification of available space, which is critical for enhancing safety, accessibility, and efficiency in minimally invasive procedures.

3.3.5 OPTIMIZATION ALGORITHM

The optimization phase aims to fit a Lamé curve (superellipse) within the available workspace contour for each slice, thereby maximizing the efficient utilization of the pelvic workspace for surgical interventions. The decision variables in this optimization include the semi-major axis (a), semi-minor axis (b), shape parameter (n), center coordinates (H, K), and orientation (θ) of the Lamé curve within each slice.

The parametric equations for a Lamé curve centered at (H, K) are given by:

$$x(\alpha) = H + a\cos^{2/n}(\alpha)$$
$$y(\alpha) = K + b\sin^{2/n}(\alpha)$$

The objective of the optimization is to maximize the enclosed area A of the Lamé curve, given by:

$$\text{Maximize}(A) = \frac{4ab\left(\Gamma\left(1+\frac{n}{2}\right)\right)^2}{\Gamma(1+n)}\cos(\theta)$$

where:

- a and b are the semi-major and semi-minor axes of the Lamé curve, respectively.
- n is the shape parameter controlling the curvature of the superellipse.
- H and K are the coordinates of the curve center.
- θ is the rotation angle of the curve.

The optimization is subject to the following constraints:

$$0 < a \leq \frac{L_x}{2\cos(\theta)}, \quad 0 < b \leq \frac{L_y}{2\sin(\theta)}$$
$$n \in \mathbb{N}, \quad -\pi \leq \theta \leq \pi$$
$$x_{\text{min}} \leq H \leq x_{\text{max}}, \quad y_{\text{min}} \leq K \leq y_{\text{max}}$$
$$M(a\cos^{2/n}(\alpha) + H,\, b\sin^{2/n}(\alpha) + K) = 1, \quad \forall\alpha \in [0, 2\pi]$$

where L_x and L_y represent half the lengths of the bounding box in the x and y directions, respectively, and $x_{\text{min}}, x_{\text{max}}, y_{\text{min}}, y_{\text{max}}$ define the bounding box limits of the workspace contour.

The initial parameters for the optimization are defined as:

$$L_x = \frac{x_{\text{max}} - x_{\text{min}}}{2}, \quad L_y = \frac{y_{\text{max}} - y_{\text{min}}}{2}$$

$$H = \frac{1}{N}\sum_{i=1}^{N} x_i,$$
$$K = \frac{1}{N}\sum_{i=1}^{N} y_i$$

where N is the number of contour points, and (x_i, y_i) are the coordinates of the i-th point. These initial parameters establish a balanced starting point for the optimization algorithm.

The optimization is implemented using MATLAB's *fmincon* function, which enforces the constraints while searching for the maximal-area Lamé curve that fits within the anatomical boundaries. The results of the Euclidean Distance Transform (EDT) are used as a reference: if the optimized Lamé curve area is smaller than the maximal inscribed circle identified by EDT, the EDT parameters are selected instead, where $n = 2$ and $a = b = r$, with r representing the radius of the circle.

Due to the anatomical complexity, uniform parameters for (a, b, H, K, n) across slices did not yield favorable results. Consequently, a two-step optimization process was employed, comprising Primary Optimization and Secondary Optimization, to account for the non-uniformity and achieve more realistic 3D workspace representations.

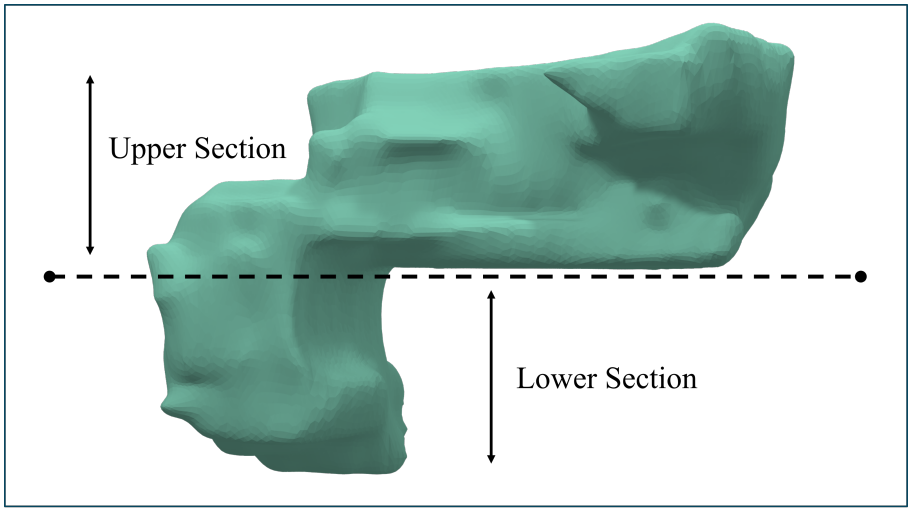

Fig. 3.8 *Anatomical Sections of workspace*

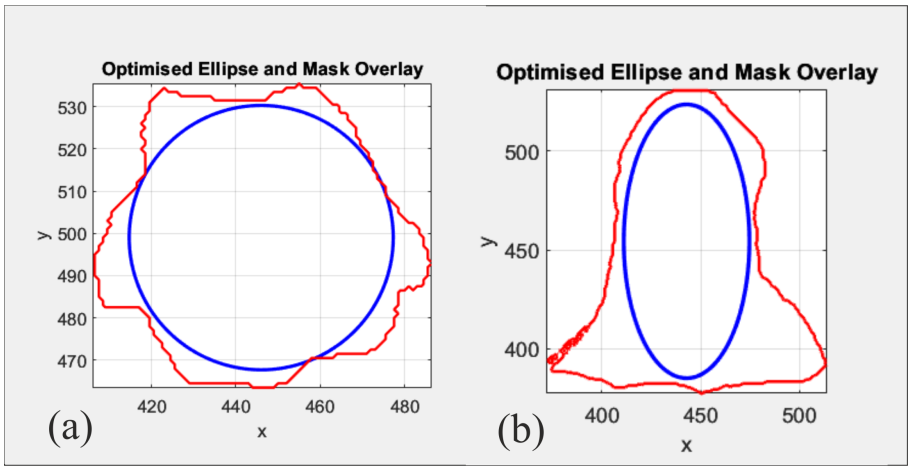

Fig. 3.9 *Optimisation Results for a layer*

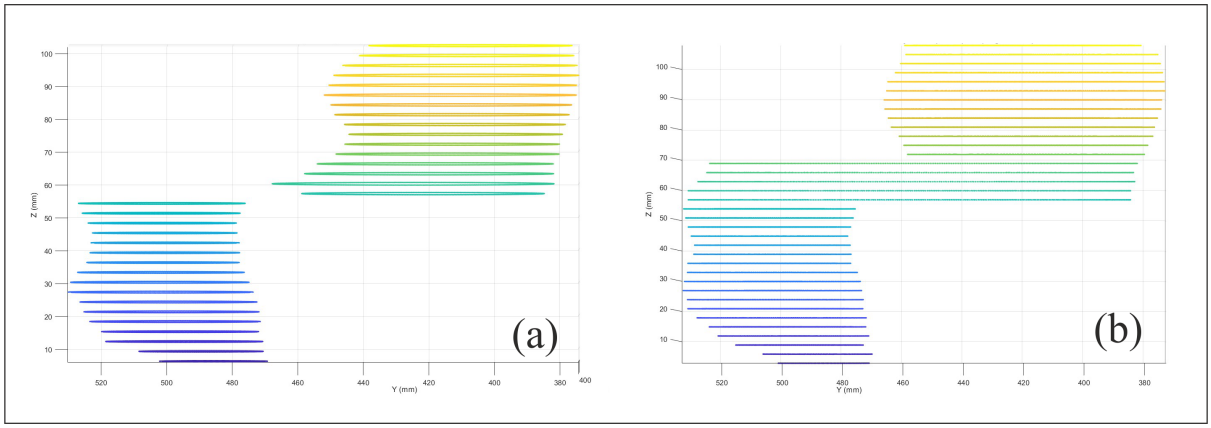

Fig. 3.10 *Overall optimisation Results in 3D space*

3.3.6 2D OPTIMISATION

The primary optimization focuses on constraining the Lamé curve to a circular shape for each slice of the workspace. This constraint simplifies the subsequent 3D reconstruction, as interpolating circles across slices naturally produces a cylindrical volume, which is easier to handle than the non-uniform 3D shapes that would result from unconstrained Lamé curves.

For this primary optimization, the shape parameter is fixed as $n = 2$ and the semi-major and semi-minor axes are set equal, $a = b = r$, ensuring that the output for each slice is a perfect circle (Fig. 3.9(a)). This approach guarantees uniformity in shape, which is particularly useful for initial visualization, volumetric analysis, and preliminary workspace evaluation.

However, the anatomical complexity of the pelvic region introduces challenges. As shown in Fig. 3.8, the workspace can be divided into lower and upper sections, and due to patient-specific anatomical variations, the positions of the centers of the circles undergo sudden shifts between these sections. This discontinuity results in a non-smooth 3D representation when the circles are interpolated along the vertical axis (Fig. 3.10(a)).

To address this issue and ensure a continuous and anatomically consistent 3D workspace, a secondary optimization step was implemented. The secondary optimization refines the positions, sizes, and orientations of the curves to accommodate anatomical variations while maintaining smoothness across slices, as described in the following section.

3.3.7 3D OPTIMISATION

The secondary optimization addresses the discontinuities observed in the primary 2D optimization, ensuring a smooth and anatomically consistent 3D workspace. The first step in this process is to identify the layer where a significant displacement of the circle center coordinates (H, K) occurs. A displacement threshold of 30 mm is used to detect abrupt shifts, and the

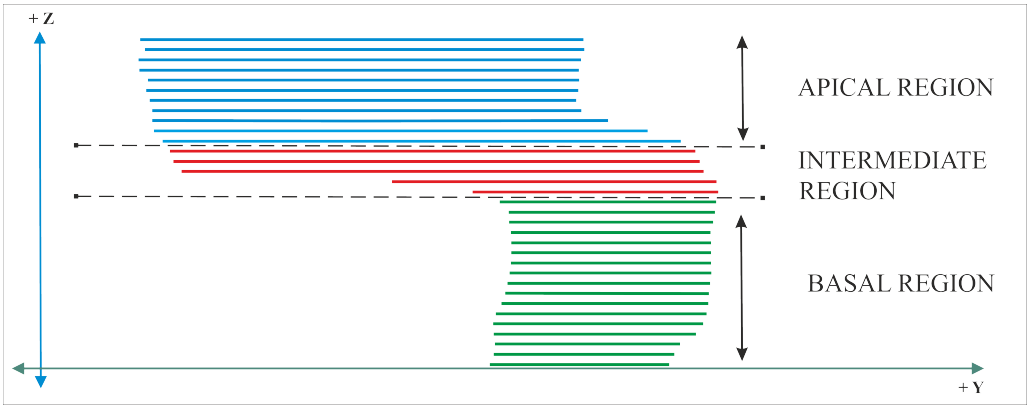

Fig. 3.11 *Optimized section of 3-dimensional workspace*

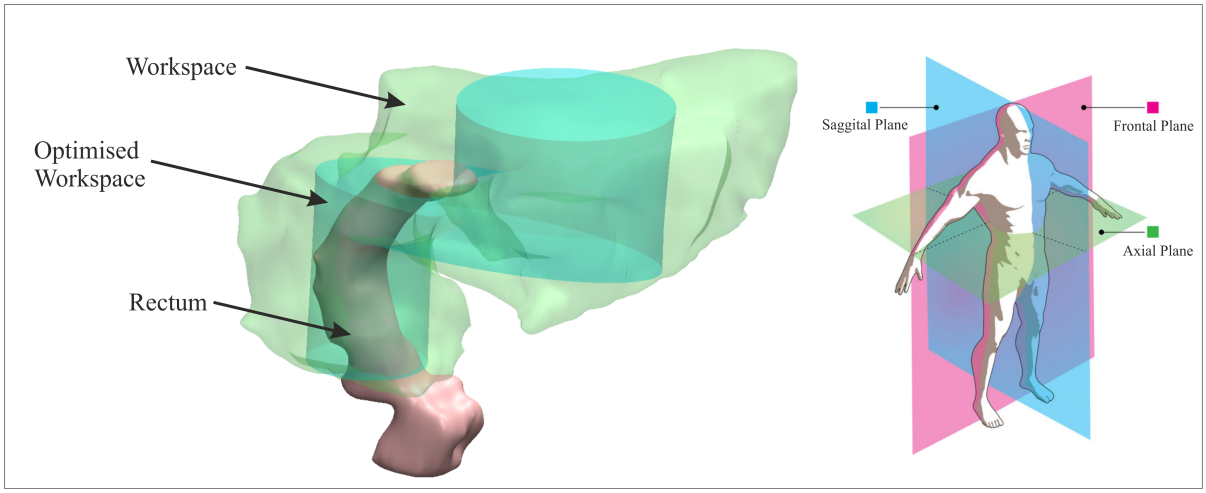

Fig. 3.12 *3D representation of optimised workspace*

corresponding slice is labeled as layer j.

Starting from layer j, the secondary optimization is applied to five consecutive layers: $j, j+1, j+2, j+3, j+4$. In this optimization, the shape parameter is fixed at $n = 2$, but the semi-major and semi-minor axes are allowed to differ ($a \neq b$), resulting in best-fit ellipses for these layers (Fig. 3.9(b)). This approach effectively resolves the discontinuity, producing a continuous 3D workspace across the affected region.

The optimized workspace reveals three distinct anatomical regions: Apical, Intermediate, and Basal (Fig. 3.11). The Apical and Basal regions are modeled as circular cylinders, while the Intermediate region is represented as an elliptical cylinder, reflecting the patient-specific anatomical variations. By combining the results from both primary and secondary optimizations, a comprehensive 3D representation of the pelvic workspace is obtained.

The geometric and positional parameters of the circles and ellipses for each layer are saved in a Comma Separated Values (.csv) file for further analysis and visualization. The final 3D workspace, integrating both optimization steps, is illustrated in Fig. 3.10(b) and Fig. 3.12. An

overall flowchart summarizing the entire workspace optimization procedure in MATLAB is presented in Fig. 3.13.

3.4 OPTIMISATION RESULTS

A detailed workspace assessment for the proposed flexible surgical stapler was carried out using preoperative MRI datasets from 77 patients (47 males and 30 females) obtained from Nantes Hospital. Each dataset underwent segmentation, 3D reconstruction, and optimization to quantify the available workspace and provide design guidelines for the surgical device. The analysis indicates that female patients generally exhibit a larger workspace compared to male patients, mainly due to anatomical differences in the bony pelvis as well as the arrangement of the genital and urinary structures.

Following the optimization step, key physiological parameters were extracted to guide the design of the flexible stapler. Although average values were obtained for both sexes, the design process was primarily based on the 5th percentile values. Percentiles express the relative standing of a measurement within the population. For example, a 5th percentile value means that 95% of the population has measurements larger than this threshold. Designing the stapler according to the 5th percentile workspace ensures operability under the most restrictive anatomical scenarios, while larger workspaces naturally allow greater flexibility for tool use.

As an illustration, for male patients, the mean (μ) basal radius is 28.36 mm with a standard deviation (σ) of 4.7 mm, while the 5th percentile radius (P_5) is 20.55 mm. The principal geometric approximations of the workspace are circular in the basal and apical regions and elliptical in the intermediate region. Table 3.1 provides a summary of the mean, standard deviation, and 5th percentile dimensions across all three regions for both male and female subjects. Figure 3.14 shows the statistical distribution of radii in the apical and basal regions, with emphasis on the 5th percentile markers.

Further analysis of positional data, summarized in Table 3.2, presents the average spatial coordinates of the centers of the primary geometric shapes for each layer in the basal, intermediate, and apical regions. Layer spacing is 3 mm along the Z-axis, consistent with MRI acquisition.

Two key observations emerge from this combined analysis of geometry and coordinates:

1. **Regional Dimensional Variation:** There is a notable difference in radii between the apical and basal regions, with the basal region being significantly smaller. The intermediate region provides sufficient width and height to act as a conduit connecting the apical entry point to the basal actuation region. This confirms the necessity of designing the tool to navigate through a constrained intermediate pathway.

2. **Alignment and Path Constraints:** In the universal coordinate system derived from MRI data, the centers of the three geometric regions lie approximately along the X-axis. No-

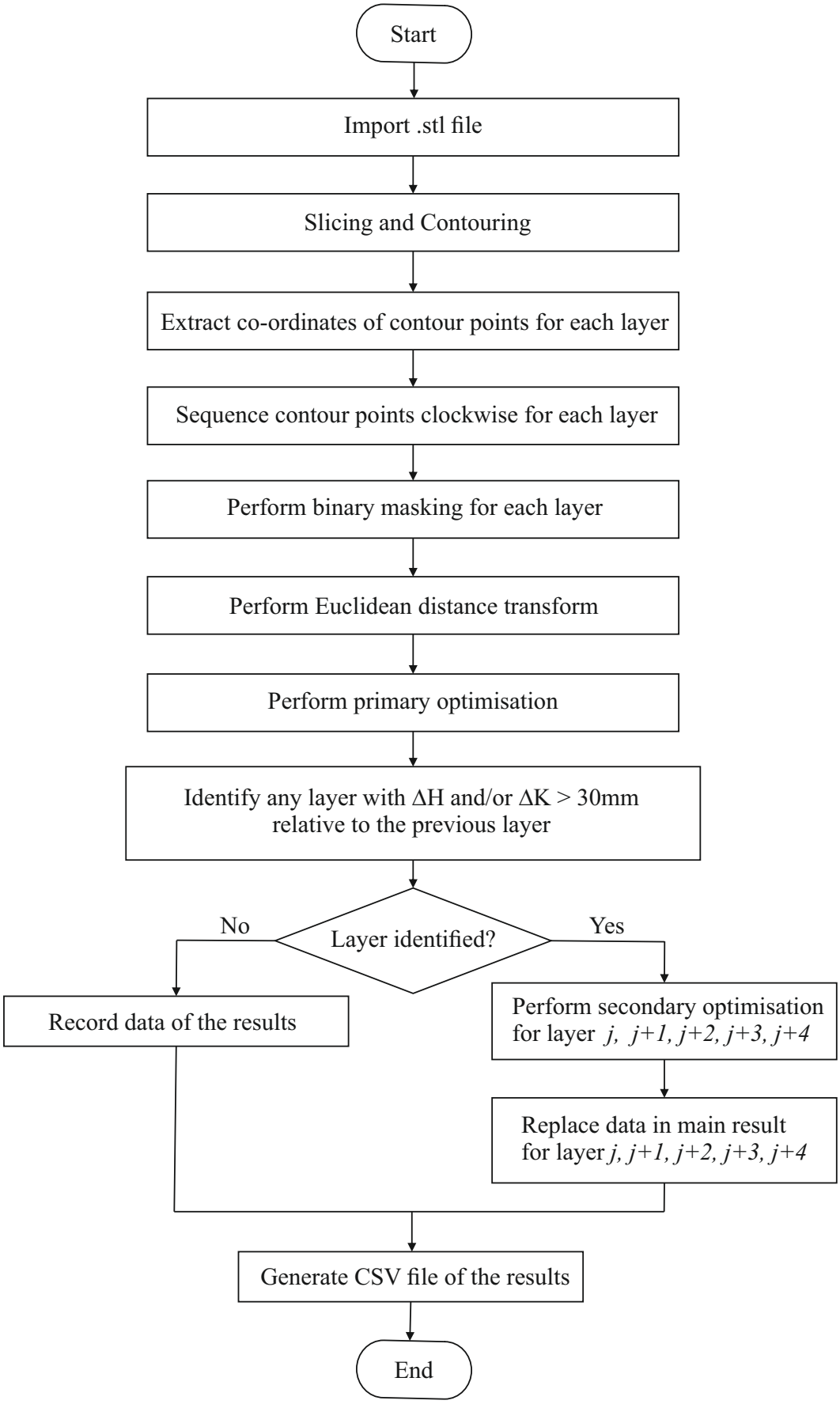

Fig. 3.13 *Flowchart of the workspace optimization process in MATLAB.*

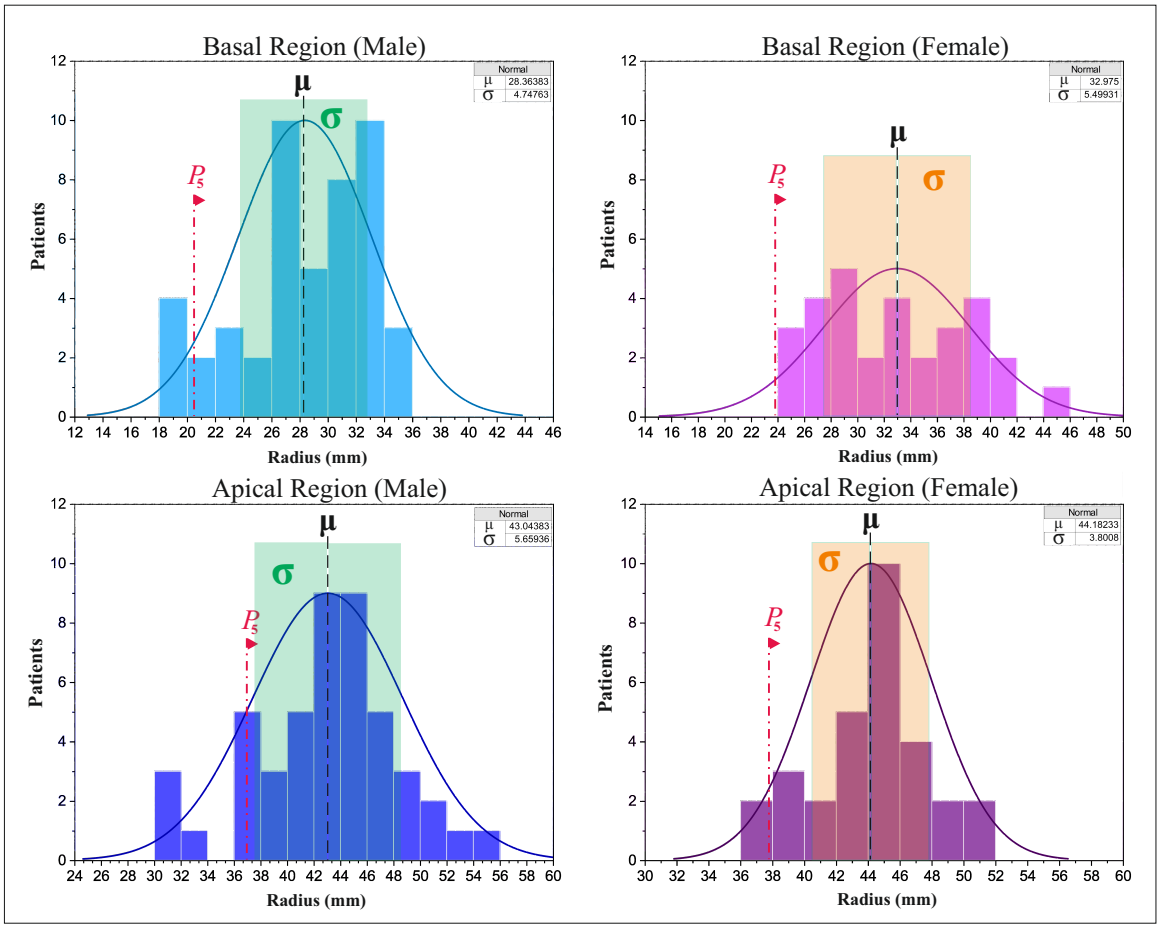

Fig. 3.14 *Statistical distribution of basal and apical radii, with* 5th *percentile marked.*

ticeable shifts are observed along the Y-axis, with mean offsets of 70 mm in males and 45 mm in females, resulting in the intermediate region being positioned between the apical and basal centers. This offset demonstrates that a straight trajectory for a 12 mm diameter stapler from the entry point (apical) to the actuation point (basal) is not feasible. Therefore, the use of a flexible wrist mechanism is required to follow the curved trajectory and achieve the correct stapling orientation.

3.5 SUMMARY OF THE CHAPTER

This chapter presents a comprehensive workspace analysis for laparoscopic rectal surgery, aimed at quantifying the highly constrained pelvic environment and guiding the design of a flexible surgical stapler. The study begins with high-resolution, patient-specific T2-weighted MRI acquisition following standardized protocols in multiple planes to capture the complex pelvic anatomy. Image quality control, artifact correction, and intensity normalization ensure that subsequent modelling is based on reliable data. Semi-automated and manual segmentation of each MRI slice classifies the pelvis into six functional zones (bone, ligaments, vascular tissues, genitourinary tract, rectum, and available workspace). Segmented slices are assem-

			Male	Female
No. of patients			47	30
Basal Region	Circle Radius (r) (mm)	Average (μ)	28.36	32.97
		St. Dev (σ)	4.7	5.4
		5th Percentile (P_5)	20.55	23.78
Intermediate Region	Major Axis (a) (mm)	Average (μ)	65.06	63.16
		St. Dev (σ)	7.3	2.9
		5th Percentile (P_5)	52.10	59.07
	Minor Axis (b) (mm)	Average (μ)	26.04	28.27
		St. Dev (σ)	4.6	3.3
		5th Percentile (P_5)	19.18	22.81
Apical Region	Circle Radius (r) (mm)	Average (μ)	43.04	44.18
		St. Dev (σ)	6.3	3.8
		5th Percentile (P_5)	37.10	37.92

Table 3.1 *Observation of data from optimization results*

		Male	Female
No. of patients		47	30
Basal Region	Avg. no. of layers	13	2
	Centre X coordinate (H) (mm)	446.34	446.45
	Centre Y coordinate (K) (mm)	492.72	475.45
Intermediate Region	Avg. no. of layers	5	5
	Centre X coordinate (H) (mm)	446.23	458.63
	Centre Y coordinate (K) (mm)	445.51	448.37
Apical Region	Avg. no. of layers	17	29
	Centre X coordinate (H) (mm)	447.29	444.89
	Centre Y coordinate (K) (mm)	420.73	432.77

Table 3.2 *Average coordinate axes of the workspace regions*

bled into accurate three-dimensional reconstructions, exported in `.stl` format and analysed in CAD software to compute volumetric and positional metrics.

These 3D models are then imported into MATLAB, where a bespoke computational pipeline discretizes the workspace (G-code generation, coordinate extraction, binary masking) and applies quantitative methods such as Euclidean Distance Transform to identify maximal collision-free areas. A two-step optimization procedure fits Lamé curves (superellipses) to each slice: a primary circular optimization to ensure uniformity and a secondary elliptical optimization

to handle anatomical discontinuities. This approach produces smooth, anatomically consistent 3D representations and reveals distinct apical, intermediate, and basal regions.

Analysis of 77 patient datasets shows significant gender- and region-specific variability. Radii, axes, and centre coordinates are statistically characterized, and 5th-percentile dimensions are extracted to ensure that the stapler design remains functional under the most restrictive conditions. The results demonstrate that a straight path between entry and actuation points is rarely available, confirming the necessity of a flexible wrist mechanism and bendable jaws. Overall, the chapter delivers an end-to-end methodology—combining imaging, segmentation, 3D reconstruction, and mathematical optimization—that directly informs the ergonomic design and safe deployment of laparoscopic instruments.

Overall, the chapter delivers an end-to-end methodology—combining imaging, segmentation, 3D reconstruction, and mathematical optimization—that directly informs the ergonomic design and safe deployment of laparoscopic instruments. Crucially, the stratification of the pelvic workspace into apical, intermediate, and basal regions, together with percentile-based dimensional constraints, establishes the precise spatial limits within which a stapling device must operate. These quantitative insights not only validate the need for flexible jaws and a wristed mechanism but also define the boundary conditions for engineering optimisation. Building on this anatomical foundation, the next chapter translates these workspace-derived parameters into a formal geometric and kinematic framework, where optimisation techniques are applied to determine the stapler's feasible dimensions, joint angles, and operating configurations.

4

Optimisation of Design Parameter for Surgical Tool

Based on the earlier workspace characterization and optimization, the available surgical field can be categorized into three anatomical zones: Apical, Intermediate, and Basal. These regions are delineated according to the vertical levels of axial or transverse planes reconstructed from MRI-based segmentation [95].

During laparoscopic rectal procedures, the patient lies in the supine position, with the frontal plane oriented parallel to the operating table. The stapler or surgical tool enters the body through a port on the lower left abdominal wall. Discussions with colorectal surgeons highlighted key constraints associated with tool maneuverability in this setting:

- The tool is introduced at an oblique angle relative to both the axial and sagittal planes.
- It first passes through the intermediate zone before progressing deeper into the basal zone.
- It rarely, if ever, traverses the apical zone during standard operations.

Thus, all translational and rotational actions of the instrument are effectively confined to the intermediate and basal zones. Recognizing this fact is essential for design optimization, as it allows tailoring of tool geometry, actuation, and flexibility specifically for the regions in use, while avoiding unnecessary complexity for the apical region.

4.1 SIMPLIFIED WORKSPACE REPRESENTATION

For analytical purposes, the workspace was further simplified by merging the geometries of the basal and intermediate zones. The basal zone, modeled as a circular cylinder, was extended

upward by the height of the intermediate zone. This yields a single cylindrical volume that serves as the effective workspace for tool motion. The parameters of this model are defined as follows:

- **Working radius** r_w: The effective cylindrical radius available for tool operation:

$$r_w = r_b - 6, \quad r_b \in [\,{}^{5}r_b,\, {}^{95}r_b\,]$$

  where r_b is the basal zone radius obtained from optimization, with ${}^{5}r_b$ and ${}^{95}r_b$ denoting the 5th and 95th percentile values, respectively. The 6 mm reduction accounts for the radial clearance required for a tool of 12 mm diameter.

- **Working height** H_w: The combined height of basal and intermediate zones, offset by the tool radius:

$$H_w = H_b + H_i - 6$$

  where H_b and H_i denote the basal and intermediate heights. The subtraction ensures the tool centerline remains safely within workspace limits.

- **Wrist joint height** h: The vertical location of the wrist joint, governing tool reach and bending analysis.

- **Offset from bottom layer** k: The distance from the cylindrical base to the tool centerline. Lower values of k minimize unnecessary intrusion into adjacent tissue.

- **Dead lengths** u and v:
  - u: Non-actuated segment between the wrist joint and bending section;
  - v: Non-bending section between the end of the bending segment and the tool tip.

- **Bending angle** β: The angular deflection at the wrist joint, defining the arc path of the tool.

- **Tool-wall angle** λ: The orientation of the tool with respect to workspace boundaries, influencing insertion mechanics.

- **Maximum length** L: The longest possible extension of the tool inside the cylindrical workspace.

This reduction results in a simplified cylindrical model that is mathematically tractable while preserving key anatomical constraints, enabling accurate trajectory, reachability, and maneuverability analysis.

4.2 GEOMETRIC POINTS AND PARAMETERS

To support trajectory planning within this workspace, three characteristic points are introduced:

- **Point** A: Located on the top face of the cylinder, denoting the upper boundary of operation.
- **Point** B: Positioned on the cylindrical wall at the wrist joint height h, corresponding to the base of the bending section.
- **Point** C: The tip of the tool, located within the lower portion of the workspace, representing the functional endpoint.

Their coordinates in 3D are given by:

$$A = (x_A,\ y_A,\ H_w) \tag{4.1}$$

$$B = (r_w \cos\varphi,\ r_w \sin\varphi,\ h) \tag{4.2}$$

$$C = (r_w t_C \cos\varphi,\ r_w t_C \sin\varphi,\ z_C) \tag{4.3}$$

with the auxiliary definitions:

$$\begin{aligned} x_A = r_w \cos\varphi(1-2t_A), \quad y_A = r_w \sin\varphi(1-2t_A), \\ t_A \in [0,1], \quad t_C \in [0,1], \\ 90^\circ \le \varphi \le 180^\circ, \quad \varphi \text{ is the azimuth angle.} \end{aligned}$$

For simplification, the motion of the stapler is considered planar. Since any azimuthal plane yields equivalent results, the XZ-plane with $\varphi = 180^\circ$ is chosen. This reduces the 3D formulation to a 2D problem while retaining the essential kinematic features.

4.3 BENDING ANGLE β AND TOOL CONSTRAINTS

The proposed flexible stapler incorporates a wrist joint with a bending capacity of up to 90°, offering greater articulation than conventional devices limited to 45°.

In this framework, the bending angle β at point B is the angle between shaft BA and the tool section BC. Practical operation imposes the following constraint:

$$95^\circ \le \beta \le 180^\circ \tag{4.4}$$

Here, the lower limit of 95° adds a 5° safety buffer beyond the nominal capability, reducing risks of jamming or excessive mechanical loading at the joint. The upper bound corresponds to the fully extended tool in a straight configuration.

4.4 OPTIMISATION OF TOOL PARAMETERS:

4.4.1 OPTIMIZATION FOR STRAIGHT TOOL

Problem Statement For a straight tool, the Euclidean distances between the wrist joint B and points A and C are defined as:

$$\|BA\| = \sqrt{(x_1 + r_w)^2 + (H_w - h_s)^2} \tag{4.5}$$

$$\|BC\| = \sqrt{(x_2 + r_w)^2 + (y_2 - h_s)^2} \tag{4.6}$$

where h_s is the height offset due to the wrist joint, and (x_1, y_1) and (x_2, y_2) are the coordinates of points A and C, respectively.

The bending angle β at the wrist joint is computed using the dot product:

$$\cos(\beta) = \frac{\overrightarrow{BA} \cdot \overrightarrow{BC}}{\|BA\| \, \|BC\|} \tag{4.7}$$

The objective is to maximize the effective length $\|BC\|$ while ensuring that β remains within safe operational limits.

Objective Function

$$\text{Maximize } f_{\text{straight}} = \|BC\| = L_s = \sqrt{(x_2 + r_w)^2 + (y_2 - h_s)^2} \tag{4.8}$$

Constraints

- **Bending Angle Constraint**:

$$\cos(180^\circ) \leq \cos(\beta) \leq \cos(95^\circ) \tag{4.9}$$

- **Geometrical Constraints**:

$$x_1 \in \left[-\frac{2r_w}{3}, r_w\right], \quad x_2 \in [0, r_w], \quad y_2 \in \left[0, \frac{H_w}{2}\right], \quad h_s \in [0, H_w - 3] \tag{4.10}$$

4.4.2 OPTIMIZATION FOR CURVED TOOL

Problem Statement For a curved tool, the total tool length $\|BC\|$ consists of a straight rigid segment of constant length u and a curved segment with bending angle $\theta = 180°$. In this configuration, $\|BC\|$ depends only on the workspace radius r_w and the rigid length u, and is independent of the bending angle β or height h_c. The goal is to maximize $\|BC\|$ while ensuring β remains within the safe operational limits.

Objective Function

$$\text{Maximize } f_{\text{curved}} = \|BC\| = L_c = \pi r_w + u \tag{4.11}$$

where r_w is the working radius and $u = 10$ mm is the constant rigid segment length.

Constraints

- **Bending Angle Constraint**:

  $$95° \leq \beta \leq 180°$$

  For the curved tool, β is enforced directly rather than using the dot product, as the curved segment cannot be represented as a straight vector.

- **Geometrical Constraints**:

$$h_c \leq H_w, \quad h_c = r_c + u + k \tag{4.12}$$

Solution Approach The straight tool optimization problem was solved using the MATLAB function *fmincon*. The curved tool optimization was performed using a linear parametric evaluation in MATLAB, considering the respective constraints. Both analyses incorporated the basal region radius R_b from the previous workspace optimization, ranging from the 5th to 95th percentile of the patient population. An illustrative example of tool length analysis for both straight and curved tools is shown in Fig. 4.1.

4.5 OPTIMISATION RESULTS

The outcomes of the tool length evaluation, i.e., the maximum tool length for the straight tool (L_s) with its associated wrist position relative to the base (h_s), and the maximum tool length for the curved tool (L_c) with the corresponding wrist position from the base (h_c), are presented in Fig. 4.2. The central aim of this analysis was to identify a tool length suitable for both the straight and curved configurations while encompassing the largest possible portion of the

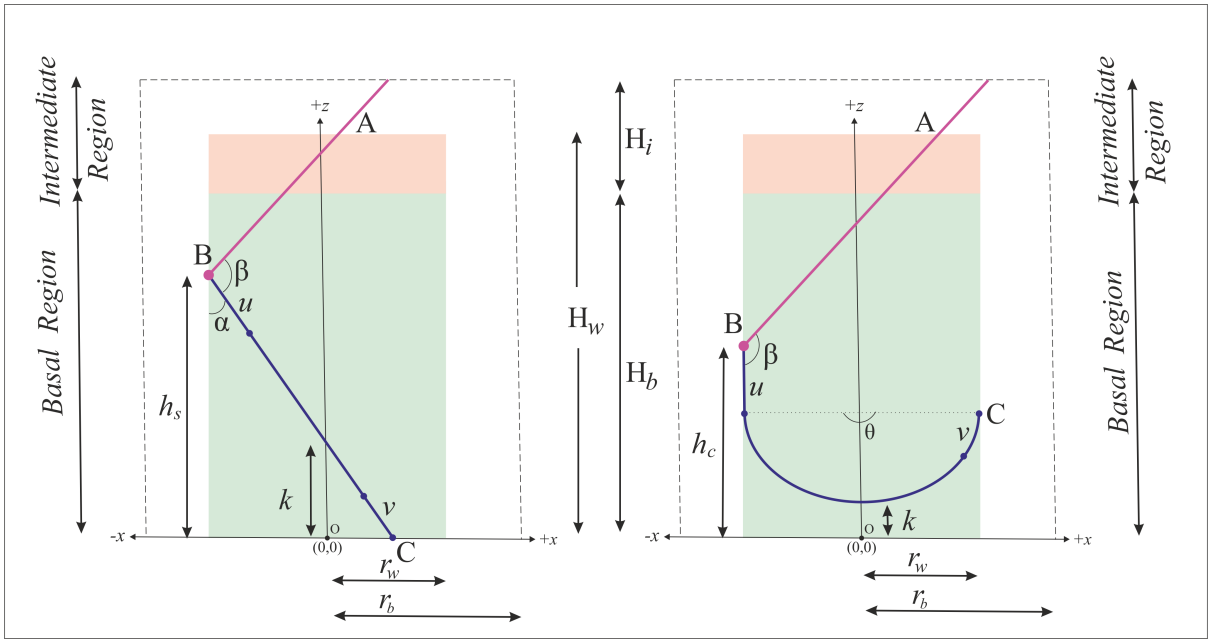

Fig. 4.1 *Depiction of tool length analysis for straight tool and curved tool, respectively.*

population, thereby enabling the development of a flexible tool of this length. To generate the tool length values, the basal radius R_b of male subjects was considered, ranging from the 5th percentile (P_5) to the 95th percentile (P_{95}). The optimization results demonstrated that female patients possess a comparatively larger workspace than male patients. Accordingly, the male dataset was selected for the design process, as their smaller dimensions provided more restrictive and hence more conservative constraint values.

Based on this analysis, two distinct tools were proposed instead of a single design: one with a length of 55.70 mm (referred to as MK1) and another with a length of 67.10 mm (referred to as MK2). This strategy ensures that the majority of the population is covered. The rationale for employing a common tool length across both straight and curved modes lies in operational flexibility: in restricted workspaces, the device can be employed in its curved configuration, while in larger workspaces it may be straightened by adjusting θ and α, as illustrated in Fig. 4.3.

After finalizing the tool lengths for the proposed endoscopic surgical stapler, their performance was benchmarked against existing rigid, straight-jawed endoscopic staplers using the same analysis procedure as for the straight tool. The comparative results are shown in Fig. 4.4. This comparison highlights that conventional staplers with a tool length of 70 mm (cutting length 45 mm) are unsuitable for patients between the P_5 and P_{18} percentiles, necessitating open surgery in those cases. By contrast, the proposed staplers extend coverage across P_5 to P_{95}, accommodating patients with narrower anatomies. Moreover, the tool's flexibility improves ease of placement and orientation during surgical procedures.

To maximize patient coverage, the MK1 and MK2 staplers were introduced. MK1 is effective from the P_5 to the P_{23} percentile, while MK2 is effective from the P_{18} to the P_{95} percentile.

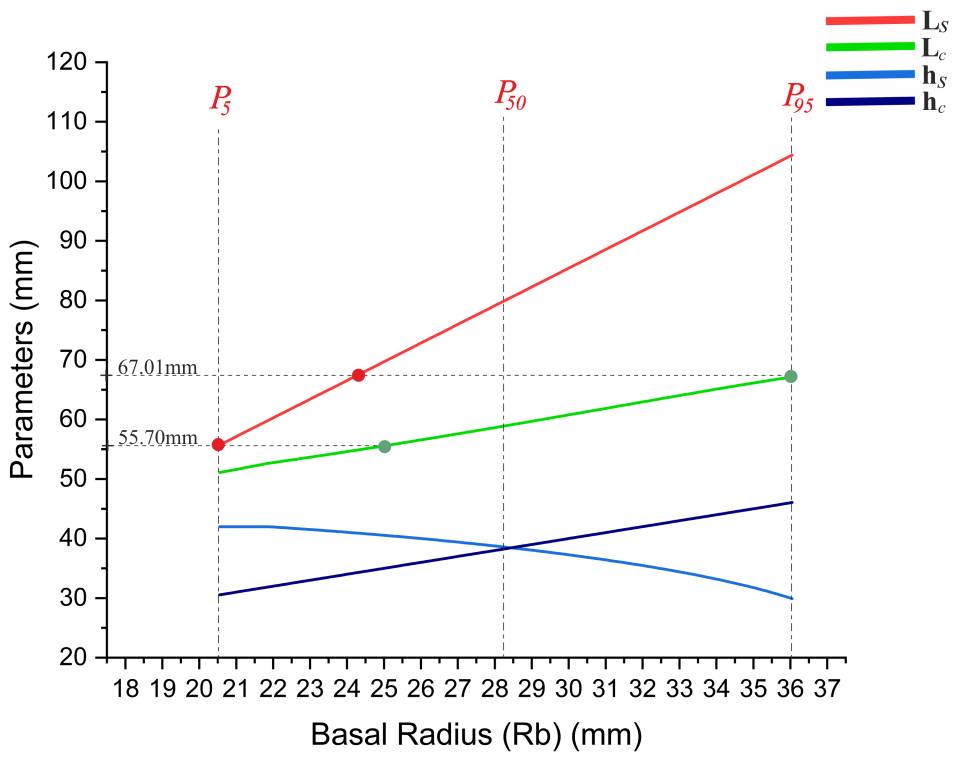

Fig. 4.2 *Maximum tool lengths for straight and curved tools along with corresponding wrist positions.*

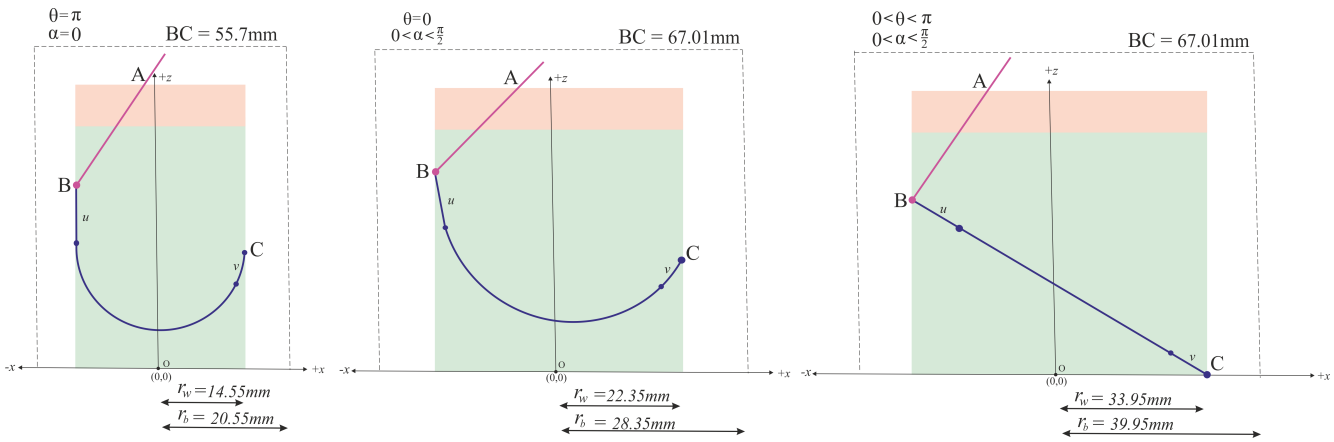

Fig. 4.3 *Operation of the designed stapler in varying workspace sizes.*

The overlapping range allows either tool to be employed for patients within that interval, giving surgeons alternative choices. A representative case is shown in Fig. 4.5 for a patient with $R_b = 25.10$ mm.

The MK1 and MK2 staplers, designed to function in curved configurations for constrained spaces, provide an extended stapling length, enhancing tissue sealing capability. Furthermore, the curved tool configuration facilitates access to deeper regions closer to the workspace base, thereby reducing unnecessary removal of healthy tissue. The proposed design enables dynamic,

independent adjustment of α and θ through the wrist joint and a stacked tensegrity mechanism, resulting in improved adaptability and operational versatility [96].

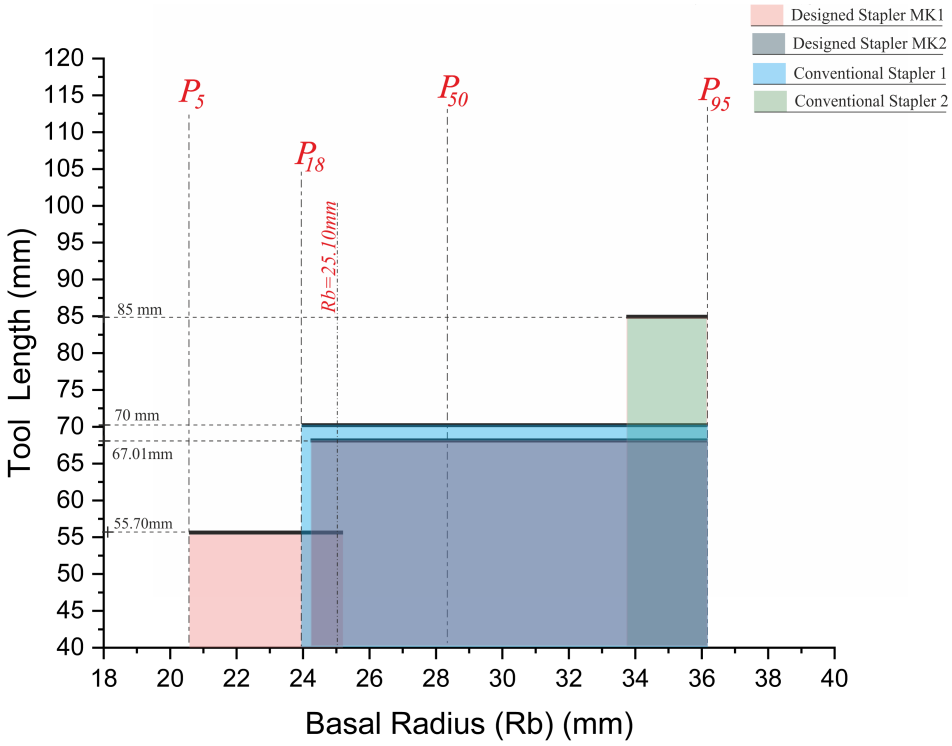

Fig. 4.4 *Population coverage comparison between conventional staplers and the designed MK1 and MK2 staplers.*

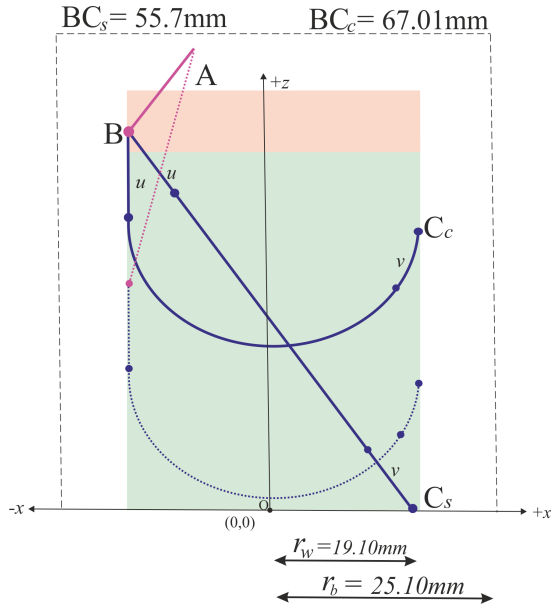

Fig. 4.5 *Example showing the utilisation of MK1 and MK2 staplers for the same patient with* $R_b = 25.10$ mm.

4.6 SUMMARY OF THE CHAPTER

This chapter translates the anatomical and kinematic constraints derived from the workspace analysis into a rigorous optimisation of the surgical stapler's key design parameters. Based on MRI-derived segmentation and 3D reconstruction, the pelvic workspace was divided into apical, intermediate, and basal regions. Clinical feedback confirmed that, during laparoscopic rectal surgery, the tool enters the body at an acute angle and primarily navigates only the intermediate and basal zones. These insights allowed the design effort to focus on the regions actually traversed, reducing unnecessary complexity in the apical zone.

To enable tractable analysis, the basal and intermediate regions were merged into a single simplified cylindrical workspace defined by a working radius r_w, working height H_w, wrist joint position h, centreline distance from the base k, dead lengths u and v, bending angle β, approach angle λ and maximum tool length L. Three key geometric points—A (upper boundary), B (wrist joint), and C (tooltip)—were parametrised in 3D space and reduced to a 2D plane for computational efficiency. Within this model, the bending angle β at the wrist joint was constrained between 95° and 180° to maintain safety margins beyond the nominal 90° capability.

Two optimisation problems were formulated. For a straight tool, the MATLAB solver *fmincon* maximised the effective length $\|BC\|$ while satisfying angle and geometric constraints. For a curved tool, a parametric evaluation maximised $\|BC\|$ as $\pi r_w + u$ under analogous constraints. Using basal radii from the 5th to 95th population percentiles (male data as the more restrictive case), optimal lengths were derived.

Results identified two designs—MK1 at 55.7 mm and MK2 at 67.1 mm—that together cover nearly the entire patient population. Compared with conventional rigid staplers (70 mm), which fail for up to 18 % of patients, the proposed flexible designs expand coverage to the 5th–95th percentile range while allowing dynamic adjustment of angles α and θ. This dual-design strategy ensures deeper reach, improved sealing, and enhanced adaptability in minimally invasive surgery.

The chapter outlines the optimal geometric parameters and tool lengths necessary for optimal pelvic workspace coverage, and it demonstrates how flexible designs can overcome the limitations of rigid staplers. However, these optimised lengths and angles remain theoretical unless embodied in mechanisms capable of delivering precise articulation, force transmission, and ergonomic control within the confined surgical environment. To bridge this gap, the next chapter turns to the development of the jaw and wrist mechanisms—the motion subsystems that physically realise the optimised kinematics. Their design, validation, and refinement ensure that the geometric gains established here can be translated into reliable, surgeon-friendly functionality.

5

Kinematic Modelling and Analysis

This chapter introduces the kinematic modeling and analysis of the proposed flexible, multi-segment tensegrity mechanism. Unlike rigid-link systems, the mechanism undergoes elastic deformations, resulting in nonlinear kinematic behavior that cannot be captured using conventional joint-based models. To address this challenge, an analytical framework based on the Piecewise Constant Curvature Approximation is adopted, enabling a tractable yet accurate description of the mechanism's bending behavior. The chapter establishes the relationship between actuation, elastic forces, and resulting curvature, and extends the formulation from a single segment to the complete structure. This modeling foundation is essential for understanding motion generation, force transmission, and design limitations of the proposed system.

5.1 KINEMATIC MODEL

The proposed multi-segment bending mechanism exhibits tensegrity characteristics due to the combination of isolated compression and tension elements. The rigid links serve as compression members, while the cables act as tension-only elements, maintaining equilibrium and functional integrity under external displacements. The flexible spine functions as a compliant pseudo-joint, enabling rotational and bending motion of the top link through elastic deformation controlled entirely by cable tension. The force-driven redistribution of tension across the cables, together with the spine's compliance, ensures that stability and motion arise from the balance of forces rather than fixed kinematic constraints, a defining feature of tensegrity systems.

Flexible mechanisms tend to show nonlinear behavior when they undergo large deformations or bending. This makes their modeling and analysis more complex compared to rigid-link mechanisms. To make the kinematic modeling of such systems more manageable, a commonly used approach is the Piecewise Constant Curvature Approximation (PCCA). This method assumes that the flexible structure can be broken down into a series of segments, each bending like a

circular arc with constant curvature. This simplification allows us to use analytical equations to describe the shape and position of the mechanism.

The PCCA method has been well established in earlier studies [97], especially for systems where cable-driven actuation is used. In such systems, the input is the tension applied to the cables, and the output is the resulting posture or shape of the mechanism. One of the key advantages of PCCA is that it remains effective even when the entire structure is formed by a single continuous flexible beam, instead of having distinct segments with joints [81]. Because of its simplicity and usefulness, this method has been widely used in designing and modeling flexible tools, particularly in medical and surgical applications where smooth and controlled bending is essential [98].

In our work, we focus on a flexible robotic mechanism made up of multiple segments stacked vertically, as shown in Figure 5.1. Each segment is based on a tensegrity-inspired design and with modifications to improve in-plane bending while keeping the structure stiff in that same plane. A single continuous flexible beam connects the base of the robot to its tip and acts as the central spine of the mechanism. We refer to this beam as $(A_1^0 A_n^0)$, which runs through all the segments and gives structural continuity to the system.

To control how the mechanism bends, we use two cables that run along the sides of the flexible beam — one from A_1^i to A_n^i and the other from A_1^j to A_n^j. By pulling on these cables, we can create a bending motion in the desired direction. Additionally, a set of springs is placed along the cables. These springs are used to model the elastic resistance offered by the outer covering or skin that wraps around the mechanism. This setup tries to mimic the conditions in real-world applications, like surgical environments, where the device interacts with soft tissue and must maintain a certain shape.

To understand the behavior of the system better, we look at a single segment of the mechanism — specifically the part between points A_1^o and A_2^o. This segment is actuated by two tendons, ρ_1^i and ρ_1^j, positioned on either side of the flexible spine. These tendons apply pulling forces to bend the segment. Alongside, two springs with stiffness values k_1^i and k_1^j are placed between the anchor points (A_1^i, A_2^i) and (A_1^j, A_2^j), respectively. This combination of cables and springs defines how each segment reacts when actuated.

The same design is repeated for all the segments in the mechanism — such as $A_2^o A_3^o$, $A_3^o A_4^o$, and so on — with the layout of cables and springs staying the same throughout. This uniformity helps maintain predictable bending behavior across the whole structure.

When one or both of the cables are pulled, the segment bends, and this local bending happens across all segments, creating an overall curved shape for the mechanism. The actual length of the cable after deformation is represented by $\rho_n^{i/j}$, and this value is critical in calculating how the mechanism bends. By applying the PCCA method, we can relate these cable lengths to the

curvature and orientation of each segment, allowing us to model and predict the shape of the mechanism during operation.

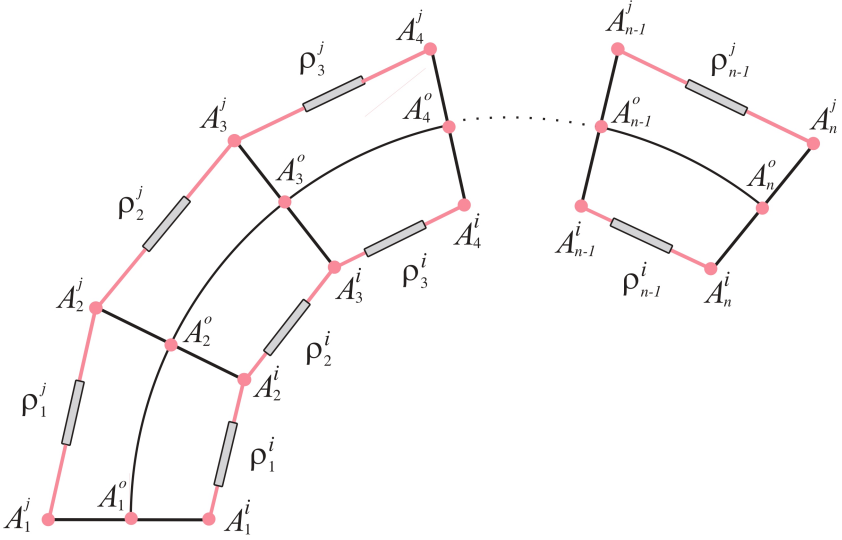

Fig. 5.1 *The tensegrity mechanism understudy with a stacked multi−segmented model with a flexible beam.*

5.2 KINEMATICS EQUATIONS OF ONE SEGMENT

In order to determine the positions of the points located on the mobile platform, it is essential to analyze the deformation behavior of a beam subjected to torsion. We consider that the distance between A_1^o and A_2^o is h_1 when the mechanism is in its neutral configuration. Furthermore, A_1^o corresponds to the midpoint of $A_1^i A_1^j$, such that $A_1^i A_1^o = A_1^o A_1^j = l_1$.

The coordinates of the fixed points are expressed as:

$$\mathbf{a}_1^j = \begin{bmatrix} -l_1 \\ 0 \end{bmatrix}^T \quad \mathbf{a}_1^i = \begin{bmatrix} l_1 \\ 0 \end{bmatrix}^T \tag{5.1}$$

and in the moving reference frame:

$$\mathbf{a}_2^j = \begin{bmatrix} -l_1 \\ 0 \end{bmatrix}^T \quad \mathbf{a}_2^i = \begin{bmatrix} l_1 \\ 0 \end{bmatrix}^T \tag{5.2}$$

where $\mathbf{a}_n^{i/j}$ denotes the vector representation of point $A_n^{i/j}$.

In constructing the multi-segmented structure, the mechanism width was maintained as specified in Equations (5.1) and (5.2). This choice followed a comparison between constant-width and tapering-width configurations, with stability analyses supporting the former, as discussed in [99].

To establish the relation between cable tensions, spring forces, and the curvature radius of one

segment, a lumped parameter model is employed. In this model, forces applied by cables and springs at the beam ends generate a torsional torque:

$$\mathcal{T}_1 = \mathcal{T}_{f_1^j} + \mathcal{T}_{f_1^i} + k_1^j(\rho_1^j - d_1^j)l_2 - k_1^i(\rho_1^i - d_1^i)l_2 \tag{5.3}$$

where $\mathcal{T}_{f_1^j} = -f_1^j l_2$ and $\mathcal{T}_{f_1^i} = f_1^i l_2$. Hooke's law, expressed in Equation (5.4), links the rotational spring to the bending moment. Here, K_θ represents the effective bending stiffness (N·m/rad), h_1 the arc length between A_1^o and A_2^o, f_1 and f_2 the cable forces, and r_1 the bending radius (see Figure 5.2). For a single section:

$$h_1/r_1 = \mathcal{T}_1/K_\theta \tag{5.4}$$

The beam deformation is thus characterized by bending radius r_1 and bending angle θ_1:

$$r_1 = h_1/\theta_1 \quad \text{and} \quad \theta_1 = \tau_1/K_\theta \tag{5.5}$$

This formulation applies for bending in either direction, left or right, allowing the position of A_2^o to be determined.

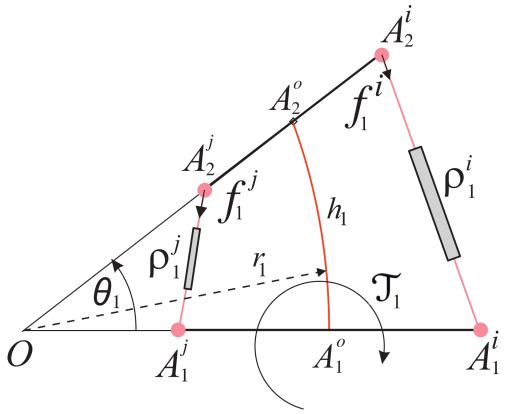

Fig. 5.2 *Equilibrium of bending moment [81], where two forces f_1 and f_2 generate the torque $\mathcal{T}_1$.*

The segment $(A_2^j A_2^i)$ is orthogonal to the beam at A_2^o, and the coordinates of these points are given as:

$$\mathbf{a}_2^o = \begin{bmatrix} r_1 - r_1\cos(\theta_1) \\ r_1\sin(\theta_1) \end{bmatrix} \tag{5.6}$$

$$\mathbf{a}_2^j = \begin{bmatrix} r_1 - r_1\cos(\theta_1) - l_2\cos(\theta_1) \\ R\sin(\theta_1) + l_2\sin(\theta_1) \end{bmatrix} \tag{5.7}$$

$$\mathbf{a}_2^i = \begin{bmatrix} r_1 - r_1\cos(\theta_1) + l_2\cos(\theta_1) \\ R\sin(\theta_1) - l_2\sin(\theta_1) \end{bmatrix} \tag{5.8}$$

The inverse kinematic relations for a flexible-beam mechanism can be written as:

$$||\mathbf{a}_1^j - \mathbf{a}_2^j|| = \rho_1^j, \quad ||\mathbf{a}_1^i - \mathbf{a}_2^i|| = \rho_1^i \tag{5.9}$$

These can also be reformulated in terms of spring lengths as:

$$(-l_1 - r_1 + r_1\cos(\theta_1) - l_2\cos(\theta_1))^2 + (-r_1\sin(\theta_1) + l_2\sin(\theta_1))^2 = (\rho_1^j)^2 \tag{5.10}$$

$$(l_1 - r_1 + r_1\cos(\theta_1) + l_2\cos(\theta_1))^2 + (-r_1\sin(\theta_1) - l_2\sin(\theta_1))^2 = (\rho_1^i)^2 \tag{5.11}$$

Following the same approach, the equations for subsequent sections can be derived similarly. The generalized inverse kinematic model for multiple sections is expressed as:

$$||\mathbf{a}_{n-1}^j - \mathbf{a}_n^j|| = \rho_{n-1}^j, \quad ||\mathbf{a}_{n-1}^i - \mathbf{a}_n^i|| = \rho_{n-1}^i \tag{5.12}$$

5.3 FORCE TRANSMISSIONS BETWEEN SEGMENTS

To understand how the mobile platform moves in response to the forces applied through the tendons (or actuation cables), we first need to estimate the resulting curvature of the flexible beam in each segment. Specifically, this involves calculating two key geometric parameters: the radius of curvature and the bending angle. These parameters directly influence the posture of the segment and must match the physical constraints defined by the kinematic model.

To compute these values, we frame the problem as an optimization task. For a single segment, we define the optimization problem $\mathcal{S}$ as shown in Equation (5.9). The goal is to find the configuration that minimizes the error between the actual cable lengths (measured between tendon attachment points) and the desired or commanded cable lengths ρ_1^i and ρ_1^j:

$$\mathcal{S} = \text{Minimize}\left((||\mathbf{a}_1^j - \mathbf{a}_2^j|| - \rho_1^j)^2 + (||\mathbf{a}_1^i - \mathbf{a}_2^i|| - \rho_1^i)^2\right) \tag{5.13}$$

This cost function ensures that the computed configuration results in tendon lengths that closely match the target values. In practice, we apply constraints such that the tendon lengths remain within physically feasible limits: $\rho_1^i, \rho_1^j \geq 0$ and $\rho_1^i, \rho_1^j \leq 3$. These bounds represent the minimum and maximum permissible cable lengths, based on the mechanical limits of the design.

For a mechanism with multiple segments, this optimization is extended by summing up the squared error terms for each segment. This provides a global cost function that considers the full structure, enabling us to find the configuration of the entire mechanism that best fits the given cable lengths.

In addition to the kinematic modeling, it is important to consider how bending forces are trans-

ferred from one segment to the next. This force transmission depends on the relative tension in the two tendons. For example, if $f_n^i > f_n^j$, the segment bends toward the right side. The tendons are routed through eyelets embedded in the mobile platform, and as they pass through these eyelets, friction comes into play. This friction is represented by the coefficient μ.

Figure 5.3 illustrates how the forces behave as they pass through the eyelets—showing both the incoming and outgoing force directions. This analysis is essential because the friction at these points affects how efficiently the force is transmitted along the structure. By taking this friction into account, we can calculate how much of the input force actually contributes to the bending motion and how much is lost, which allows us to derive accurate force transmission coefficients, as discussed in [81].

This combination of optimization-based kinematic modeling and force analysis gives us a complete picture of how the mechanism behaves when actuated and helps in predicting its posture under various loading and friction conditions.

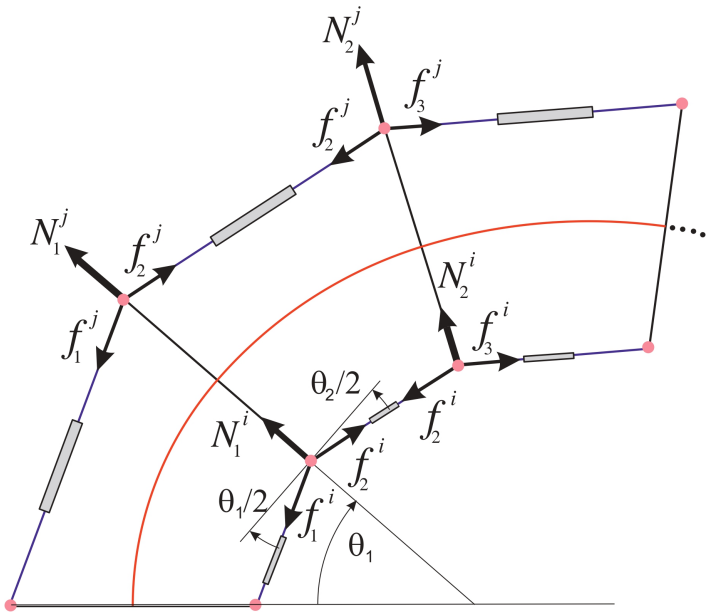

Fig. 5.3 *Static equilibrium of three segments.*

For actuators on the right side of the central axis, the tensions in the cables reduce from the base to the end as

$$\frac{f_{n+1}^i}{f_n^i} = \left(\frac{1-\mu\sin(\theta_1/2)}{1+\mu\sin(\theta_1/2)}\right) \tag{5.14}$$

For actuators on the left side of the central axis, the tensions in the cables increase from the base to the end as

$$\frac{f_{n+1}^j}{f_n^j} = \left(\frac{1+\mu\sin(\theta_1/2)}{1-\mu\sin(\theta_1/2)}\right) \tag{5.15}$$

5.4 SIMULATION-BASED EVALUATION OF BENDING BEHAVIOUR

To understand how the mechanism behaves under actuation, we performed a simulation study using the SIROPA library [100] within the MAPLE software (Version 2023, Maplesoft, Waterloo, Canada). The goal of this simulation was to evaluate how the structure bends under different force conditions and how various constraints affect its performance. At this stage, some of the model parameters (such as exact material properties) are yet to be finalized. Hence, this simulation also acts as a tool to inform material selection and workspace analysis.

MOTION SIMULATION

To visualize the basic bending motion of a single segment, we simulated how the structure deforms under increasing differences in cable forces. Figure 5.4 shows this deformation, where the red curve represents the central spine of the segment and the blue lines represent the actuation cables. The simulation was performed over a force difference range from $f_1 - f_2 = 0 + \epsilon$ to 17 N, where ϵ is a small offset added to avoid singular conditions (i.e., infinite curvature when the forces are exactly equal). This upper limit of 17 N was chosen based on mechanical limits relevant to the design described in this study.

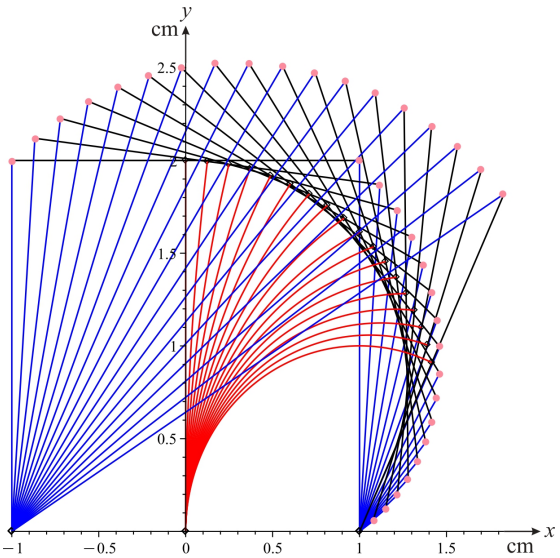

Fig. 5.4 *Simulation of the bending of one segment with $l_1 = l_2 = 1$ cm and $h_1 = 2$ cm.*

However, the use of springs (each with a stiffness of 100 N/m) introduces practical constraints. The spring elements can either become fully compressed or stretched beyond their limits, or the cable may align tangentially to the curvature of the beam, all of which can lead to a degenerate configuration. To prevent this, we imposed a constraint that restricts the spring to compress no more than 40% of its initial length in the neutral (home) pose. With this condition, the maximum achievable bending angle per segment is about 1.15 radians (approximately $130°$). This angle becomes a benchmark for assessing the range of motion achievable within mechanical safety margins.

For multi-segment simulations, we applied the same inverse kinematics optimization approach described earlier (based on Equations 5.9 and 5.12). MAPLE's optimization tools were used to solve for the curvature, using the applied cable forces and spring tensions as inputs. In the absence of friction, the bending profile of the entire mechanism is smooth and continuous, as shown in Figure 5.5 (left).

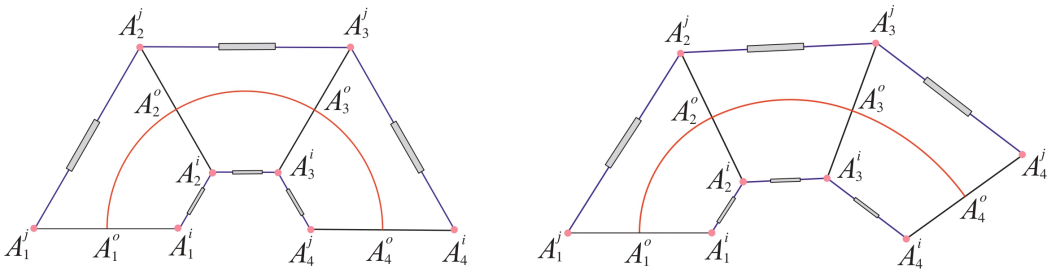

Fig. 5.5 *Simulation of bending for three segments with $\mu = 0$ **(left)** and $\mu = 0.2$ **(right)**.*

EFFECT OF FRICTION ON CABLE TENSION AND CURVATURE

Friction plays a significant role in how the mechanism behaves during actuation. In the real system, cables pass through guiding eyelets embedded in the mobile platform. As they do so, frictional forces (represented by the coefficient μ) resist their motion. When friction is introduced in the model (e.g., $\mu = 0.2$), we observe an imbalance in tension between the two cables in a segment, which alters the effective curvature.

This effect is visualized in Figure 5.5 (right). Compared to the frictionless case, the bending curve is no longer perfectly smooth, and segments begin to exhibit asymmetrical deformation. This highlights the importance of accounting for friction in both modeling and physical design, as it directly affects accuracy and responsiveness.

It is also worth noting that our current model assumes a uniform curvature angle across segments. While this helps simplify the simulation and maintain consistency, it is a limitation that may need to be relaxed in future versions of the model for more realistic behavior.

BENDING SINGULARITY DUE TO CROSS-SECTION CONSTRAINTS

One of the critical design trade-offs in implementing a flexible stapler mechanism based on tensegrity principles is the reduction in cross-sectional dimensions. This design choice is necessary to ensure that the instrument can navigate the constrained anatomical spaces in surgical environments. However, making each segment thinner introduces new challenges.

As shown in Figure 5.6, when the cross-section becomes very narrow, even small deviations in cable tension can cause the flexible beam to collide or interfere with the actuation cables. This leads to a significant increase in the radius of curvature and, in extreme cases, a loss of controllability, known as a *bending singularity*.

To address this problem, one solution is to include an extra joint that is similar to a wrist before

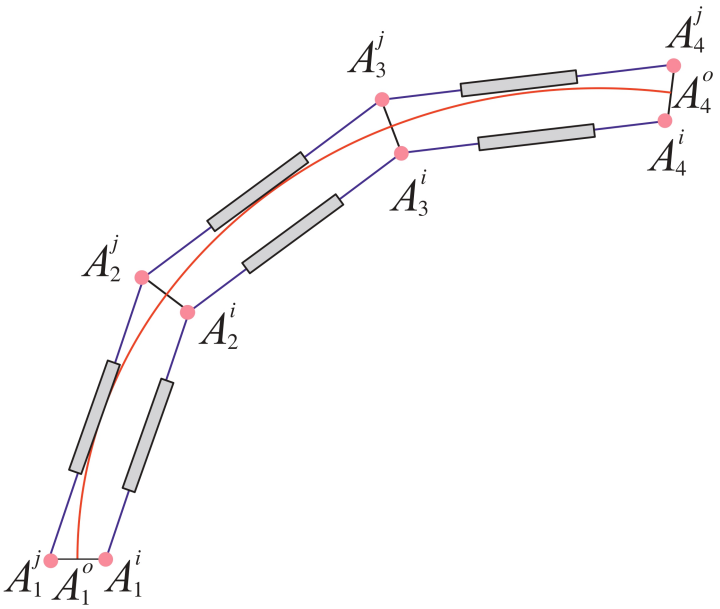

Fig. 5.6 *Bending singularity occurring due to reduced cross-section.*

the stapler tip, offering more degrees of freedom to adjust the tool's orientation without relying only on bending. Another strategy is to increase the number of segments in the mechanism, which distributes the curvature more evenly and reduces the risk of interference. However, adding more segments may increase the number of eyelets, which can also amplify the total friction in the system. Therefore, a careful balance between segment count, mechanical clearance, and frictional losses must be achieved through design iteration

The proposed multi-segment bending mechanism exhibits tensegrity characteristics due to the combination of isolated compression and tension elements. The rigid links serve as compression members, while the cables act as tension-only elements, maintaining equilibrium and functional integrity under external displacements. The flexible spine functions as a compliant pseudo-joint, enabling rotational and bending motion of the top link through elastic deformation controlled entirely by cable tension. The force-driven redistribution of tension across the cables, together with the spine's compliance, ensures that stability and motion arise from the balance of forces rather than fixed kinematic constraints, a defining feature of tensegrity systems.

5.5 SUMMARY OF THE CHAPTER

This chapter develops a kinematic modeling and analysis framework for a multi-segment flexible robotic mechanism inspired by tensegrity principles. Due to the nonlinear behavior of large deformations, the Piecewise Constant Curvature Approximation is adopted to describe bending in an analytically tractable form. A detailed single-segment model is derived and extended to the full structure, relating cable lengths, forces, and bending curvature through geometric and elastic considerations. An optimization-based inverse kinematics approach is introduced

to compute feasible configurations. Force transmission, frictional effects, and simulation-based evaluations are presented, highlighting practical design constraints, workspace limits, and bending singularities relevant to surgical robotic applications. This chapter also establishes a strong foundation to the design and development of the structure and mechanism of the endoscopic flexible surgical stapler as illustrated in the following chapter.

6

Mechanical Design and Prototyping of the Flexible Surgical Stapler

The design of the flexible endoscopic surgical stapler jaw represents a critical step in translating a conceptual surgical instrument into a functional prototype. This chapter presents the iterative development of the stapler jaw, detailing the design rationale, fabrication techniques, and experimental evaluation. Particular emphasis is placed on maintaining structural integrity while providing controlled flexibility necessary for minimally invasive procedures.

6.1 DESIGN RATIONALE AND REQUIREMENTS

The primary functional requirements for the stapler jaw were defined based on its intended clinical use, specifically for safe and precise tissue manipulation within the constrained pelvic workspace. The jaw must provide controlled flexibility along its length to navigate confined anatomical regions, while simultaneously maintaining sufficient rigidity to ensure consistent tissue compression and stapling. Additionally, the design needed to accommodate modular components to facilitate ease of assembly, cleaning, and future modifications. Compatibility with cable-driven actuation mechanisms was also essential to allow precise and repeatable motion control.

6.2 FIRST-GENERATION STAPLER JAW DESIGN

The initial jaw design employed a flexible slotted tube configuration, which permits bending along the longitudinal axis while maintaining structural continuity. The assembly included a flexible lower jaw with integrated slots for controlled bending, a corresponding flexible upper jaw to coordinate motion, and a flexible cartridge and knife assembly aligned with the jaw axis. Cable-driven actuation tendons were routed along the jaw to transmit motion from the handle to the tip. The design strategy was designed to balance flexibility and mechanical stability while minimizing the risk of overextension or permanent deformation. The CAD model of this

first-generation design is shown in Figure 6.1.

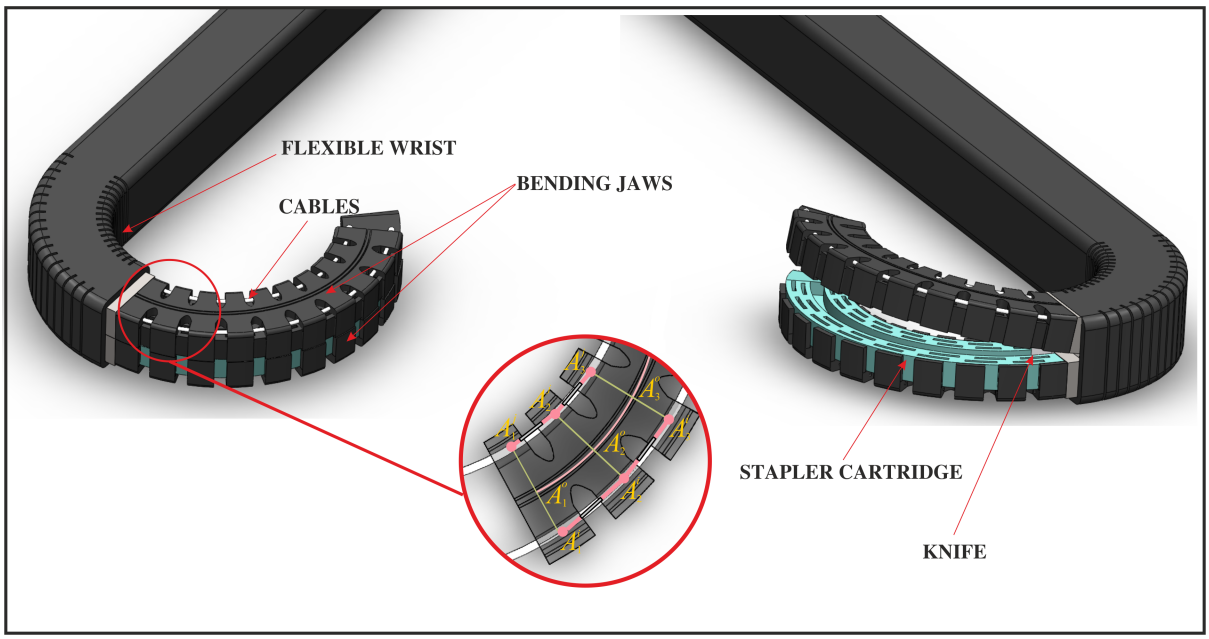

Fig. 6.1 *CAD model of the first-generation flexible stapler jaw.*

6.2.1 PROTOTYPE FABRICATION AND MATERIAL SELECTION

To evaluate mechanical behavior and validate design assumptions, a scaled-up prototype, twice the actual size, was fabricated using stereolithography (SLA) 3D printing. A mixture of flexible and rigid resins in a 20:80 volume ratio was used to emulate the compliance and stiffness of the intended design. This material combination was selected to provide sufficient flexibility for bending tests while maintaining the structural integrity of the jaw segments. The prototype enabled detailed observation of bending behavior, tendon routing, and mechanical response, as illustrated in Figure 6.2.

Table 6.1 *Material properties of 3D-printed parts*

Properties	**Values**
Density (ρ)	1290.57 kg/m^3
Ultimate Tensile Strength (UTS)	1.6416 MPa
Poisson's ratio (ν)	0.35
Young's Modulus (E)	4.83 MPa

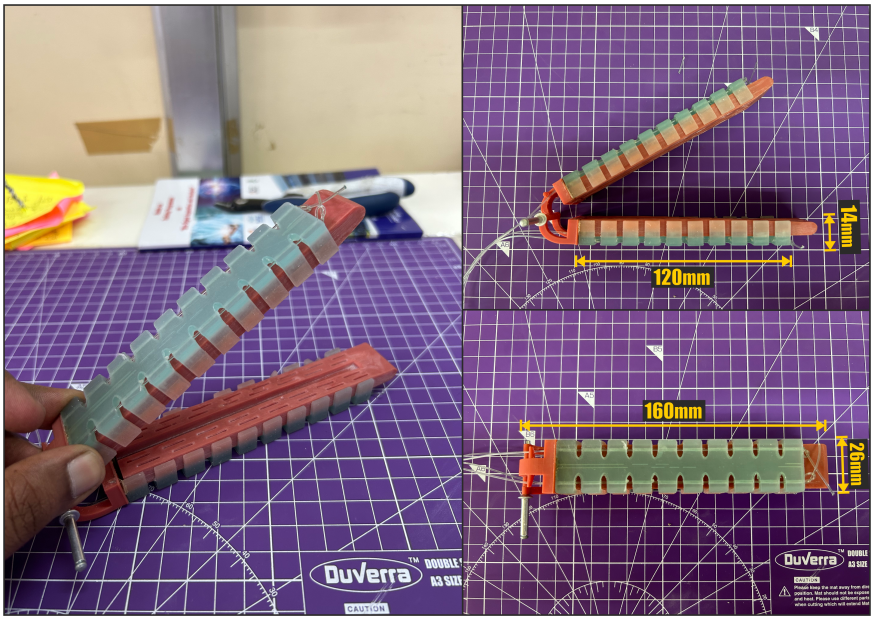

Fig. 6.2 *SLA 3D-printed prototype of the first-generation flexible jaw.*

6.2.2 EXPERIMENTAL EVALUATION

The bending performance of the first-generation prototype was assessed experimentally under variable loads. One tendon was loaded incrementally while the opposing tendon remained free. Optical tracking was used to measure the tip angular displacement (α) and its corresponding x and y coordinates. The experimental results revealed a linear relationship between the applied load and angular displacement, indicating predictable and controlled bending without sudden deflection or structural instability. The experimental setup is shown in Figure 6.3, and the recorded displacement and angle data are presented in Figure 6.4. These results confirmed that the slotted tube design could reliably achieve the desired range of motion under controlled loading conditions [101].

6.3 SECOND-GENERATION STAPLER JAW DESIGN

Although the first-generation jaw successfully demonstrated feasibility, several limitations were identified. The structure exhibited reduced rigidity under higher loads, which could compromise precise tissue compression. Control over the jaw tip orientation during insertion was limited, and integration of a removable anvil was challenging due to the continuous tube design. These observations motivated the development of a second-generation jaw that incorporated both flexibility and enhanced structural stability.

The second-generation design introduced a segmented solid-sectioned jaw connected by a flexible spine, allowing controlled articulation while preserving overall rigidity. The mechanical hinge was integrated to restrict the jaw's opening angle to 15 degrees, ensuring consistent deployment and preventing overstretching during use. Additionally, the previously fused anvil

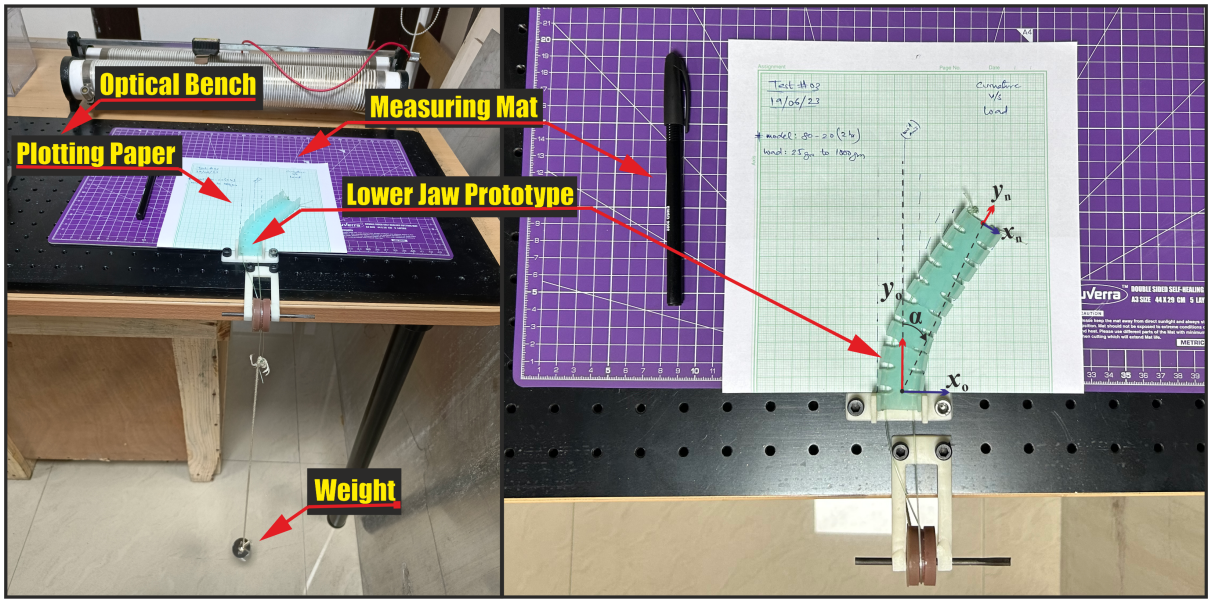

Fig. 6.3 *Experimental setup for testing the bending behavior of the first-generation jaw.*

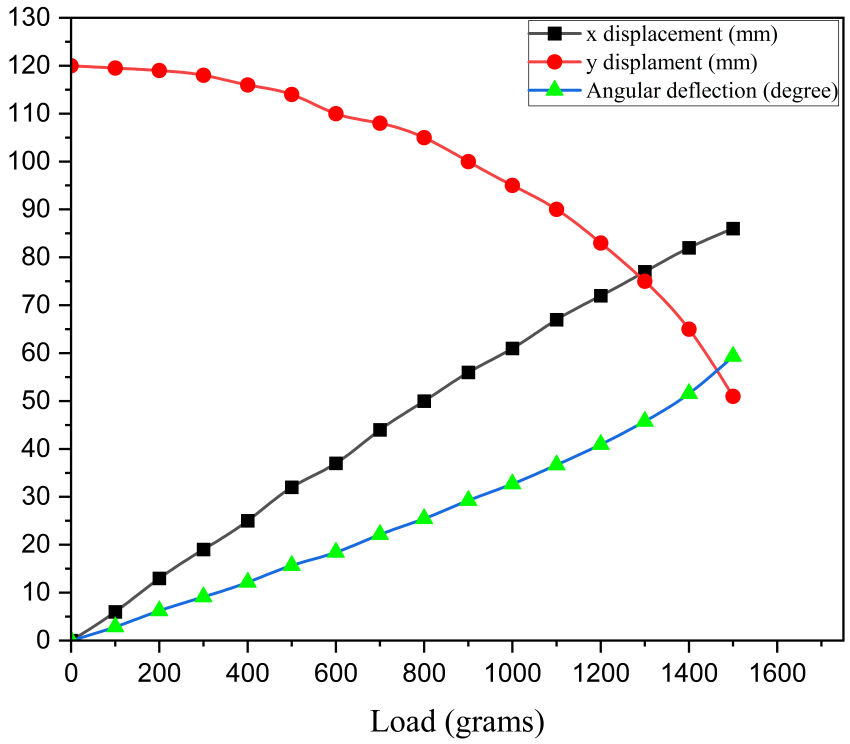

Fig. 6.4 *Experimental results showing angular displacement (α) and tip coordinates (x, y) versus applied load.*

was redesigned as a flexible, removable component, fitting within a newly developed flexible upper jaw. This modular configuration enhanced assembly, cleaning, and future adaptability, while enabling testing with different jaw configurations to further optimize design performance. The second-generation design is illustrated in Figure 6.5.

Table 6.2 *Table for load v/s deflection of the tip of the 3D-printed lower jaw prototype.*

Sl. No.	Load (g)	X Displacement (mm)	Y Displacement (mm)	Angular Deflection (α) (deg)
1	0	0	120	0
2	100	6	119.5	2.86
3	200	13	119	6.23
4	300	19	118	9.14
5	400	25	116	12.16
6	500	32	114	15.67
7	600	37	110	18.43
8	700	44	108	22.16
9	800	50	105	25.46
10	900	56	100	29.24
11	1000	61	95	32.70
12	1100	67	90	36.66
13	1200	72	83	40.94
14	1300	77	75	45.75
15	1400	82	65	51.59
16	1500	86	51	59.33

6.3.1 PROTOTYPE FABRICATION AND SCALING

Functional prototypes of the second-generation design were fabricated using SLA 3D printing, incorporating both rigid and flexible resins to accurately represent the mechanical behavior of the jaw segments. Two sets of prototypes were produced: one at actual size for functional evaluation in simulated surgical environments, and another scaled to 250% for detailed observation of kinematics, bending behavior, and actuation response. The comparison of the original and scaled-up models is shown in Figure 6.6, while the bending capability of the jaw is depicted in Figure 6.7.

6.3.2 KINEMATIC AND STRUCTURAL CONSIDERATIONS

The second-generation jaw maintained the functional principles of the first design while improving control and rigidity. The flexible spine allowed smooth bending along the jaw length, guiding the tip along the intended trajectory. The mechanical hinge ensured reproducible opening angles during tissue engagement, while the cable-driven actuation system provided a low-friction transmission of force for precise tip control. The modular anvil design facilitated experimentation with different jaw configurations and allowed iterative improvements without requiring complete redesigns of the entire assembly. These design enhancements collectively contributed to a more robust, controllable, and versatile stapler jaw suitable for minimally invasive surgical procedures.

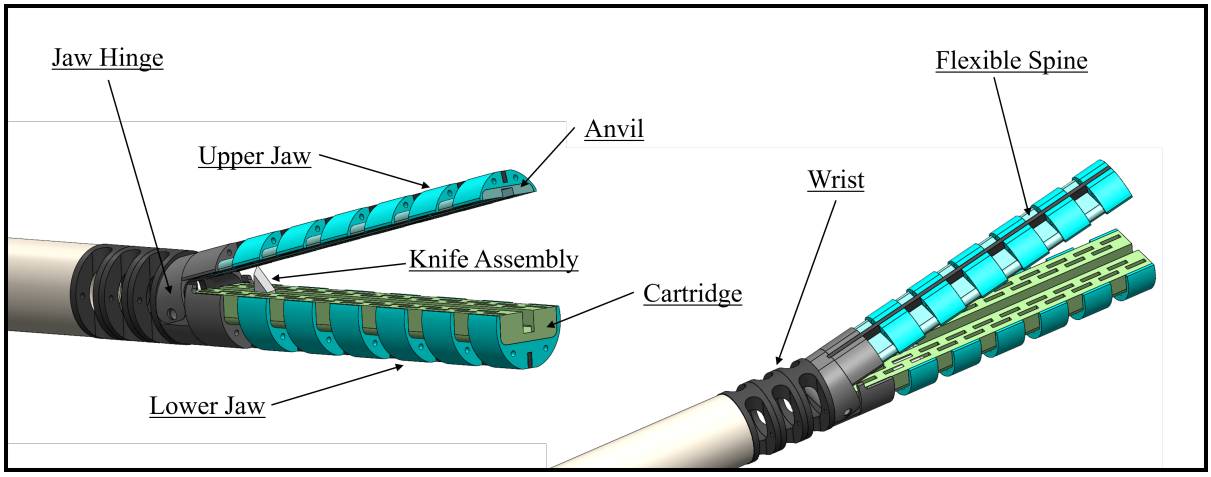

Fig. 6.5 *Second-generation flexible stapler jaw with segmented solid sections joined by a flexible spine.*

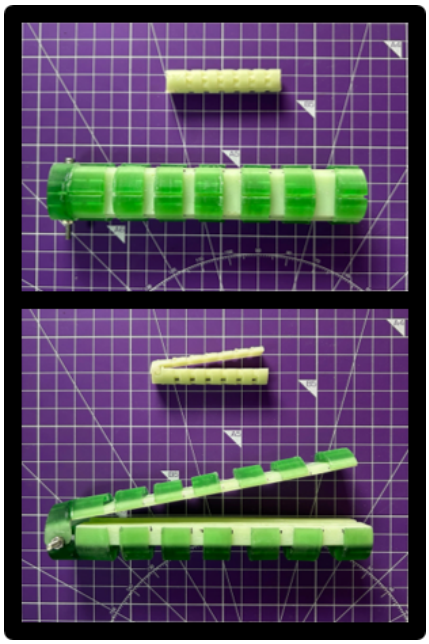

Fig. 6.6 *Comparison of actual-size and 250% scaled-up 3D-printed prototypes of the second-generation jaw.*

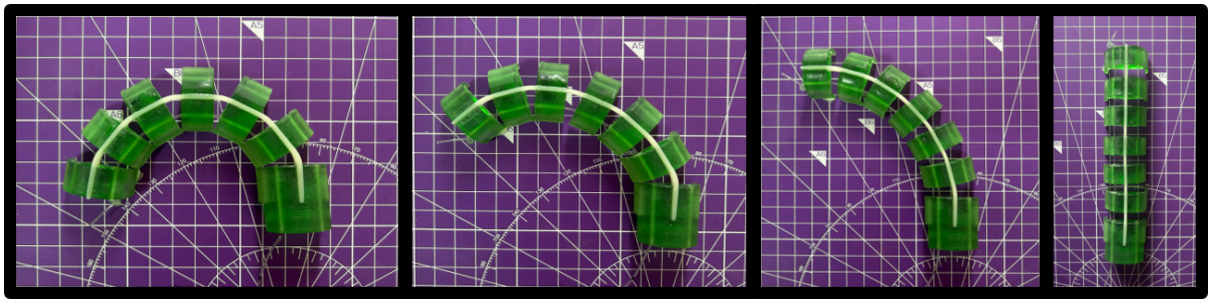

Fig. 6.7 *Demonstration of the bending capability of the second-generation jaw using the 3D-printed prototype.*

6.4 STAPLER WRIST DESIGN

A multi-segmented wrist mechanism was developed to provide controlled articulation within the spatial constraints of minimally invasive surgical procedures. The wrist employs flexural hinges, which achieve motion through elastic deformation rather than discrete mechanical joints. This approach offers several advantages, including frictionless operation, high precision, and reduced mechanical complexity, making it particularly suitable for compact surgical tools. Unlike conventional flexure geometries, the proposed wrist design features a tailored arrangement of hollow cylindrical segments with semi-circular cuts. To ensure predictable bending behavior and structural stability, a detailed mechanical analysis was conducted, focusing on the area moment of inertia about the principal axes, I_{xx} and I_{yy}. This analysis enabled the prediction of directional stiffness and deformation under external loading, ensuring the wrist provides sufficient compliance while maintaining stability during actuation.

6.4.1 MATHEMATICAL FORMULATION

6.4.1.1 Geometric Parameters

The wrist segment consists of a hollow cylindrical element with a semi-circular cut, as illustrated in Figure 6.8. The primary geometric parameters considered in the analysis include the inner radius R_i, outer radius R_o, flexure hinge width w, flange thickness T, and cut radius R_c, along with the cut offset s, the length of the cut L, applied force F, and the material's Young's modulus E (Figure 6.9). These parameters define the segment geometry and serve as inputs for subsequent bending and stiffness calculations.

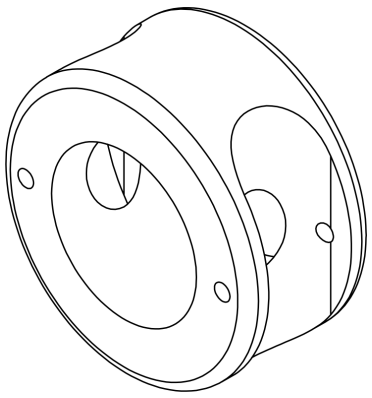

Fig. 6.8 *Single wrist segment with a flexural hinge.*

6.4.1.2 Area Moment of Inertia

To evaluate bending performance, the wrist segment is divided longitudinally into three regions. Regions 1 and 3 are uniform hollow cylinders, for which the area moment of inertia is calculated

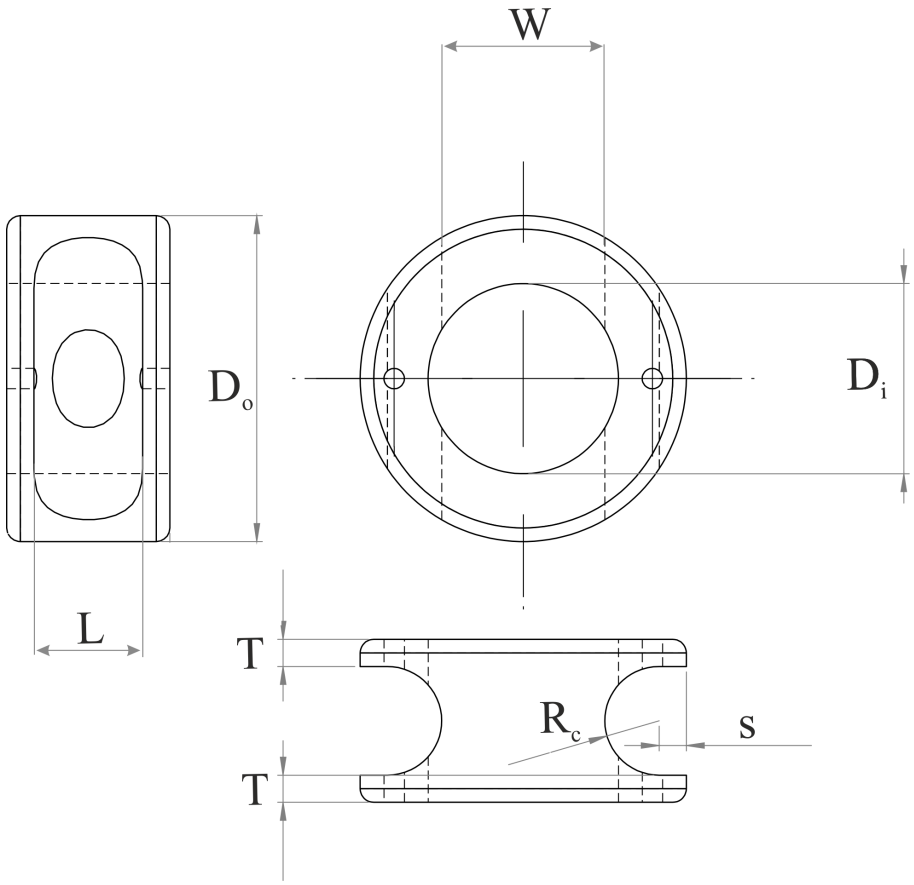

Fig. 6.9 *Key dimensions of the wrist segment used in bending analysis.*

using standard formulas:

$$I_{\text{R1}} = I_{\text{R3}} = \frac{\pi}{64}(D_o^4 - D_i^4) \tag{6.1}$$

These regions are symmetric, leading to $I_{xx} = I_{yy}$. Cable holes are sufficiently small relative to the segment cross-section, allowing their influence on the moment of inertia to be neglected. Region 2, corresponding to the flexural cut, has a variable cross-section along its length, requiring a more detailed computation. Using vertical strips of width dx and height $H(x)$, the area moment of inertia about the y-axis is given by:

$$H(x) = \begin{cases} \sqrt{R_o^2 - x^2}, & R_i < x < R_o \\ \sqrt{R_o^2 - x^2} - \sqrt{R_i^2 - x^2}, & 0 < x < R_i \end{cases} \tag{6.2}$$

The segment is symmetric about both axes, so only one-quarter of the cross-section is considered. The area moment of inertia along the segment length L is then calculated as:

$$I_{yy}(l) = \begin{cases} 4\int_0^{R_i} x^2 \left(\sqrt{R_o^2 - x^2} - \sqrt{R_i^2 - x^2}\right) dx + 4\int_{R_i}^{R_X} x^2 \sqrt{R_o^2 - x^2} dx, & R_i < R_X \\ 4\int_0^{R_X} x^2 \left(\sqrt{R_o^2 - x^2} - \sqrt{R_i^2 - x^2}\right) dx, & R_X \leq R_i \end{cases} \tag{6.3}$$

where $R_X = R_o - X_l - s$ and $X_l = \sqrt{R_c^2 - (l - R_c)^2}$, as shown in Figure 6.10. Similarly, the area moment of inertia about the x-axis, I_{xx}, is computed using horizontal strips of width $W(y)$ and height dy to account for the variable geometry:

$$I_{xx} = 4\int_0^R y^2 \cdot W(y)\, dy$$

with

$$I_{xx}(l) = 4\int_0^r W(y) \cdot y^2\, dy + 4\int_r^R \min\left(X_c(l), X_R(y)\right) \cdot y^2\, dy$$

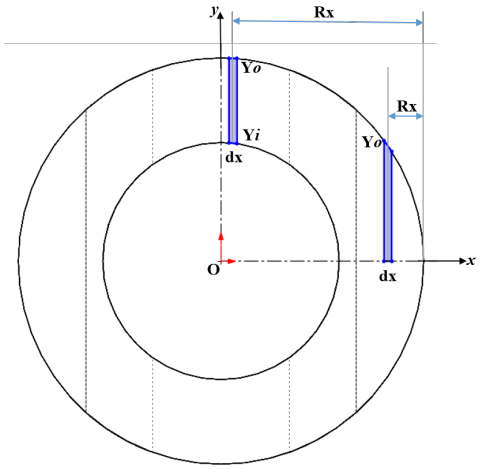

Fig. 6.10 *Cross-sectional area considered for I_{yy} calculation.*

6.4.2 ANGULAR DEFLECTION OF A SINGLE SEGMENT

The angular deflection of a single segment under an applied transverse force F is computed independently for each region, with the total deflection obtained by summing contributions from Regions 1, 2, and 3:

$$\theta_{\text{R1}} = \frac{F(L + 2T)T}{EI_{\text{R1}}}, \quad \theta_{\text{R3}} = \frac{FT^2}{EI_{\text{R3}}}, \quad d\theta(l) = \frac{F(L + T - l)dl}{EI(l)} \tag{6.4}$$

The cumulative deflection of the segment is then:

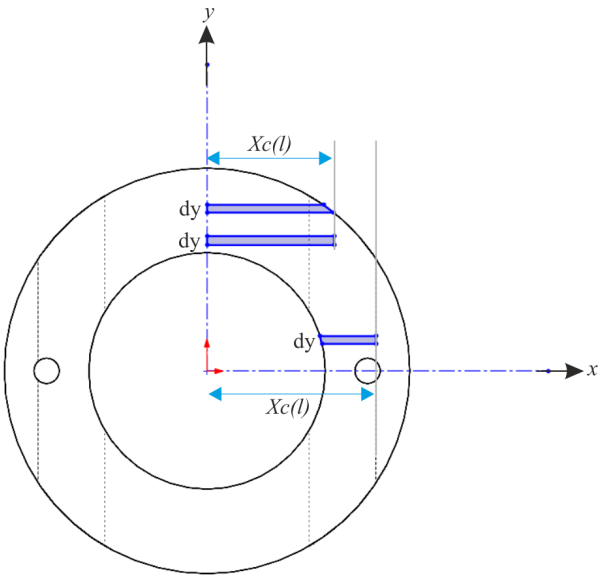

Fig. 6.11 *Cross-sectional area considered for I_{xx} calculation.*

$$\theta = \theta_{\mathrm{R1}} + \int_0^L d\theta(l)\, dl + \theta_{\mathrm{R3}} \tag{6.5}$$

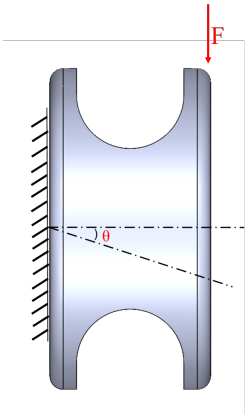

Fig. 6.12 *Schematic of angular deflection in a single wrist segment under applied load F.*

6.4.3 MULTISEGMENT DEFLECTION

In the multi-segmented wrist, uniform bending along all segments is desirable for predictable tip motion. To achieve this, a second cable is routed along the opposite side of the central axis, terminating at the penultimate segment. This arrangement produces equal bending moments at the base of each segment (Figure 6.13), ensuring uniform angular deflection:

$$\theta_{seg} = \frac{M_{seg}\, L}{EI} \tag{6.6}$$

While this requires twice the number of cables and applied force compared to a single-cable design, the necessary actuation force (35 N) remains well below typical human grip forces, making the design feasible for compact surgical wrists.

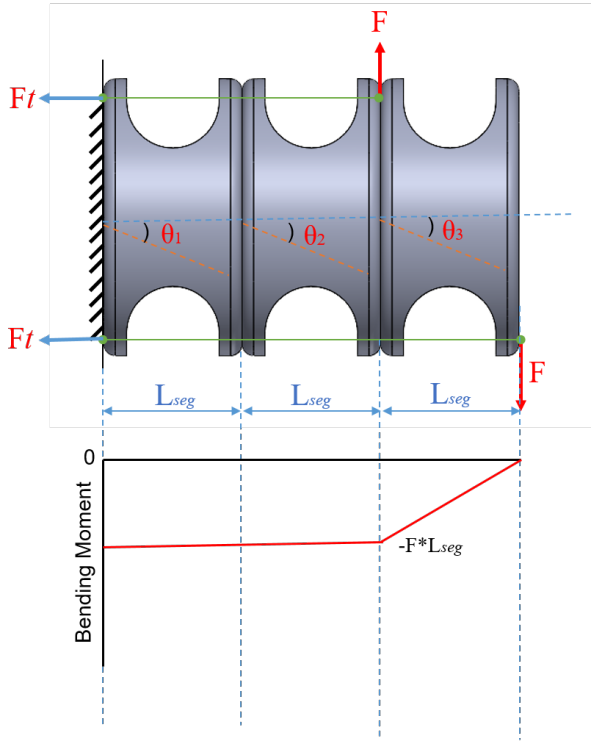

Fig. 6.13 *Bending moment distribution for a multi-segment wrist under load.*

6.4.4 FORCE OPTIMIZATION USING MATLAB

To minimize the required actuation force while achieving a target deflection θ_{target}, optimization of the flexural hinge geometry was performed. Flange thickness T and hinge width w were varied within physical and manufacturing constraints. The total angular deflection of a single segment was calculated as:

$$\theta_y = \theta_{R1} + \theta_{R3} + \int_0^L \frac{F(L+T-l)}{E \cdot I_{yy}(l)}\, dl$$

Using MATLAB's `fmincon` function with the Sequential Quadratic Programming (SQP) algorithm, the optimal combination of T and w that maximized bending while minimizing actuation force was determined. The required force was then scaled relative to the target deflection.

6.4.5 EXPERIMENTAL VALIDATION

A scaled prototype of the wrist segment was manufactured at twice its original dimensions using stereolithography (SLA) 3D printing. The printing material consisted of a blend of flexible and rigid resins in an 80:20 ratio, resulting in an effective Young's modulus of $E = 4.83$ MPa. To evaluate the mechanical response, incremental loads up to 1400 grams were applied to one end of the segment while the opposite end was constrained. Angular deflections were recorded for each loading condition (Figure 6.14). The experimentally measured deflections exhibited strong agreement with the theoretical predictions, as presented in Table 6.3 and illustrated in Figure 6.15. These results validate the underlying mathematical model, the assumed material properties, and the numerical integration approach employed.

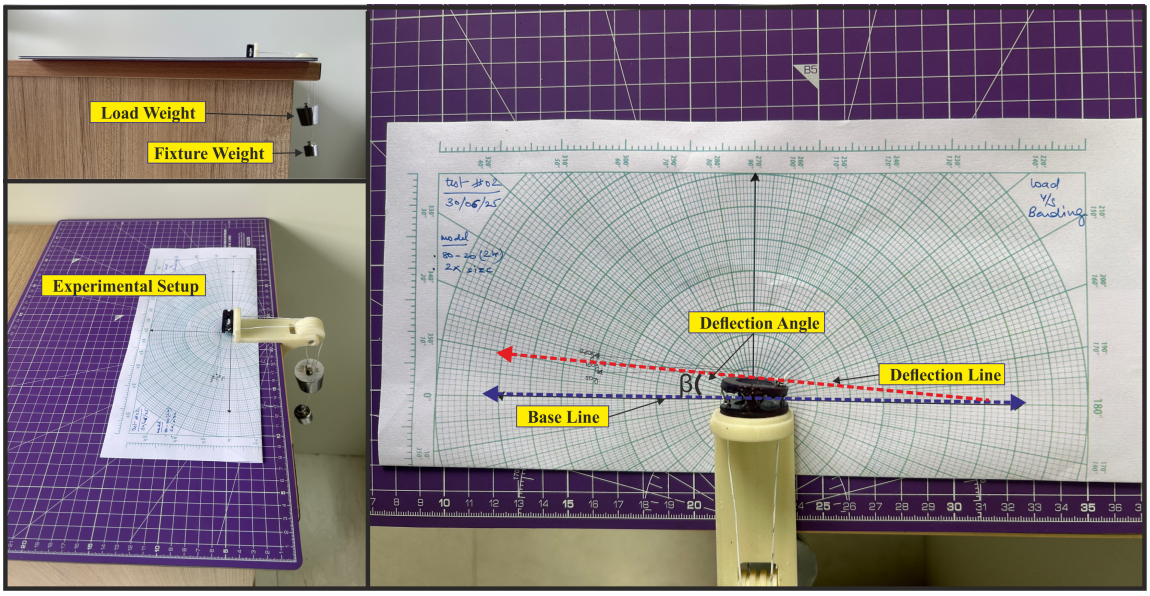

Fig. 6.14 *Experimental setup for measuring angular deflection of a single wrist segment.*

6.5 STAPLER ACTUATION MECHANISM

Following the successful development of the jaw and wrist mechanisms, attention was directed towards designing an integrated handheld instrument capable of housing, supporting, and actuating these subsystems. This instrument, referred to as the *stapler gun*, was conceptualized to enable intuitive single-handed operation while maintaining mechanical precision, ergonomic comfort, and full functional control over all subsystems. The design objectives included minimizing the user's physical effort, ensuring accurate translation of applied forces to the jaw and wrist mechanisms, and enabling repeated operation without mechanical degradation. The complete device, highlighting its major components and actuation interfaces, is illustrated in Figure 6.16.

The primary actuation lever is responsible for firing the staple pins as well as deploying the integrated cutting knife. The lever is ergonomically positioned for engagement using the palm

Table 6.3 *Experimental vs Calculated Angular Deflection for Wrist Segment*

Load (grams)	Experimental (°)	Calculated (°)
0	0	0
50	1	1.08
100	2	2.15
200	4	4.30
300	6	6.45
400	9	8.60
500	10	10.75
600	14	12.90
700	15	15.05
800	17	17.21
900	20	19.36
1000	21	21.51
1100	23	23.66
1200	25	25.81
1300	28	27.96
1400	30	30.11

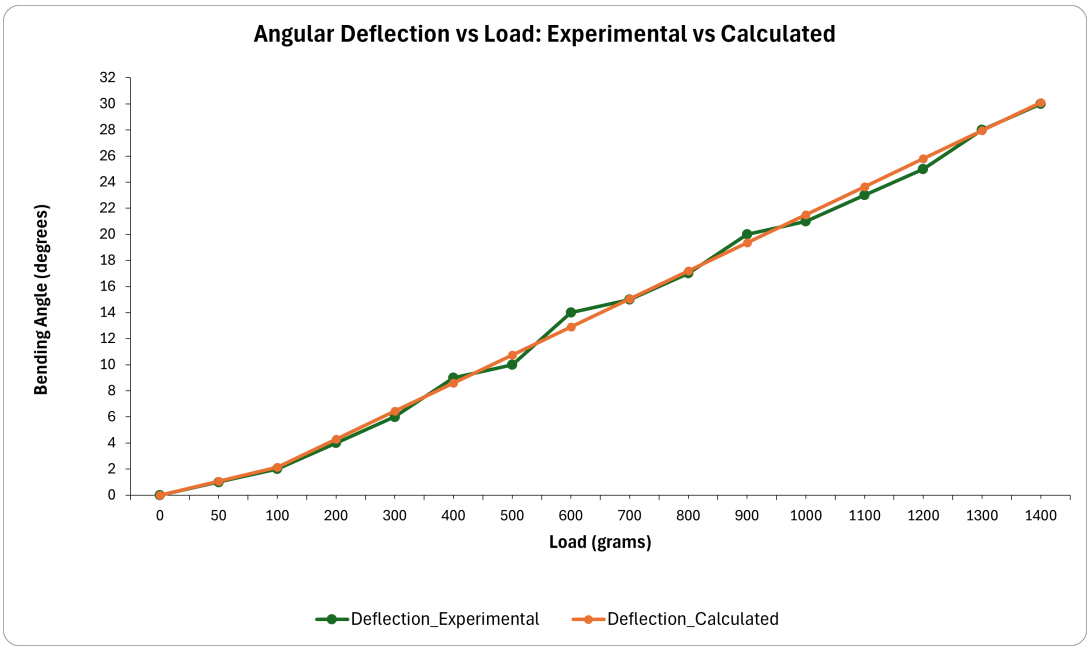

Fig. 6.15 *Comparison of experimental and calculated deflections for wrist segment under applied load.*

and fingers, allowing controlled actuation with minimal hand fatigue. The thumb-operated knob provides articulation of the jaw, permitting up to 180° of bending in either direction, whereas the wrist roller, manipulated by the index finger, enables up to 90° of angular motion in both directions. Axial rotation of the front assembly, facilitated through a spindle mechanism, allows 180° rotation in either direction. Finally, a retraction slider returns the knife to its original position after firing, enabling the device to be reset quickly for subsequent operations.

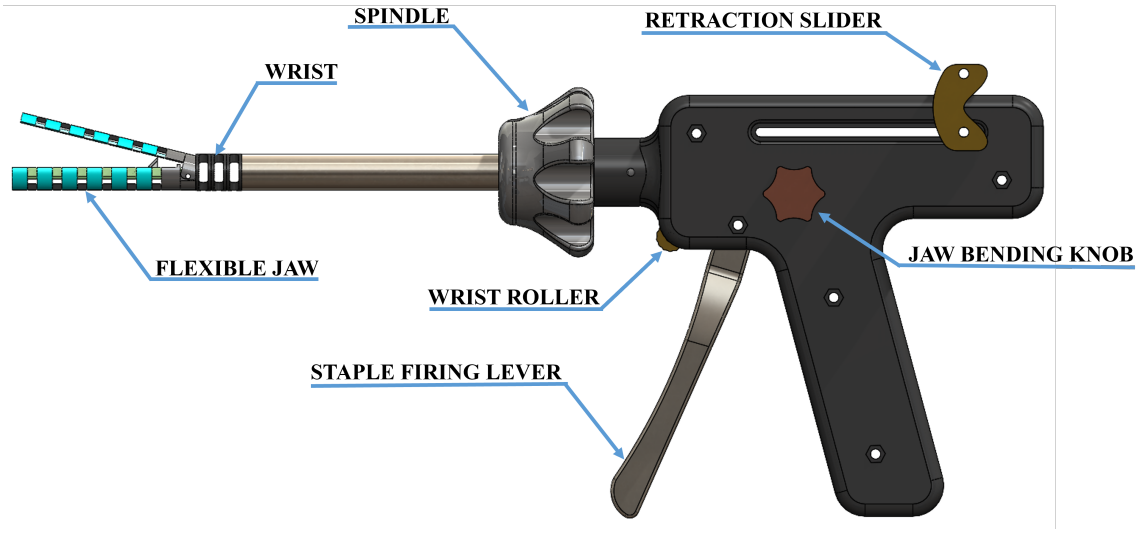

Fig. 6.16 *Complete design of the surgical stapling instrument, showing all major components and actuation interfaces.*

The combination of these mechanisms ensures that the stapler gun provides comprehensive control over the position and orientation of the distal end while maintaining a compact form factor suitable for minimally invasive procedures.

6.5.1 TRANSMISSION ASSEMBLY

To achieve reliable and precise actuation, the stapler gun utilizes dedicated cable-based transmission systems for each functional subsystem. For stapler firing and knife deployment, a *ratchet-and-pawl mechanism* was coupled with a *compound pulley train* featuring an overall pulley ratio of 1:6. This configuration ensures mechanical advantage and actuation speed amplification while keeping the required input displacement within ergonomic limits. Full actuation of the stapling and cutting mechanism requires a cable displacement of 25 mm, which corresponds to a 180° angular rotation of the output pulley. This arrangement guarantees consistent staple deployment with minimal input force while also preventing unintentional misfires.

Jaw and wrist articulation mechanisms employ a compound transmission based on a *worm-and-worm wheel assembly* coupled with output pulleys. For jaw articulation, the thumb-operated knob is directly connected to a worm gear system with a gear ratio of 16:1, enabling full jaw deflection with only 6.13 mm of cable displacement. This corresponds to a 45° angular rotation of the output pulley, providing sufficient motion for tissue manipulation without exceeding the elastic limits of the jaw flexures. Similarly, wrist actuation utilizes an Iworm gear-based transmission system with a 9:1 gear ratio, operated via a roller, and actuated using an Index Finger, allowing precise control over the wrist rotation with 9.23 mm cable displacement, achieved by the angular rotation of 60° from the neutral position of the output pulley. This design ensures that both subsystems operate smoothly under low input forces while maintaining mechanical

integrity over repeated cycles.

The selection of pre-tensed cable-based transmissions was motivated by their high flexibility, low mechanical backlash, and the ability to route forces through confined geometries without adding significant bulk. The compound pulleys and worm gear assemblies also provide intrinsic locking capabilities, preventing undesired movement of the distal mechanisms when the actuating force is removed.

6.5.2 MATHEMATICAL REPRESENTATION OF STAPLER FIRING, JAW, AND WRIST TRANSMISSION ASSEMBLIES

The torque transmission mechanisms of the stapler firing, jaw articulation, and wrist articulation differ in their input actuation but converge at the principle of converting human-applied forces into cable tensions at the distal end. To distinguish them, subscripts s, j, and z are used for the stapler firing, jaw, and wrist assemblies, respectively. Figure 6.17 depicts the actuation sub-assemblies for the surgical stapler.

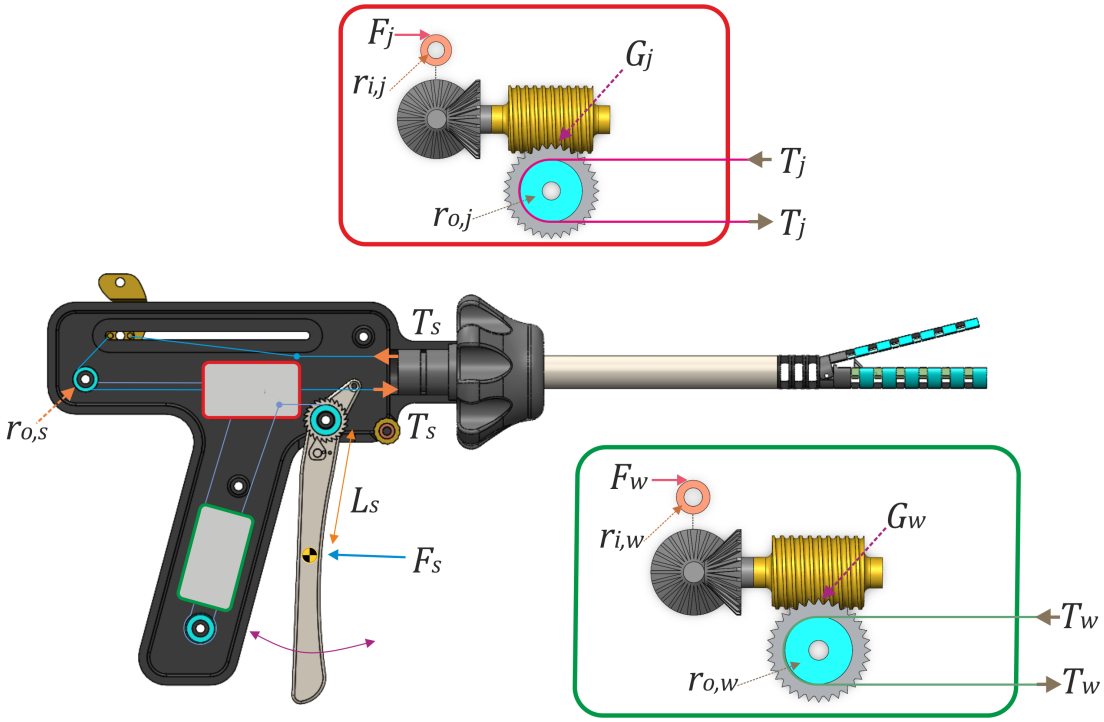

Fig. 6.17 *Actuation Sub-assemblies for the surgical stapler*

Stapler Firing Assembly

The stapler firing mechanism is actuated by a hand-operated lever of effective length L_s, pivoted at one end. When a grip force F_s is applied at the lever, it generates a torque about the pivot:

$$\tau_{in,s} = F_s \cdot L_s \tag{6.7}$$

This torque is transmitted via a pawl–ratchet system to the input pulley of radius $r_{i,s}$. Through a two-stage pulley train with overall ratio $G_{p,s}$ (with $G_{p,s} < 1$ since the pulley train provides a torque reduction while amplifying displacement speed) and efficiency $\eta_{p,s}$, the output torque becomes

$$\tau_{o,s} = \tau_{in,s} \cdot G_{p,s} \cdot \eta_{p,s} \tag{6.8}$$

The final stage is the output pulley of radius $r_{o,s}$, where torque is converted into cable tension:

$$T_s = \frac{\tau_{o,s}}{r_{o,s}} \tag{6.9}$$

Thus, the cable tension for the stapler firing system is

$$T_s = \frac{F_s \cdot L_s \cdot G_{p,s} \cdot \eta_{p,s}}{r_{o,s}} \tag{6.10}$$

Jaw Assembly

For the jaw articulation mechanism, the actuator knob of radius $r_{i,j}$ is subjected to a tangential input force F_j, producing torque

$$\tau_{in,j} = F_j \cdot r_{i,j} \tag{6.11}$$

This torque is transmitted through a $1:1$ bevel gear stage:

$$\tau_{b,j} = \tau_{in,j} \tag{6.12}$$

The worm–worm wheel stage with gear ratio G_j and efficiency η_j modifies the torque:

$$\tau_{w,j} = \tau_{b,j} \cdot G_j \cdot \eta_j \tag{6.13}$$

At the output pulley of radius $r_{2,j}$, cable tension is given by

$$T_j = \frac{\tau_{w,j}}{r_{o,j}} = \frac{F_j \cdot r_{i,j} \cdot G_j \cdot \eta_j}{r_{o,j}} \tag{6.14}$$

Wrist Assembly

The wrist articulation system follows the same pathway as the jaw assembly. For an input force F_w applied at knob radius $r_{i,w}$, the final cable tension is

$$T_w = \frac{F_w \cdot r_{i,w} \cdot G_w \cdot \eta_w}{r_{o,w}} \tag{6.15}$$

This formulation highlights the distinct input mechanisms: a lever–pulley transmission for stapler firing, and knob-driven worm–wheel transmissions for jaw and wrist bending. Despite these differences, all subsystems share the common principle of torque transformation followed by cable tension generation.

By linking ergonomic input forces (F_s, F_j, F_w) with distal cable tensions, the model allows systematic validation against human physiological capabilities, ensuring that stapler firing remains feasible with grip strength, while jaw and wrist articulation remain smooth and fatigue-free using the Thumb and Index Finger, respectively.

6.5.3 ACTUATION FORCES AND ERGONOMICS

Ergonomic considerations were integral to the design of the stapler gun, with each actuation control strategically mapped to different parts of the hand to maximize operator comfort and control. Biomechanical data indicate that an average human male can generate a grip force of approximately 334 N, whereas females can exert around 179 N [102]. Considering these physiological limits, the actuation lever, which governs both stapling and knife deployment, was designed to require a maximum tissue dissection force of 12 N. This value is well within the operator's comfortable exertion range and ensures that repeated actuation does not cause hand fatigue.

The thumb-controlled jaw knob is capable of generating tangential forces of up to 62 N for males and 51 N for females [103, 104]. With this input, the system delivers a cable tension of up to 360 N, sufficient to bend the jaw over its full intended range. For wrist articulation, the index-finger roller can apply forces of 45 N for males and 40 N for females [105, 106], producing cable tensions up to 400 N. Both subsystems thus operate safely below human physiological limits while achieving the necessary mechanical deflections, ensuring consistent performance even during prolonged surgical procedures (Figure 6.18).

Additionally, the design of the transmission system accounts for mechanical efficiency and energy losses. Friction in the pulleys and worm gears was minimized through careful material selection and surface finishing, ensuring smooth motion. Furthermore, the placement of cables and gear interfaces was optimized to reduce angular misalignment, torsional stress, and

hysteresis during repeated actuation cycles. The system's modular construction also allows easy maintenance, replacement of worn components, and adjustments to accommodate varying patient anatomies or surgical scenarios.

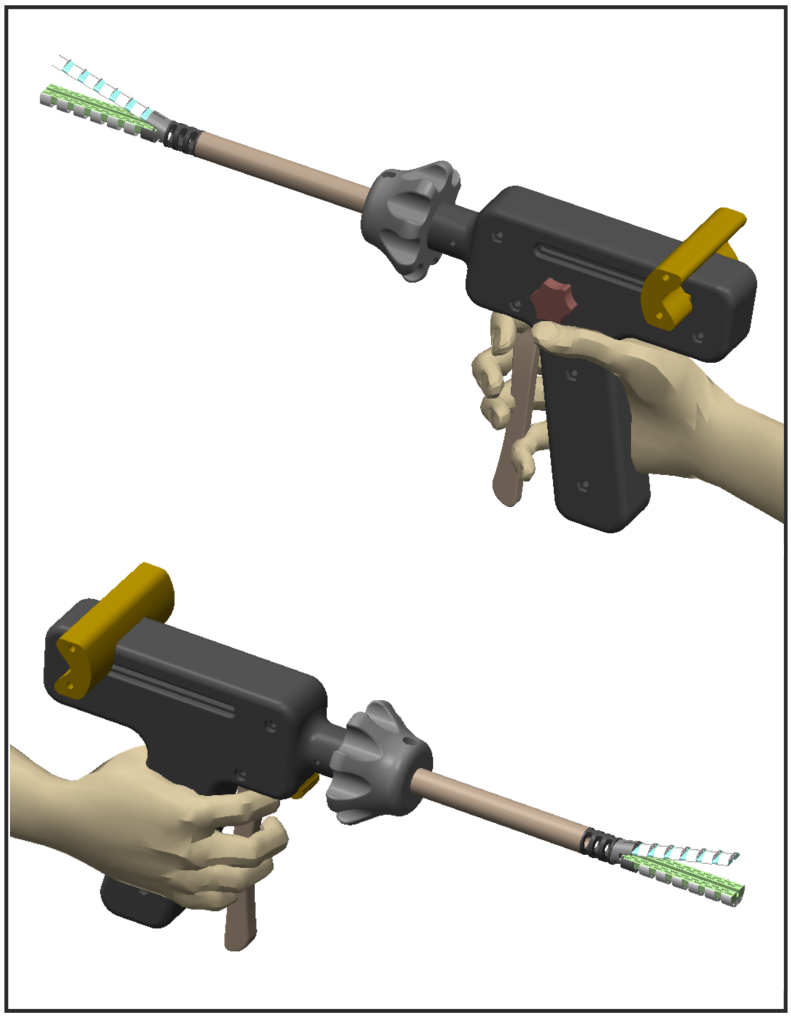

Fig. 6.18 *Surgical Stapler with Ergonomic Handheld Design*

6.5.4 FORCE ANALYSIS AND SAFETY MARGINS

The forces required for operating the stapler gun were evaluated considering both maximum actuation needs and safety margins. Calculations indicate that the actuation lever requires only 3.5% of the average male gripping force and 6.7% of the average female grip strength, providing ample safety margin to prevent operator fatigue [107]. Similarly, jaw and wrist actuation demand forces well below the maximum capabilities of the human hand, ensuring that mechanical failure or hand strain is highly unlikely. These considerations are critical for minimally invasive surgery, where precise control of delicate tissue is essential, and inadvertent overexertion could compromise patient safety.

6.6 ERGONOMIC EVALUATION OF DESIGN FROM SURGEONS

The ergonomic assessment of the stapler handle design commenced with the fabrication of an initial prototype, designated as *Prototype Noir* (Figure 6.19). This version incorporated two actuation levers positioned side by side. However, this configuration was rapidly identified as ergonomically suboptimal. The side-by-side placement of the levers impeded intuitive handling, constrained natural hand movements, and complicated the actuation process. Consequently, the design was deemed unsuitable for practical use and was excluded from further development.



Fig. 6.19 *First 3D printed prototype,* ***Prototype Noir***

To systematically address these limitations, a second prototype, named *Prototype Christmas*, was developed (Figure 6.20). This model incorporated modular elements that enabled direct assessment of user comfort and accessibility through variations in control placement. The design included two levers of different lengths—one short and one long—two possible thumb knob positions, and four alternative rotation knob positions. In addition, a roller located beneath the handle was tested. This modularity provided a structured approach for evaluating surgeon

interaction with the device and identifying the most ergonomic configuration.

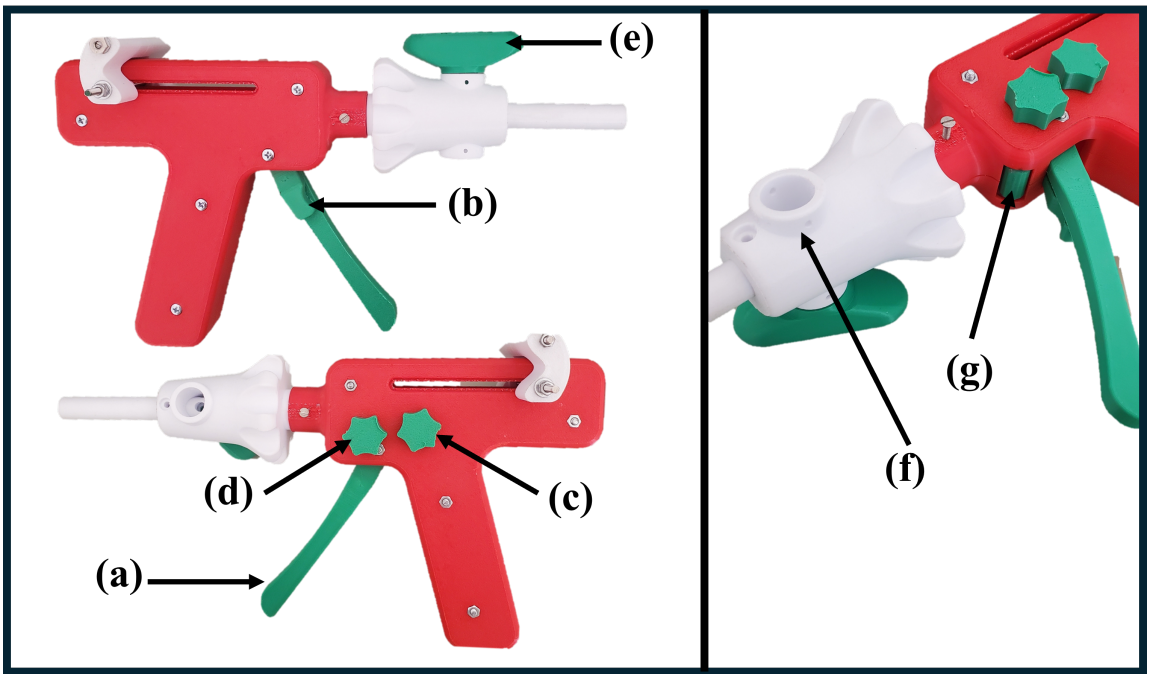

Fig. 6.20 *Second 3D-printed prototype,* ***Prototype Christmas****, showing its key components: (a) long trigger, (b) short trigger, (c) thumb knob in position 1, (d) thumb knob in position 2, (e) rotation knob in position 1, (f) rotation knob in position 2, and (g) roller under the handle.*

The evaluation process engaged a panel of sixteen digestive surgeons practicing visceral surgery, with one quarter being women and one quarter left-handed. The average glove size was 7 (median 7, range 6–7.5), serving as a standardized proxy for hand anthropometry. The cohort represented a broad spectrum of surgical experience, including interns in the basic internship phase and advanced internship phase, junior doctors in years one and two (DJ1 and DJ2), Chef de Clinique Assistants (CCA/assistants), and senior consultants such as Praticiens Hospitaliers (PH) and Professeurs des Universités–Praticiens Hospitaliers (PU-PH), both specialized and non-specialized in colorectal surgery. Ten of the participants had at least DJ2-level training, ensuring sufficient expertise in rectal stapling procedures.

Testing was conducted using structured questionnaires with Likert scales, complemented by free comments. These surveys captured both anthropometric and professional profiles of the surgeons, alongside detailed ergonomic feedback on handle, triggers, and control mechanisms. Overall, accessibility of the controls was deemed satisfactory, with up to 93% of surgeons finding some buttons easy to reach and 81% considering them practical or very practical (Table 6.4). However, accessibility did not always translate into practicality, and significant ergonomic shortcomings were noted.

Surgeons indicated that staplers are most commonly introduced via the right iliac fossa trocar during laparoscopic rectal surgery. While most surgeons operated with their dominant hand,

some alternated between both hands depending on case complexity. Rectal stapling was generally considered moderately difficult, with anatomical and clinical factors such as a narrow pelvis, obesity, low tumors, and prior radiotherapy consistently reported as increasing technical difficulty. These realities provided essential context for evaluating *Prototype Christmas*.

User feedback regarding the handle design revealed notable variability. While some participants considered the overall size to be functional, others described it as excessively bulky and angular, thereby limiting its suitability for users with smaller hands. In the evaluation of the trigger system, the long lever was accessible to approximately 75% of participants; however, only half found it practical. Its operation often required engagement of the third or fourth fingers and interfered with the use of the short lever. The short lever, although easier to reach, was generally deemed impractical for consistent use. Preferences regarding lever functionality were divided: some participants favored the short lever for jaw closure due to its accessibility, whereas others preferred the long lever for its mechanical advantage.

The evaluation of the rotation control mechanisms yielded conclusive insights. The knob located distally from the handle (Position 1) was frequently reported as inaccessible or impractical, particularly by surgeons with smaller hands. Additional concerns included excessive friction and unfavorable actuation angles. In contrast, the proximally positioned knob (Position 2) was consistently rated as the most ergonomic, offering universal accessibility and ease of use. Although the roller situated beneath the handle presented operational challenges—primarily due to finger length limitations and friction—it was recognized as a promising alternative, contingent upon future redesigns to increase its size and reduce resistance.

One-handed operation was judged feasible but not optimal. While a few participants managed the device entirely with one hand, most considered it nearly manageable but limited by handle bulk, distal control placement, and interference between levers.

Table 6.4 *Summary of ergonomic evaluations for the* ***Prototype Christmas***

Category	**Response option**	**Distribution**
	Participant Demographics	
Gender	Female	75%
	Male	25%
Hand dominance	Right-handed	75%
	Left-handed	25%
Glove size (hand size)	Size 7	56.3%
	Size 7.5	37.5%
Professional status	Resident – IPS	12.5%
	Resident – IPA	25%

Category	Response option	Distribution
	DJ1	18.8%
	DJ2	12.5%
	CCA / Assistant	25%
	PH / PU-PH (spec./non-spec.)	6.2%
	Surgical Context	
Trocar used for stapling	Right iliac fossa	100%
Hand use during stapling	Dominant hand only	44%
	Both hands	66.7%
	With assistance	44%
Perceived stapling difficulty	Easy	11.1%
	Moderate	77.8%
	Difficult	11.1%
	Ergonomic Evaluation	
Handle size	Appropriate	50%
	Slightly too large	50%
Long trigger	Accessible	90%
	Comments	Requires 3rd–4th fingers; interferes with short trigger
Short trigger	Accessible	81.3%
	Judged impractical	62.5%
Jaw closure preference	Short trigger	50%
	Long trigger	37.5%
Articulation preference	Trigger / Wheel or button	Mixed (no consensus)
Thumb knob (close, Pos. 1)	Accessible	Universally accessible; preferred
Thumb knob (far, Pos. 2)	Inaccessible	Often inaccessible; friction issues
Rotation knob (far, Pos. 1)	Inaccessible	Fails Single Hand Operation
Rotation knob (close, Pos. 2)	Inaccessible	Fails Single Hand Operation
Roller under handle	Inaccessible	Poor accessibility; suggested larger size
One-hand usability	Perfect	13.3%

Category	Response option	Distribution
	Almost perfect	53.3%
	Moderate–Difficult	33.3%

6.6.1 DESIGN INTEGRATION

The final stapler design emerged through the integration of mathematical modeling, ergonomic force analysis, and surgeon evaluation into a unified instrument architecture. The mathematical representation of the firing, jaw, and wrist transmissions established the relationships between ergonomic input forces and distal cable tensions, ensuring that the required torques and deflections could be achieved within the physiological capabilities of the hand. This modeling guided the selection of lever arms, pulley ratios, and worm–wheel assemblies to balance mechanical advantage with compactness and smooth operation.

Force and safety analyses further validated these transmission pathways, demonstrating that actuation demands represent only a small fraction of human gripping, thumb, and finger strengths. These results confirmed that the instrument can be operated reliably without fatigue while maintaining wide safety margins against overexertion. Ergonomic mapping of controls—lever, thumb knob, and index-finger roller—distributed actuation responsibilities across different digits, enabling efficient single-handed operation.

Based on the structured evaluation and comprehensive feedback for the ergonomics from the surgeons, the final prototype underwent significant refinements. The distal rotation knob was removed to streamline operation and ensure true one-handed usability, while the proximal thumb knob was retained at the preferred position for improved handling. Between the two levers, the long lever was selected for its functional advantages, with the short lever eliminated. The grip profile was reshaped to enhance comfort and accommodate a wider range of hand sizes.

By systematically combining validated mechanical models, quantitative force analysis, and ergonomic evaluation, the final stapler gun design integrates the firing, jaw, and wrist mechanisms into a robust, modular, and user-friendly device. Figure 6.21 summarizes the implemented solution by illustrating the complete cable-based transmission network and how the modeled torques and tensions are routed to achieve stapler firing, jaw bending, and wrist articulation. This convergence of analytical, experimental, and user-centered insights—together with surgeon feedback—ensures that the instrument is mechanically sound while achieving the required precision, repeatability, safety margins, and practical usability for minimally invasive surgical procedures.

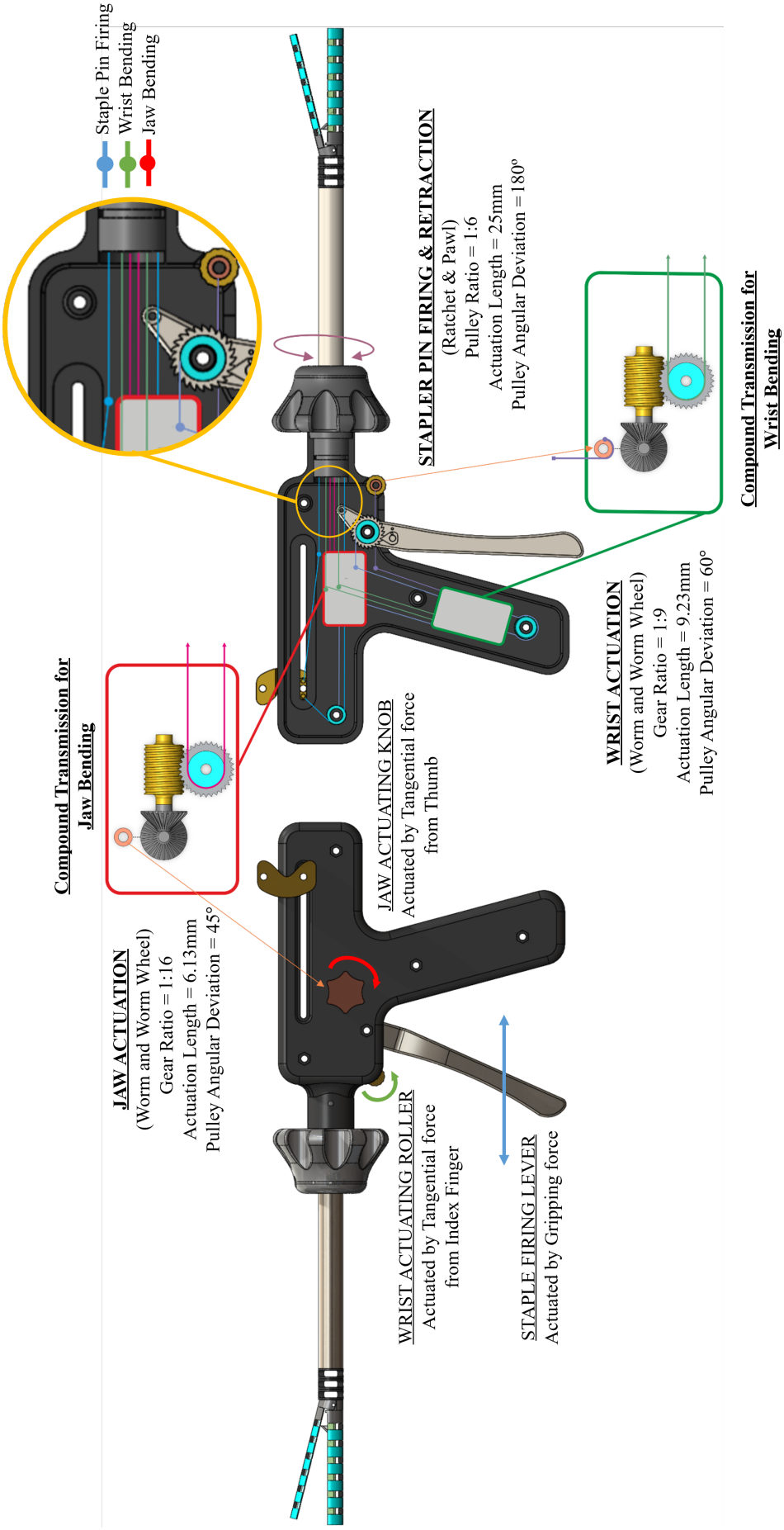

Fig. 6.21 *Detailed view of the cable-based actuation system for the surgical stapler, illustrating the transmission pathways for jaw, wrist, and firing mechanisms.*

6.7 SUMMARY OF THE CHAPTER

This chapter details the design, modeling, and integration of a handheld surgical stapler developed using analytical modeling, Piecewise Constant Curvature Approximation (PCCA), kinematic analysis, and CAD-based design. The work begins with the jaw mechanism, modeled through PCCA to capture compliant bending behavior while maintaining structural integrity. Analytical and kinematic models established the relationships between applied forces, angular deflections, and stress distribution. Prototypes and experimental tests validated the predictions, demonstrating repeatable performance under surgical loading conditions.

The wrist mechanism was subsequently developed to extend articulation capabilities at the distal end. Based on cable-driven actuation and compliant joints, it enables smooth angular deflection with precise control. Kinematic analysis quantified input–output relationships, and CAD prototypes confirmed reliable articulation across repeated cycles. Together, the jaw and wrist mechanisms form a compliant, cable-actuated articulation system suitable for minimally invasive procedures.

The stapler actuation mechanism was subsequently developed as an integrated handheld device, conceptually modeled after a stapler gun. The design objectives emphasized ergonomic single-handed operation, intuitive control layout, and mechanical robustness. The configuration comprises a primary lever for simultaneous stapling and cutting, a thumb-operated knob for jaw articulation, an index-finger roller for wrist movement, a spindle mechanism enabling axial rotation, and a retraction slider for knife reset. Computer-aided design modeling facilitated the integration of these subsystems while preserving overall compactness and user comfort.

To ensure efficient force transmission, the device employs cable-based systems, compound pulleys, and worm–worm wheel assemblies. Mathematical formulations for stapler firing, jaw articulation, and wrist motion describe torque transformation and cable tension generation. These models explicitly link ergonomic input forces with distal actuation requirements, verifying feasibility against human physiological capabilities.

Force and safety analyses confirmed that the actuation forces required for operation remained well below the maximum grip, thumb, and finger strength thresholds, thereby ensuring minimal user fatigue and high safety margins. Ergonomic testing conducted with sixteen digestive surgeons validated the accessibility and functional practicality of the majority of control elements, while also highlighting areas for refinement in the trigger and rotation knob designs. These insights were incorporated into the final iteration, resulting in a compact, modular, and ergonomically optimized instrument.

7

Conclusions

Minimally invasive colorectal surgeries—and other procedures in anatomically constrained regions—face significant challenges due to the limitations of conventional rigid-jaw endoscopic staplers. These devices often fail to achieve precise positioning and orientation within confined pelvic anatomy, restricting surgical access and potentially compromising procedural efficiency and patient safety. This doctoral work was motivated by the need to address these challenges, aiming to develop a flexible endoscopic surgical stapler capable of adapting to complex anatomical geometries while ensuring precision, safety, and ergonomic operation.

A critical aspect of the work was understanding the anatomical constraints for device operation. Using T2-weighted pelvic MRI scans from 77 subjects (47 male, 30 female), the feasible operational workspace for the proposed stapler was systematically identified through segmentation of relevant anatomical structures. This analysis allowed precise mapping of the usable workspace and its subsequent optimization into a geometrically uniform form. Two optimal working lengths, 67.10 mm and 55.70 mm, were determined, effectively accommodating over 95% of the patient population. This patient-oriented design approach ensured clinical relevance and provided a solid benchmark for the development of flexible surgical tools.

The research began with the development of a kinematic model for the flexible jaw mechanism. A stacked tensegrity framework, combined with the Piecewise Constant Curvature Approximation (PCCA) method, was employed to model the flexible segments and predict their articulation behavior. This approach facilitated a detailed analysis of intersegmental force transmission, frictional effects, and potential singularities within the mechanism. Simulations provided essential insights into mechanical limits, stability, and responsiveness, serving as a foundation for both design optimization and subsequent prototyping.

The theoretical design was translated into practical prototypes through CAD modeling and 3D printing. Two major iterations were developed. The first iteration validated the predicted

kinematic behavior of the flexible jaw, confirming the accuracy of the modeling approach. The second iteration introduced modularity, featuring rigid segments connected by a flexible spine and a removable anvil to enhance functionality. Experimental evaluations of these prototypes demonstrated effective articulation and mechanical reliability, highlighting the importance of iterative prototyping in bridging theoretical design and practical feasibility.

To further enhance tool maneuverability, a flexural hinge-based wrist mechanism was developed. Due to its unconventional geometry, detailed analytical models were derived to evaluate area moments of inertia (Ixx and Iyy) and their influence on bending behavior. Theoretical predictions were validated through controlled experimental bending tests using 3D-printed prototypes. Parameter optimization identified wrist configurations that maximized bending while minimizing the required actuation force, ensuring precision, ease of use, and ergonomic feasibility.

An integrated actuation system was designed to combine firing, jaw articulation, and wrist bending into a cohesive, single-handed interface. The system included a compound pulley system for staple deployment, worm and worm-wheel assemblies with compound pulleys for jaw and wrist actuation, and ergonomic controls: firing operated by the palm and fingers, jaw articulation via a thumb knob, and wrist manipulation through an index-finger roller. This design ensures intuitive and precise operation, minimizing surgeon fatigue and improving procedural control in confined surgical spaces.

This thesis establishes a systematic framework for the design, modeling, and prototyping of flexible endoscopic surgical staplers. By integrating advanced kinematic modeling, patient-specific anatomical analysis, iterative prototyping, and ergonomic actuation design, the research demonstrates that flexible staplers can achieve both mechanical reliability and clinical practicality. The outcomes validate the feasibility of flexible surgical staplers and provide actionable design principles for future developments in minimally invasive surgery, robotic-assisted tools, and patient-specific surgical devices. This work lays the groundwork for further exploration and optimization of flexible, adaptable, and ergonomic surgical instruments, contributing to enhanced safety, efficiency, and precision in challenging surgical environments.

8

Future Work

Although this thesis presents a comprehensive framework for the design, modeling, and prototyping of a flexible endoscopic surgical stapler, several critical areas remain to be addressed in order to translate this research into a fully clinically viable instrument. The most immediate and pressing challenge lies in the design and implementation of the stapler cartridge. In conventional rigid staplers, the cartridge functions as a detachable, reloadable unit containing surgical staples in a fixed, mechanically stable configuration. In contrast, the flexible design requires the cartridge to bend and articulate along with the jaw while maintaining precise alignment and uniform spacing of the staples during deployment. Ensuring reliable and consistent staple formation under these dynamic conditions is a significant engineering challenge. Future research will need to explore novel cartridge architectures, potentially integrating compliant mechanisms, micro-guiding structures, or flexible materials that preserve the geometric constraints of the staples while maintaining mechanical integrity. These investigations will be critical to ensure compliance with established medical standards and guarantee safe clinical operation.

As part of this ongoing effort, an envisioned staple pin positioning concept has been developed in this work, accompanied by a preliminary CAD model and a primitive 3D-printed prototype as depicted in Figure 8.1 and Figure 8.2. This prototype serves primarily as a proof of concept, providing an initial validation of the design intent. However, it remains an early-stage construct that requires substantial refinement in geometry, mechanics, and materials to progress toward a clinically applicable solution. Future iterations will need to address not only functional reliability but also manufacturability, biocompatibility, and integration with the overall stapler system.

Beyond cartridge design, the selection of materials for all functional components of the device—including the jaw, cartridge, anvil, and wrist—remains a key area for further development. The device's manual actuation imposes inherent limitations on the forces available for operation. Consequently, the materials must be lightweight, mechanically compliant, and capa-

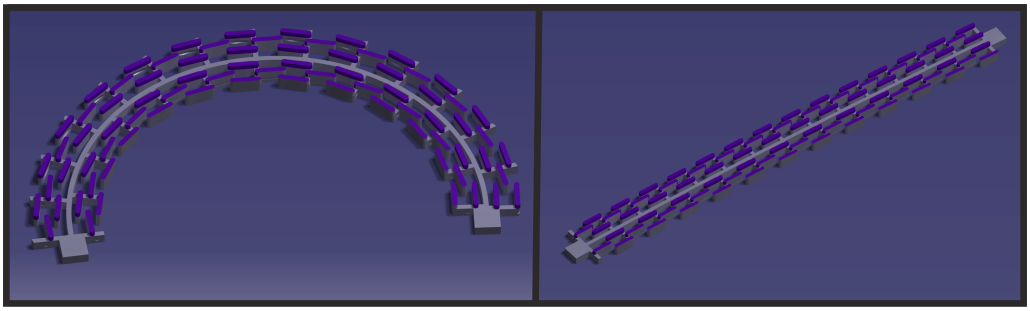

Fig. 8.1 *Envisioned CAD Design of Pin Arrangement in Flexible Cartridge*

ble of transmitting sufficient force for reliable function. At the same time, these materials must demonstrate resilience under repeated actuation, bending, and load cycles to support long-term reusability. Advanced material characterization, including fatigue testing, stress-strain analysis, and dynamic compliance evaluation, will be essential to identify suitable candidates that meet both mechanical and operational requirements.

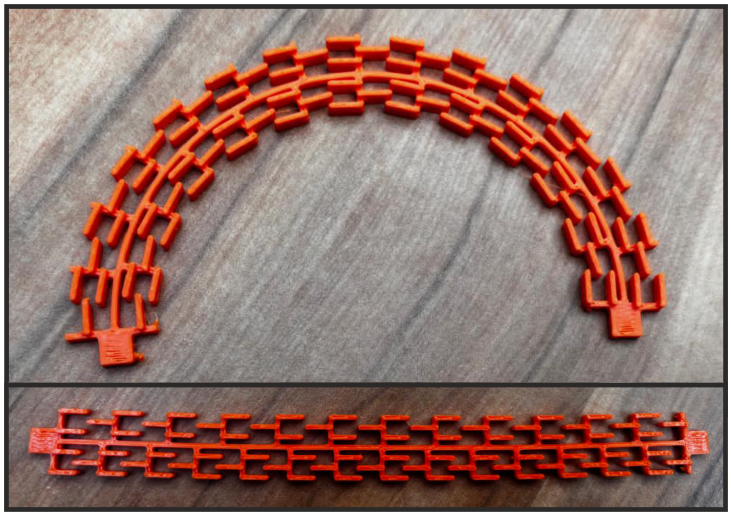

Fig. 8.2 *3D-Printed Prototype of Stapler Pin Arrangement in Flexible Cartridge*

Simultaneously, all materials employed must satisfy stringent biomedical criteria. Biocompatibility, non-toxicity, sterilizability, and long-term durability under repeated clinical use are non-negotiable requirements for any surgical instrument. Future work will therefore involve rigorous testing protocols, including sterilization cycle studies, wear analysis, and long-term mechanical reliability assessments. Integrating these studies with iterative prototyping of the jaw and cartridge assemblies will enable validation of material choices in conditions that closely replicate the surgical environment, bridging the gap between theoretical design and practical application.

Clinical validation represents the final and perhaps most critical step in the development trajectory of the flexible stapler. Controlled clinical studies will be required to evaluate device performance in real-world surgical settings, assessing parameters such as accuracy of staple deploy-

ment, ease of maneuverability within confined anatomical spaces, and overall ergonomics for the surgeon. Comparative studies with existing rigid staplers will provide quantitative benchmarks, while structured feedback from experienced surgeons will inform iterative refinements. Such studies will not only ensure that the device meets clinical efficacy and safety standards but will also guide design modifications that enhance usability, reduce fatigue, and optimize workflow during minimally invasive procedures.

Looking further ahead, the principles and methodologies established in this thesis open avenues for additional research in the field of flexible surgical instruments. An envisioned design for a motor-actuated surgical stapler has also been conceptualized, representing a potential pathway toward enhancing precision, control, and ease of operation beyond the limitations of manual actuation as shown in Figure 8.3. Integration with robotic actuation, development of sensorized feedback mechanisms, and incorporation of patient-specific anatomical customization are promising directions for future exploration. Additionally, the flexible stapler platform could be extended to other constrained surgical environments beyond colorectal procedures, broadening the impact of the research and contributing to the advancement of minimally invasive surgical technologies more broadly.

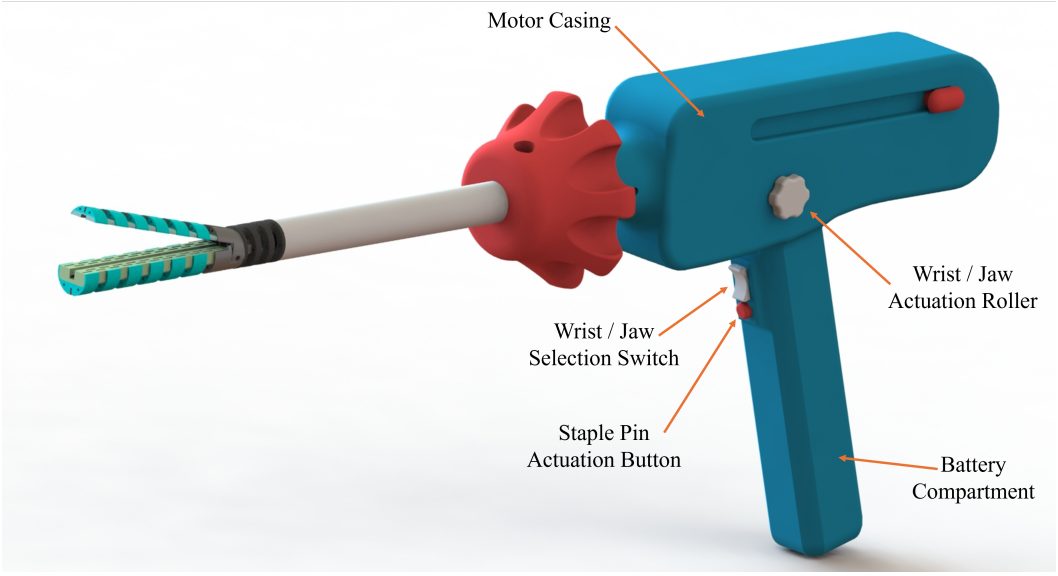

Fig. 8.3 *Envisioned Design of Motor Actuated Flexible Endoscopic Surgical Stapler*

In summary, while this thesis has laid a solid foundation for the development of a flexible endoscopic surgical stapler, the outlined future work highlights a clear roadmap toward clinical translation. By addressing the challenges of cartridge design, material selection, mechanical reliability, and clinical validation, subsequent research will ensure that the device achieves the dual goals of surgical efficacy and patient safety. The proposed investigations will consolidate the contributions of this thesis and provide a pathway for the next generation of ergonomically optimized, flexible surgical instruments capable of transforming minimally invasive surgery.

REFERENCES

[1] M. Vierra, MD, "Minimally invasive surgery," *Annual review of medicine*, vol. 46, no. 1, pp. 147–158, 1995.

[2] K. Miller and M. Curet, "Intuitive surgical: an overview," *Robotic-Assisted Minimally Invasive Surgery: A Comprehensive Textbook*, pp. 3–11, 2018.

[3] J. Chang and D. W. Rattner, "History of minimally invasive surgical oncology," *Surgical Oncology Clinics*, vol. 28, no. 1, pp. 1–9, 2019.

[4] A. Akopov, D. Y. Artioukh, and T. F. Molnar, "Surgical Staplers: The History of Conception and Adoption," *The Annals of Thoracic Surgery*, vol. 112, pp. 1716–1721, nov 2021.

[5] S. Lee-Kong and D. L. Feingold, "The history of minimally invasive surgery," in *Seminars in Colon and Rectal Surgery*, vol. 24, pp. 3–6, Elsevier, 2013.

[6] S. D. S. Peter and G. W. Holcomb III, *History of minimally invasive surgery*. Philadelphia: Elsevier Health Sciences, 2008.

[7] I. Alkatout, U. Mechler, L. Mettler, J. Pape, N. Maass, M. Biebl, G. Gitas, A. S. Laganà, and D. Freytag, "The development of laparoscopy—a historical overview," *Frontiers in surgery*, vol. 8, p. 799442, 2021.

[8] C. C. L. or Open Resection Study Group *et al.*, "Laparoscopic surgery versus open surgery for colon cancer: short-term outcomes of a randomised trial," *The lancet oncology*, vol. 6, no. 7, pp. 477–484, 2005.

[9] P. J. Guillou, P. Quirke, H. Thorpe, J. Walker, D. G. Jayne, A. M. Smith, R. M. Heath, and J. M. Brown, "Short-term endpoints of conventional versus laparoscopic-assisted surgery in patients with colorectal cancer (mrc clasicc trial): multicentre, randomised controlled trial," *The lancet*, vol. 365, no. 9472, pp. 1718–1726, 2005.

[10] H. J. Bonjer, C. L. Deijen, G. A. Abis, M. A. Cuesta, M. H. Van Der Pas, E. S. De Lange-De Klerk, A. M. Lacy, W. A. Bemelman, J. Andersson, E. Angenete, *et al.*, "A randomized trial of laparoscopic versus open surgery for rectal cancer," *New England Journal of Medicine*, vol. 372, no. 14, pp. 1324–1332, 2015.

[11] T. de Rooij, M. Z. Lu, M. W. Steen, M. F. Gerhards, M. G. Dijkgraaf, O. R. Busch, D. J. Lips, S. Festen, M. G. Besselink, D. P. C. Group, *et al.*, "Minimally invasive versus open pancreatoduodenectomy: systematic review and meta-analysis of comparative cohort and registry studies," *Annals of surgery*, vol. 264, no. 2, pp. 257–267, 2016.

[12] G. P. Marchetti, V. Pinelli, and G. F. Tassi, "100 years of thoracoscopy: historical notes," *Respiration*, vol. 82, no. 2, pp. 187–192, 2011.

[13] R. W. Jackson, "A history of arthroscopy," *Arthroscopy*, vol. 26, no. 1, pp. 91–103, 2010.

[14] S. G. Vitale, A. Giannini, J. Carugno, B. van Herendael, G. Riemma, L. A. Pacheco, A. Drizi, L. Mereu, S. Bettocchi, S. Angioni, *et al.*, "Hysteroscopy: where did we start, and where are we now? the compelling story of what many considered the "cinderella" of gynecological endoscopy," *Archives of gynecology and obstetrics*, vol. 310, no. 4, pp. 1877–1888, 2024.

[15] H. Alenezi and J. D. Denstedt, "Flexible ureteroscopy: Technological advancements, current indications and outcomes in the treatment of urolithiasis," *Asian Journal of Urology*, vol. 2, no. 3, pp. 133–141, 2015.

[16] E. D. Auyang, B. F. Santos, D. H. Enter, E. S. Hungness, and N. J. Soper, "Natural orifice translumenal endoscopic surgery (notes®): a technical review," *Surgical endoscopy*, vol. 25, no. 10, pp. 3135–3148, 2011.

[17] R. R. Shamir, I. Tamir, E. Dabool, L. Joskowicz, and Y. Shoshan, "A method for planning safe trajectories in image-guided keyhole neurosurgery," in *International Conference on Medical Image Computing and Computer-Assisted Intervention*, pp. 457–464, Springer, 2010.

[18] J. B. Adams, P. G. Schulam, R. G. Moore, A. W. Partin, and L. R. Kavoussi, "New laparoscopic suturing device: initial clinical experience," *Urology*, vol. 46, no. 2, pp. 242–245, 1995.

[19] A. Kuthe, A. Haemmerle, K. Ludwig, S. Falck, W. Hiller, F. Mainik, S. Freys, L. Dubovoy, J. Jaehne, and K. Oldhafer, "Multicenter prospective evaluation of a new articulating 5-mm endoscopic linear stapler," *Surgical Endoscopy*, vol. 30, no. 5, pp. 1883–1893, 2016.

[20] G. M. Mari, J. Crippa, P. Achilli, A. Miranda, L. Santurro, V. Riggio, M. Gerosa, P. Ascheri, G. Cordaro, A. T. Costanzi, *et al.*, "4k ultra hd technology reduces operative time and intraoperative blood loss in colorectal laparoscopic surgery," *F1000Research*, vol. 9, p. 106, 2020.

[21] N. Mayor, A. S. J. Coppola, and B. Challacombe, "Past, present and future of surgical robotics," *Trends in Urology and Men's Health*, vol. 13, no. 1, pp. 7–10, 2022.

[22] Y. S. Kwoh, J. Hou, E. A. Jonckheere, and S. Hayati, "A robot with improved absolute positioning accuracy for ct guided stereotactic brain surgery," *IEEE transactions on biomedical engineering*, vol. 35, no. 2, pp. 153–160, 1988.

[23] E. H. Spencer, "The robodoc clinical trial: a robotic assistant for total hip arthroplasty," *Orthopaedic Nursing*, vol. 15, no. 1, pp. 9–14, 1996.

[24] T. Ginoya, Y. Maddahi, and K. Zareinia, "A historical review of medical robotic platforms," *Journal of Robotics*, 2021.

[25] F. Pugin, P. Bucher, and P. Morel, "History of robotic surgery: from aesop® and zeus® to da vinci®," *Journal of visceral surgery*, vol. 148, no. 5, pp. e3–e8, 2011.

[26] R. Bogue, "Surgical robots: history, applications and future prospects," *Industrial Robot*, vol. 51, no. 6, pp. 873–880, 2024.

[27] H. R. H. Patel, A. Amodeo, and J. V. Joseph, "Robotic oncological surgery: technology that's here to stay?," *European Urology Supplements*, vol. 8, no. 10, pp. 819–824, 2009.

[28] P. Iranmanesh, P. Morel, O. J. Wagner, I. Inan, F. Pugin, and M. E. Hagen, "Set-up and docking of the da vinci® surgical system: prospective analysis of initial experience," *The international journal of medical robotics and computer assisted surgery*, vol. 6, no. 1, pp. 57–60, 2010.

[29] H.-X. Zhou, Y.-H. Guo, X.-F. Yu, S.-Y. Bao, J.-L. Liu, Y. Zhang, Y.-G. Ren, and Q. Zheng, "Clinical characteristics of remote zeus robot-assisted laparoscopic cholecystectomy: a report of 40 cases," *World journal of gastroenterology: WJG*, vol. 12, no. 16, p. 2606, 2006.

[30] F. Fanfani, G. Monterossi, A. Fagotti, C. Rossitto, S. G. Alletti, B. Costantini, V. Gallotta, L. Selvaggi, S. Restaino, and G. Scambia, "The new robotic telelap alf-x in gynecological surgery: single-center experience," *Surgical endoscopy*, vol. 30, no. 1, pp. 215–221, 2016.

[31] D. M. Herron and M. Dong, "Upcoming robotic systems," in *Robotic-Assisted Minimally Invasive Surgery: A Comprehensive Textbook*, pp. 319–321, Springer, 2018.

[32] D. Collins, H. M. Paterson, R. J. Skipworth, and D. Speake, "Implementation of the versius robotic surgical system for colorectal cancer surgery: first clinical experience," *Colorectal Disease*, vol. 23, no. 5, pp. 1233–1238, 2021.

[33] S. G. Alletti, V. Chiantera, G. Arcuri, A. Gioè, R. Oliva, G. Monterossi, F. Fanfani, A. Fagotti, and G. Scambia, "Introducing the new surgical robot hugo™ ras: system description and docking settings for gynecological surgery," *Frontiers in oncology*, vol. 12, p. 898060, 2022.

[34] S. P. Srivastava, V. P. Srivastava, A. Singh, S. Dwivedi, M. Batra, S. Gupta, S. Singh, S. S. Kulkarni, A. Paul, A. Kumar, and M. Agwan, "Evaluating the efficacy of telesurgery with dual console ssi mantra surgical robotic system: experiment on animal model and clinical trials," *Journal of Robotic Surgery*, vol. 18, no. 1, p. 391, 2024.

[35] R. Llombart-Blanco, G. Mariscal, C. Barrios, P. Vera, and R. Llombart-Ais, "Mako robot-assisted total hip arthroplasty: a comprehensive meta-analysis of efficacy and safety outcomes," *Journal of Orthopaedic Surgery and Research*, vol. 19, no. 1, p. 698, 2024.

[36] J. C. R. Burbano, N. I. Ruiz, G. A. R. Burbano, J. S. G. Inca, C. A. A. Lezama, and M. S. González, "Robot-assisted general surgery: Current applications and future trends in general surgery," *World Journal of Surgery*, 2024. PMC12080974.

[37] A. Ragusa, F. Prata, A. Iannuzzi, F. Tedesco, L. Cacciatore, A. Brassetti, G. Muto, R. M. Scarpa, and R. Papalia, "The evolution of robotic surgery through the machine design innovation," *Uro*, vol. 4, no. 3, pp. 124–135, 2024.

[38] J. A. Van Koughnett, S. Jayaraman, R. Eagleson, D. Quan, A. van Wynsberghe, and C. M. Schlachta, "Are there advantages to robotic-assisted surgery over laparoscopy from the surgeon's perspective?," *Journal of robotic surgery*, vol. 3, no. 2, pp. 79–82, 2009.

[39] P. R. Acharya, "Robotic surgery: an overview," *Journal of Biomedical Engineering and Medical Devices*, vol. 6, no. 1, 2021.

[40] H. Alemzadeh, J. Raman, N. Leveson, Z. Kalbarczyk, and R. K. Iyer, "Adverse events in robotic surgery: a retrospective study of 14 years of fda data," *PloS one*, vol. 11, no. 4, p. e0151470, 2016.

[41] J. C. R. Burbano, N. I. Ruiz, G. A. R. Burbano, J. S. G. Inca, C. A. A. Lezama, and M. S. González, "Robot-assisted surgery: Current applications and future trends in general surgery," *Cureus*, vol. 17, no. 4, 2025.

[42] G. Hubens, H. Coveliers, L. Balliu, and M. Ruppert, "Advantages and limits of robot-assisted laparoscopic surgery: preliminary experience," *Acta Chirurgica Belgica*, vol. 104, no. 4, pp. 409–413, 2004.

[43] C. e. a. Gouillat, "Impact of robotic assistance on complications in bariatric surgery at expert laparoscopic surgery centers: a retrospective comparative study with propensity score," *Surgery for Obesity and Related Diseases*, vol. 19, no. 7, pp. 567–575, 2023.

[44] J. J. Uicker, G. R. Pennock, and J. E. Shigley, *Theory of Machines and Mechanisms*. Oxford University Press, 5 ed., 2016.

[45] J. M. McCarthy and G. S. Soh, *Geometric Design of Linkages*. Springer, 2 ed., 2010.

[46] J. Angeles, *Fundamentals of Robotic Mechanical Systems: Theory, Methods, and Algorithms*. Springer, 3 ed., 2007.

[47] K. M. Lynch and F. C. Park, *Modern Robotics: Mechanics, Planning, and Control*. Cambridge University Press, 2017.

[48] K. J. Waldron and J. H. Schmiedeler, "Kinematic analysis of mechanisms and robots: mobility, constraints, dof," in *Springer Handbook of Robotics* (B. Siciliano and O. Khatib, eds.), pp. 9–32, Springer, 2008.

[49] J. L. Meriam and L. G. Kraige, *Engineering Mechanics: Dynamics*. Wiley, 6 ed., 2006.

[50] M. W. Spong, S. Hutchinson, and M. Vidyasagar, *Robot Modeling and Control*. Wiley, 2 ed., 2020.

[51] J. J. Craig, *Introduction to Robotics: Mechanics and Control*. Pearson, 3 ed., 2004.

[52] S. R. Buss, "Introduction to inverse kinematics with jacobian transpose, pseudoinverse and damped least squares methods," *IEEE Journal of Robotics and Automation*, 2004. Tutorial notes, originally 1995; widely cited.

[53] J. Denavit and R. S. Hartenberg, "A kinematic notation for lower-pair mechanisms based on matrices," *Journal of Applied Mechanics*, vol. 23, no. 2, pp. 215–221, 1955.

[54] C. R. Rocha, C. P. Tonetto, and A. Dias, "A comparison between the denavit–hartenberg and the screw-based methods used in kinematic modeling of robot manipulators," *Robotics and Computer-Integrated Manufacturing*, vol. 27, no. 4, pp. 723–728, 2011.

[55] L. Wu, R. Crawford, and J. Roberts, "Geometric interpretation of the general poe model for a serial-link robot via conversion into d-h parameterization," *arXiv preprint arXiv:1902.00198*, 2019.

[56] T. Yoshikawa, "Manipulability of robotic mechanisms," *The International Journal of Robotics Research*, vol. 4, no. 2, pp. 3–9, 1985.

[57] I. Zaplana, S. Hadfield, and J. Lasenby, "Singularities of serial robots: Identification and distance computation using geometric algebra," *Mathematics*, vol. 10, no. 12, p. 2068, 2022.

[58] N. Simaan and M. Shoham, "Singularity analysis of a class of composite serial-in-parallel robots," *IEEE Transactions on Robotics and Automation*, vol. 17, no. 3, pp. 301–311, 2001.

[59] "Working modes and aspects in fully parallel manipulators," in *Proceedings. 1998 IEEE International Conference on Robotics and Automation (Cat. No. 98CH36146)*, vol. 3, pp. 1964–1969, IEEE, 1998.

[60] C. Gosselin and J. Angeles, "Singularity analysis of closed-loop kinematic chains," *IEEE Transactions on Robotics and Automation*, vol. 6, no. 3, pp. 281–290, 1990.

[61] J.-P. Merlet, "Singular configurations of parallel manipulators and grassmann geometry," in *Proceedings of the IEEE International Conference on Robotics and Automation*, pp. 738–743, IEEE, 1989.

[62] D. Zlatanov, I. A. Bonev, and C. Gosselin, "Constraint singularities as configuration space singularities," in *Proceedings of ARK 2002: Advances in Robot Kinematics*, pp. 183–192, Springer, 2002.

[63] R. J. Webster III and B. A. Jones, "Design and kinematic modeling of constant curvature continuum robots: A review," *The International Journal of Robotics Research*, vol. 29, no. 13, pp. 1661–1683, 2010.

[64] H. Yuan, H. Yu, H. Ding, F. Alambeigi, and R. H. Taylor, "Workspace analysis of cable-driven continuum robots based on piecewise constant curvature approximation," *Mechanism and Machine Theory*, vol. 125, pp. 208–222, 2018.

[65] T. Kato, A. Degani, and H. Choset, "Tendon-driven continuum robot for endoscopic surgery: experimental evaluation of piecewise constant curvature model," *Medical Image Analysis*, vol. 25, no. 1, pp. 86–95, 2015.

[66] T. Zhang, X. Wang, N. Simaan, and H. Zhao, "Millimeter-scale soft continuum robots for large-angle and complex 3d motions," *IEEE Robotics and Automation Letters*, vol. 6, no. 4, pp. 7529–7536, 2021.

[67] H. Liu, Y. Dong, Y. Jiang, L. Sun, X. Zhang, and S. Guo, "Shape sensing for single-port continuum surgical robot using few multicore fiber bragg grating sensors," *Journal of Shanghai Jiao Tong University (Science)*, vol. 27, no. 5, pp. 663–672, 2022.

[68] D. Surovik, J. Bruce, K. Wang, M. Vespignani, and K. E. Bekris, "Any-axis tensegrity rolling via symmetry-reduced reinforcement learning," in *Proceedings of the 2018 International Symposium on Experimental Robotics (ISER 2018)*, vol. 11 of *Springer Proceedings in Advanced Robotics*, pp. 411–421, Springer, Cham, 2018.

[69] J. C. G. Alba, A. J. Valencia-Casteneda, M. S. Dutra, and M. Mauledoux, "Tensegrity approaches for flexible robots: A review," in *Synergetic Cooperation between Robots and Humans*, pp. 52–62, Springer, 2024.

[70] R. Motro, *Tensegrity: Structural Systems for the Future*. London: Kogan Page Science, 2003.

[71] R. E. Skelton and M. C. de Oliveira, "An introduction to the mechanics of tensegrity structures," in *Tensegrity Systems*, pp. 19–60, Springer, 2009.

[72] P. Wenger and D. Chablat, "Kinetostatic analysis and solution classification of a class of planar tensegrity mechanisms," *Robotica*, vol. 37, no. 7, pp. 1214–1224, 2019.

[73] M. Furet, M. Lettl, and P. Wenger, "Kinematic analysis of planar tensegrity 2-x manipulators," in *Springer Proceedings in Advanced Robotics*, vol. 8, pp. 153–160, 2019.

[74] A. P. Sabelhaus, J. Bruce, K. Caluwaerts, R. F. Firoozi, S. Dobi, N. Jansen, P. Friesen, D. Lu, and V. SunSpiral, "System design and locomotion of superball, an untethered tensegrity robot," in *2015 IEEE International Conference on Robotics and Automation (ICRA)*, pp. 2867–2873, IEEE, 2015.

[75] V. Muralidharan, P. Wenger, and C. Chevallereau, "Kinematic and static analysis of a cable-driven 2-x tensegrity manipulator for two actuation strategies," in *Advances in Robot Kinematics 2022 (ARK 2022)*, vol. 24 of *Springer Proceedings in Advanced Robotics*, pp. 149–159, Springer, Cham, 2022.

[76] Y. S. Chung, J.-H. Lee, J. H. Jang, H. R. Choi, and H. Rodrigue, "Jumping tensegrity robot based on torsionally prestrained sma springs," *ACS Applied Materials and Interfaces*, vol. 11, no. 43, pp. 40793–40799, 2019.

[77] D. B. Camarillo, C. F. Milne, C. R. Carlson, M. R. Zinn, and J. K. Salisbury, "Mechanics modeling of tendon-driven continuum manipulators," *IEEE Transactions on Robotics*, vol. 24, no. 6, pp. 1262–1273, 2008.

[78] J. Burgner-Kahrs, D. C. Rucker, and H. Choset, "Continuum robots for medical applications: A survey," *IEEE Transactions on Robotics*, vol. 31, no. 6, pp. 1261–1280, 2015.

[79] R. M. Grassmann, P. Rao, Q. Peyron, and J. Burgner-Kahrs, "Fas — a fully actuated segment for tendon-driven continuum robots," *Frontiers in Robotics and AI*, vol. 9, p. 873446, 2022.

[80] F. Renda and C. Laschi, "A general mechanical model for tendon-driven continuum manipulators," in *Proceedings of the IEEE International Conference on Robotics and Automation (ICRA)*, 2012.

[81] T. Kato, I. Okumura, S.-E. Song, A. J. Golby, and N. Hata, "Tendon-driven continuum robot for endoscopic surgery: Preclinical development and validation of a tension propagation model," *IEEE/ASME Transactions on Mechatronics*, vol. 20, no. 5, pp. 2252–2263, 2015.

[82] M. P. Huertas Niño, M. Boutayeb, and D. Martinez, "A hybrid tendon-driven continuum robot that avoids torsion under external load," *Frontiers in Robotics and AI*, 2025.

[83] A. Ghoul, S. Djeffal, H. Wang, K. Kara, and M. L. Hadjili, "Enhancing surgical robotics: A dynamic model and optimized control strategy for cable-driven continuum robots," *Journal of Mechanisms and Robotics*, vol. 17, p. 021002, 07 2024.

[84] H. Peng, A. Lewis, Y.-H. Su, S. Lin, D.-T. Chiang, W. Jiang, H. Lai, and B. Hannaford, "Efficient data-driven joint-level calibration of cable-driven surgical robots," *npj Robotics*, vol. 2, no. 1, pp. 1–16, 2024.

[85] M. Varga, P. J. Sinčák, T. Merva, P. Marcinko, L. Miková, E. Prada, M. Schnitzer, and I. Virgala, "Design and analyses of tendon-driven continuum robots for minimally invasive surgery," *IFAC-PapersOnLine*, vol. 58, no. 9, pp. 25–30, 2024. 18th IFAC Conference on Programmable Devices and Embedded Systems PDES 2024.

[86] F. Robicsek and I. Konstantinov, "Hümer hültl: the father of the surgical stapler," *Journal of Medical Biography*, vol. 9, no. 1, pp. 16–19, 2001.

[87] S. Demertzis, O. Beslac, D. Mettler, D. Zalokar, T. Spangler, B. Hausen, and L. Swanstrom, "Beyond the b: a new concept of the surgical staple enabling miniature staplers," *Surgical Endoscopy*, vol. 29, pp. 3674–3684, 2015.

[88] A. D. Gaidry, L. Tremblay, D. Nakayama, and R. C. Ignacio, "The History of Surgical Staplers: A Combination of Hungarian, Russian, and American Innovation," *The American Surgeon*, vol. 85, pp. 563–566, jun 2019.

[89] J. McGuire, I. Wright, and J. Leverment, "Surgical staplers: a review.," *Journal of the Royal College of Surgeons of Edinburgh*, vol. 42, no. 1, pp. 1–9, 1997.

[90] T. Ema, "The experience of using Endo GIA Radial Reload with Tri-Staple Technology for various lung surgery," *Journal of Thoracic Disease*, vol. 6, no. 10, pp. 1482–1484, 2014.

[91] P. Schemmer, H. Friess, C. Dervenis, J. Schmidt, J. Weitz, W. Uhl, and M. W. Büchler, "The Use of Endo-GIA Vascular Staplers in Liver Surgery and Their Potential Benefit:A Review," *Digestive Surgery*, vol. 24, no. 4, pp. 300–305, 2007.

[92] D. E. Rivadeneira, J. C. Verdeja, and T. Sonoda, "Improved access and visibility during stapling of the ultra-low rectum: a comparative human cadaver study between two curved staplers," *Annals of Surgical Innovation and Research*, vol. 6, p. 11, dec 2012.

[93] J. L. Holzmacher, S. Luka, M. Aziz, R. L. Amdur, S. Agarwal, and V. Obias, "The use of robotic and laparoscopic surgical stapling devices during minimally invasive colon and rectal surgery: a comparison," *Journal of Laparoendoscopic and Advanced Surgical Techniques*, vol. 27, no. 2, pp. 151–155, 2017.

[94] A. Thomieres, D. Khanzode, E. Duchalais, R. Jha, and D. Chablat, "Workspace analysis for laparoscopic rectal surgery: A preliminary study," in *International Conference on Robotics in Alpe-Adria Danube Region*, pp. 139–146, Springer, 2024.

[95] D. Khanzode, A. Thomieres, R. Jha, E. Duchalais, L. Baron, D. Pisla, and D. Chablat, "Optimization of design parameters for a flexible endoscopic surgical tool using medical imaging data for minimally invasive surgery (mis)," *Mechanism and Machine Theory*, vol. 209, p. 105987, 2025.

[96] D. Khanzode, R. Jha, A. Thomieres, E. Duchalais, and D. Chablat, "Design of a surgical stapler for laparoscopic colectomy," in *New Trends in Medical and Service Robotics* (D. Tarnita, N. Dumitru, D. Pisla, G. Carbone, and I. Geonea, eds.), (Cham), pp. 71–80, Springer Nature Switzerland, 2023.

[97] I. Gravagne, C. Rahn, and I. Walker, "Large deflection dynamics and control for planar continuum robots," *IEEE/ASME Transactions on Mechatronics*, vol. 8, no. 2, pp. 299–307, 2003.

[98] D. Khanzode, R. Jha, D. Chablat, and E. Duchalais, "Stapler design with stacked tensegrity mechanisms for surgical procedures," in *International Design Engineering Technical Conferences and Computers and Information in Engineering Conference*, vol. 86281, p. V007T07A037, American Society of Mechanical Engineers, 2022.

[99] D. Khanzode, R. Jha, E. Duchalais, and D. Chablat, "Stacked tensegrity mechanism for medical application," in *International Symposium on Advances in Robot Kinematics*, pp. 139–148, Springer, 2022.

[100] R. Jha, D. Chablat, L. Baron, F. Rouillier, and G. Moroz, "Workspace, joint space and singularities of a family of delta-like robot," *Mechanism and Machine Theory*, vol. 127, pp. 73–95, 2018.

[101] D. Khanzode, R. Jha, A. Thomieres, E. Duchalais, and D. Chablat, "Surgical staplers in laparoscopic colectomy: A new innovative flexible design perspective," *Robotics*, vol. 12, no. 6, p. 156, 2023.

[102] M. O. Conrad and R. W. Marklin, "Evaluation of forearm muscle fatigue from operating a motorcycle clutch," *Journal of Ergonomics*, 2014.

[103] G. P. Slota, M. L. Latash, and V. M. Zatsiorsky, "Tangential finger forces use mechanical advantage during static grasping," *Journal of applied biomechanics*, vol. 28, no. 1, pp. 78–84, 2012.

[104] N. Arnold, A. Chrzan, K. Chan, D. Hess, L. Hinkleman, S. Duquette, J. Kelpin, and T. R. Bush, "Comparing isolated thumb force generation, wrist rotation, and clinical measurements in healthy and osteoarthritic individuals before and after surgery," *Bioengineering*, vol. 11, no. 9, p. 948, 2024.

[105] F. Gao, M. L. Latash, and V. M. Zatsiorsky, "Maintaining rotational equilibrium during object manipulation: linear behavior of a highly non-linear system," *Experimental Brain Research*, vol. 169, no. 4, pp. 519–531, 2006.

[106] Z.-M. Li, H. J. Pfaeffle, D. G. Sotereanos, R. J. Goitz, and S. L.-Y. Woo, "Multidirectional strength and force envelope of the index finger," *Clinical Biomechanics*, vol. 18, no. 10, pp. 908–915, 2003.

[107] Z.-M. Li and R. J. Goitz, "Biomechanical evaluation of the motor function of the thumb," *Technology and Health Care*, vol. 11, no. 4, pp. 233–243, 2003.

Publications

JOURNAL PUBLICATIONS

1. Khanzode, D.; Jha, R.; Thomieres, A.; Duchalais, E.; Chablat, D. “Surgical Staplers in Laparoscopic Colectomy: A New Innovative Flexible Design Perspective”. *Robotics*, 2023, 12, 156. doi:10.3390/robotics12060156.

2. Khanzode, D.; Thomieres, A.; Jha, R.; Duchalais, D.; Baron, L.; Pisla, D.; Chablat, D. “Optimisation Of Design Parameters For A Flexible Endoscopic Surgical Tool Using Medical Imaging Data For Minimally Invasive Surgery (MIS)”. *Mechanism and Machine Theory*, 209 (2025) 105987. doi:10.1016/j.mechmachtheory.2025.105987.

OTHER PUBLICATIONS

1. N. Gupta, D. Khanzode, and R. Jha. ”Design and Mathematical Modelling of a Novel Two-Degree-of-Freedom Robot-Assisted Cardiac Catheterization System.” *IEEE Transactions on Medical Robotics and Bionics*. doi:10.1109/TMRB.2024.3503911.

2. Varsha, B., Dhruva Khanzode, Sanjeev Verma’a, and S. Senthil Kumaran. “Quantitative Finger Flexion Assessment Using Flex-Sensor Smart Gloves: Calibration and Application.” *Journal of Hand Therapy*, 2025 (manuscript submitted).

CONFERENCE PROCEEDINGS

1. Khanzode, D., Jha, R., Duchalais, E., Chablat, D. (2022). Stacked Tensegrity Mechanism for Medical Application. In: Altuzarra, O., Kecskeméthy, A. (eds) *Advances in Robot Kinematics 2022*. ARK 2022. Springer Proceedings in Advanced Robotics, vol 24. Springer, Cham. doi:10.1007/978-3-031-08140-8_16.

2. Khanzode, D., Jha, R., Chablat, D., Duchalais, E. (2022). ”Stapler Design With Stacked Tensegrity Mechanisms for Surgical Procedures.” *ASME 2022 International Design Engineering Technical Conferences*. V007T07A037. St. Louis, Missouri, USA. doi: 10.1115/DETC2022-89714.

3. Khanzode, D., Jha, R., Thomieres, A., Duchalais, E., Chablat, D. (2023). Design of a Surgical Stapler for Laparoscopic Colectomy. In: Tarnita, D. et al. (eds) *New Trends in Medical and Service Robotics*. MESROB 2023. Mechanisms and Machine Science, vol 133. Springer, Cham. doi:10.1007/978-3-031-32446-8_8.

4. Thomieres, A., Khanzode, D., Duchalais, E., Jha, R., Chablat, D. (2024). Workspace Analysis for Laparoscopic Rectal Surgery: A Preliminary Study. In: Pisla, D. et al. (eds) *Advances in Service and Industrial Robotics*. RAAD 2024. Mechanisms and Machine Science, vol 157. Springer, Cham. doi:10.1007/978-3-031-59257-7_15.

5. Khanzode, D., Thomieres, A., Jha, R., Duchalais, E., Chablat, D. (2024). A novel method for 3D workspace estimation of robotic surgical instruments in minimally invasive surgery using medical imaging data. *Mechanism and Machine Theory Symposium*, Jun 2024, Guimaraes, Portugal. hal-04658045v1.

ORAL/POSTER PRESENTATION

1. Dhruva Khanzode, et al., "Robot Assisted Cardiac Catheterization," *IETE Zonal Seminar on Emerging Sensors and Electronic Systems (ESES 2023)*, Chandigarh, India, April 28, 2023.

2. Dhruva Khanzode, et al., "Design of a Surgical Stapler for Laparoscopic Colectomy," *Advancement in Healthcare Technologies (AiHT 2023)*, Chandigarh, India, June 28, 2023.

AWARDS

- Best Student Paper Award: "Design of a Surgical Stapler for Laparoscopic Colectomy," *MESROB 2023*, Craiova, Romania, June 7–10, 2023.

Appendices

A

Ethical Clearance certificate: CSIR-CSIO



सीएसआइआर – केन्द्रीय वैज्ञानिक उपकरण संगठन
(वैज्ञानिक तथा औद्योगिक अनुसंधान परिषद)
सैक्टर 30 – सी, चण्डीगढ़ (भारत)
CSIR-Central Scientific Instruments Organisation
(Council of Scientific & Industrial Research)
Sector 30-C, Chandigarh (India)
www.csio.res.in

सूचना का अधिकार
RIGHT TO INFORMATION

75 years of CSIR Touching Lives
CSIO

Date: 8th February 2022
Ref: IEC/CSIO/2021
Project No: 23

INSTITUTIONAL ETHICAL COMMITTEE

Dr. Archana Bhatnagar, Chairperson Department of Biochemistry, Panjab University, Chandigarh

Prof Rajesh Gill, Member, Social scientist Department of Sociology, Panjab University, Chandigarh

Dr. Rohit Jindal, Member, Clinician Department of Orthopaedics GMCH, Sector 32-Chandigarh

Dr. Viren Sardana, Member, Basic Medical CSIR-IGIB, New Delhi

Mr. Sunil Saharan, Member Legal expert Panjab & Haryana High Court

Mrs. Garima Saini, Member, Lay person, NITTTR, Chandigarh

Dr. Suman Singh, Member Secretary CSIR-CSIO, Chandigarh

Name of Supervisor/PI:	Dr. Ranjan Jha Scientist, Biomedical Applications (BMA) CSIR-CSIO, Chandigarh
Name of Co-PI:	Prof. Damien Chablat Directeur de Recherché CNRS LS2N, Central Nantes, France
Title of Proposal:	A flexible robotic medical device based on a novel underactuated tensegrity mechanism for minimally invasive surgical (MIS) procedure
Duration of project/fellowship:	3 Year (2022-2025)
Funding Agency:	ICMR, New Delhi
Names of people involved in the experiments:	Dr. Ranjan Jha, Prof. Damien Chablat, Mr. Dhruva Rajesh Khanzode
IEC Comments:	The committee has reviewed the project. Since the study doesn't involve any testing on human or animals, the project is approved for ethical clearance.

Dr. Suman Singh
Member Secretary, IEC
Senior Scientist
CSIR-CSIO, Chandigarh

Dr. Archana Bhatnagar
Chairperson, IEC
Department of Biochemistry
Panjab University, Chandigarh

Note: It is the responsibility of the PI to provide SOPs and experimental training to the students/staff whose name is approved to conduct the experiments and handle the organism requested for IEC approval. The IEC member would periodically inspect the SOPs and facility.

EPBAX LINE : (0172) 2672 & Three Digit Extension No. **Director Office : Tel.** : (0172) 2657190, 2672200,
COA's Office : (0172) 2657900, **Fax** : (0172) 2657082, **COSP**: (0172) 2672212, **Tele Fax**: (0172)2652651
SPO's Office : (0172) 2652082, **COFA's Office** : (0172) 2642167, 2672296, **Fax** : (0172) 2651756

B

Ethical Clearance certificate: CHU Nantes

AVIS 24-88-07-170
Groupe Nantais d'Ethique dans le Domaine de la Santé (GNEDS)

Nom du protocole Code et versioning	**LIME**

Investigateur principal	Dr E. Duchalais
Lieu de l'étude	CHU Nantes, ICO Nantes
Type de l'étude	Bicentrique, rétrospective sur données existantes et prospective sur questionnaires
Type patients/participants	Population atteinte d'un cancer du bas, moyen et haut rectum en vue d'une chirurgie d'exérèse totale du méso rectum
Nombre de patients/participants prévus	Non précisé
Objectif principal	Mesurer l'association entre la volumétrie pelvienne et la morbidité post opératoires chez les patients opérés d'une exérèse totale du mésorectum pour cancer
Objectif secondaire	Évaluation de l'association avec les difficultés peropératoires (durée opératoire, perte de sang) Évaluation de l'association avec la survenue du syndrome de résection antérieure du rectum par le score LARS. (19) Évaluation de l'association avec la survenue de dysfonctions urinaires par le score IPSS chez l'homme (20) et le score USP chez la femme (21). Évaluation de l'association avec la survenue de dysfonctions sexuelles par le score IIEF-5 chez l'homme (22) et le score FSFI chez la femme (23). Évaluation de l'association avec l'incidence du taux de fistule post opératoires Évaluation de l'association avec la survie à long terme Évaluation de l'association sur la survie sans récidive Analyse des différents volumes pelviens dans l'objectif de la conception future d'une agrafeuse chirurgicale robotisée.

Titre : **Un dispositif médical robotique flexible basé sur un mécanisme de tensegrité sous-actionné pour la chirurgie mini-invasive (MIS).**

Mots clés : *Instruments chirurgicaux, Imagerie médicale, Chirurgie mini-invasive, Agrafeuse chirurgicale.*

Résumé : Les chirurgies colorectales mini-invasives, ainsi que les interventions réalisées dans des régions anatomiques contraintes, sont limitées par les agrafeuses endoscopiques conventionnelles à mâchoires rigides, dont le positionnement et l'orientation optimaux restent difficiles à atteindre. Cette thèse répond à ce défi clinique en développant une ***agrafeuse chirurgicale endoscopique flexible***, conçue pour s'adapter aux géométries complexes du pelvis tout en assurant une utilisation sûre, précise et ergonomique. Une analyse approfondie des contraintes anatomiques, basée sur des IRM pelviennes pondérées T2 de 77 sujets, a permis de caractériser l'espace de travail opératoire et d'optimiser deux longueurs de travail, 67,10 mm et 55,70 mm, couvrant plus de 95% de la population étudiée. Ces résultats fournissent des références essentielles pour la conception d'outils adaptés aux spécificités morphologiques des patients. Un modèle cinématique du mécanisme flexible de la mâchoire a été élaboré à partir de structures de tenségrité empilées et d'une approximation de courbure constante par morceaux (PCCA), permettant de prédire le comportement d'articulation, la transmission des forces intersegmentaires et les singularités potentielles. Ces prédictions ont guidé l'optimisation de la conception, validée par un prototypage itératif en CAO. Deux générations de prototypes ont démontré une articulation fiable et des performances mécaniques robustes, la seconde intégrant des segments rigides modulaires et une enclume amovible pour une fonctionnalité accrue. Un mécanisme de poignet à charnière flexible a également été conçu pour améliorer la manœuvrabilité, optimisé pour maximiser la flexion tout en minimisant la force d'actionnement. Enfin, un système d'actionnement manuel a été développé pour intégrer le déclenchement, l'articulation de la mâchoire et la flexion du poignet dans une interface intuitive, répondant aux exigences ergonomiques des environnements chirurgicaux contraints. Ce travail établit ainsi un cadre méthodologique complet pour la conception d'agrafeuses chirurgicales flexibles, ouvrant la voie à des dispositifs mini-invasifs de nouvelle génération

Title: **A Flexible robotic medical device based on under actuated tensegrity mechanism for minimally invasive surgery (MIS).**

Keywords : *Surgical Tools, Medical Imaging, Minimally Invasive Surgery, Surgical Stapler*.

Abstract: Limitations of Conventional Endoscopic Staplers and Proposed Innovation Minimally invasive colorectal surgeries, along with procedures performed in anatomically constrained regions, are hindered by the limitations of conventional rigid-jaw endoscopic staplers, which often struggle to achieve optimal positioning and orientation. This thesis addresses this clinical challenge by developing a ***flexible endoscopic surgical stapler*** designed to adapt to the complex geometries of the pelvis while ensuring safe, precise, and ergonomic operation. Relevant anatomical constraints were characterized using T2-weighted pelvic MRI scans from 77 subjects, enabling the definition of a feasible operational workspace. Two optimal working lengths, 67.10 mm and 55.70 mm, were identified, effectively accommodating over 95% of the studied population and providing benchmarks for patient-specific tool design. Based on these constraints, a kinematic model of the flexible jaw mechanism was developed using a stacked tensegrity framework and Piecewise Constant Curvature Approximation (PCCA). This approach enabled the prediction of articulation behaviour, intersegmental force transmission, and potential singularities, guiding the optimization of the design. The model's predictions were validated through iterative prototyping using CAD, with two prototype generations demonstrating reliable articulation and robust mechanical performance. The second iteration incorporated modular rigid segments and a removable anvil for enhanced functionality. To further improve maneuverability, a flexural hinge-based wrist mechanism was designed and analytically modelled, optimizing parameters to maximize bending while minimizing actuation force. Finally, a manual actuation system was developed to integrate firing, jaw articulation, and wrist bending into an intuitive control interface, informed by ergonomic considerations. This work presents a comprehensive framework for designing and prototyping flexible surgical staplers that are mechanically reliable, anatomically optimized, and ergonomically practical, paving the way for a new generation of minimally invasive surgical devices.